View metadata, citation and similar papers at core.ac.uk
brought to you by CORE
provided by UT Digital Repository

CRWR Online Report 06-05

Physical and Conceptual Modeling of Sedimentation Characteristics in Stormwater Detention Basins

by

Masatsugu Takamatsu, Ph.D.

Michael Barrett, Ph.D.

Randall J. Charbeneau, Ph.D.

December 2006

Center for Research in Water Resources
The University of Texas at Austin
J.J. Pickle Research Campus
Austin, TX 78712-4497

This document is available online via the World Wide Web at
http://www.crwr.utexas.edu/online.shtml

Acknowledgements

This research was funded by the Texas Department of Transportation (TxDOT) under grant number 0-4611, "Non-Proprietary, Small Footprint Stormwater Quality Structures for Use in Urban Areas". The TxDOT Program Coordinator was David Stolpa and TxDOT Project Director was David Zwernemann. The research project, led by Dr. Harlow Landphair, was a joint project with Texas A&M University (TAMU). Full scale experiments were conducted by the research team from TAMU. We appreciate the research funding from TxDOT and the support from the TAMU research team.

TABLE OF CONTENTS

List of Tables

List of Figures

Chapter 1 Introduction

1.1 BACKGROUND

The importance of stormwater management has increased from controlling floods in urban areas to include preventing the spread of polluted stormwater runoff to the environment. According to Walesh (1987), "stormwater management is primarily concerned with limiting future flood damages and environmental impacts due to development, whereas flood control aims at reducing the extent of flooding that occurs under current conditions."

Polluted runoff from highways may cause serious water quality problems such as excess loadings of nutrient and metals to rivers and lakes. Many of the pollutants that are emitted by heavy traffic are accumulated on the roadway surface, where they attach to soil particles, and are carried by storm water runoff into receiving water bodies. Thus, there is a need for appropriate treatment of stormwater runoff. Many factors should be considered in the treatment design process, such as the type, cost, size and detention time of the treatment device, as well as the physical and chemical properties of stormwater runoff.

Many treatment structures have been developed to improve the quality of stormwater runoff. The most common treatment structures are passive processes that rely on gravity and naturally occurring biological processes. Pollutant removal efficiencies are different for each constituent depending on the specific technology used (TTI Research Report 2000). It has been found that some types of pollutants (*e.g.*, lead, zinc, oil and grease) are well attached to particles and can be effectively removed by removing the suspended solids in storm water runoff (Urbonas and Stahre 1993).

Stormwater has been cited in regulations as one of the major contributors of non-point source pollution. In response to the 1987 Amendments to the Clean Water Act (CWA), the U.S. Environmental Protection Agency (EPA) developed the National Pollutant Discharge Elimination System (NPDES) Stormwater Program in 1990 (US EPA NPDES Website). The NPDES program regulates stormwater discharge from industrial facilities, construction activities, and municipal separate storm sewer systems (MS4s) to receiving water bodies. Many local governments intending to improve the quality of their runoff-impacted streams are incorporating best management practices (BMPs) into their stormwater management plans. EPA defines stormwater BMPs as "methods that have been determined to be the most effective, practical means of preventing or reducing pollution from non-point sources" (Bartosh 2004).

To utilize stormwater BMPs in a limited space, it is necessary that they be installed underground. Several different proprietary stormwater BMPs are already being marketed for use underground. While they are effective, these marketed BMPS are more expensive than simple precast units such as pipe and box culverts. Texas Department of Transportation (TxDOT) funded a research project that was launched in September 2003. The primary objective of the project is

> To develop simple effective stormwater quality treatment structures that are composed of off the shelf materials including pipe and box culvert sections with specialized inlet and outlet controls. These structures will be designed for low head loss and will affect efficient, low maintenance and cost effective stormwater quality treatment in limited right-of-way conditions.

1.2 MOTIVATION

Several areas of research are needed to fully accomplish the project objective, as shown in Figure 1.1, a project overview diagram. These various research needs and the related approaches are discussed below.

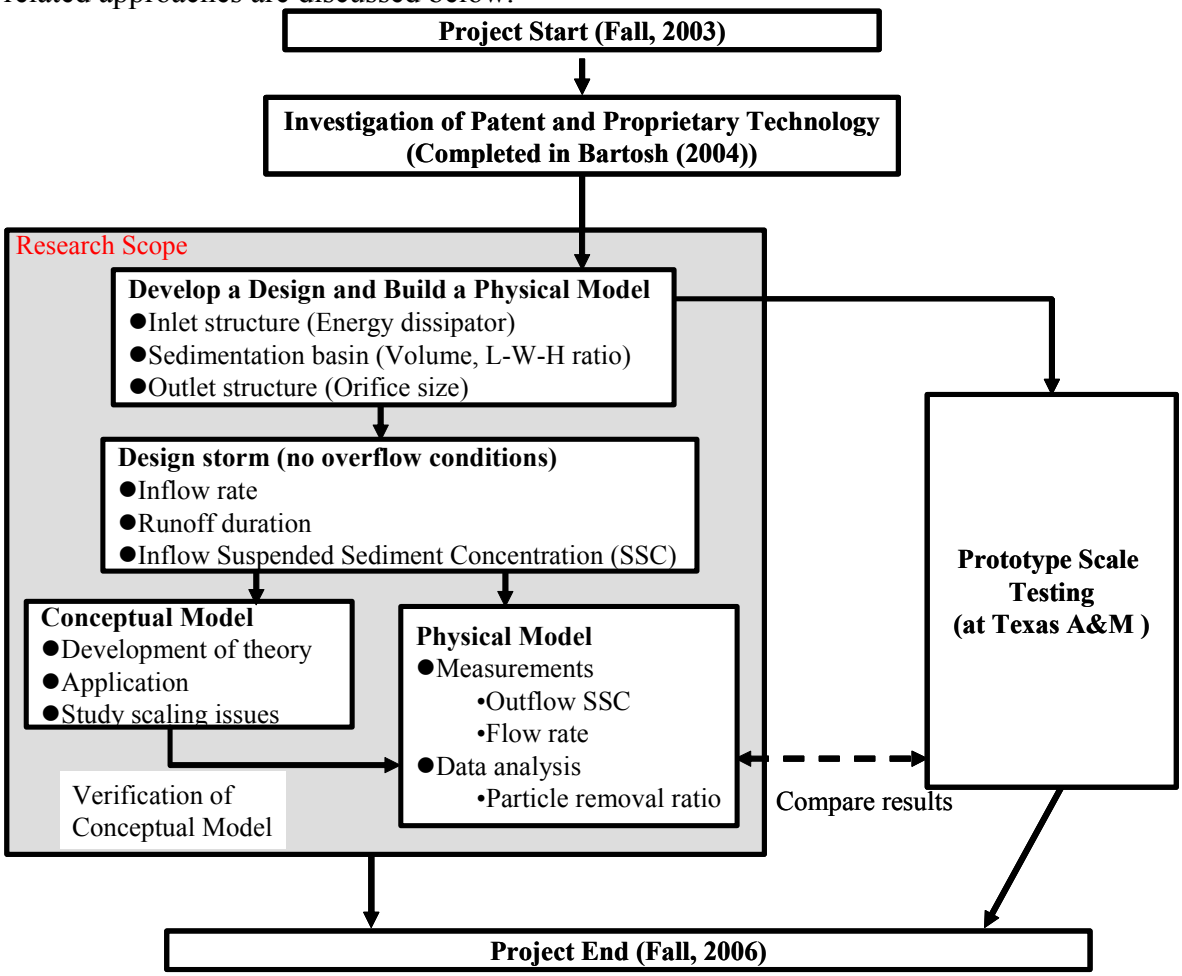

Figure 1.1. Research project overview diagram

1.2.1 Need for Investigation of Patent and Proprietary Technology

A survey of manufactured stormwater BMPs currently on the market was necessary to determine how each BMP works and to avoid violating any patents that may exist. For this purpose, Bartosh (2004) did an extensive survey on marketed small-

footprint stormwater BMPs and established which parts of each product, if any, are proprietary. Because of this research, the design process for new small-footprint stormwater BMPs, including inlet and outlet structures, became much easier. Also according to the research, box type culverts and baffles are not allowed to be patented because they are fundamental hydraulic structures (Bartosh, 2004). This fact is important to consider within the context of the design process.

1.2.2 Need for Design Development

After the review of proprietary BMPs was completed, a design process for a nonproprietary BMP was begun. There were three major components to be designed.

- Inlet structure
- Sedimentation basin
- Outlet structure

Figure 1.2 shows a schematic figure of box culvert type stormwater sedimentation basin.

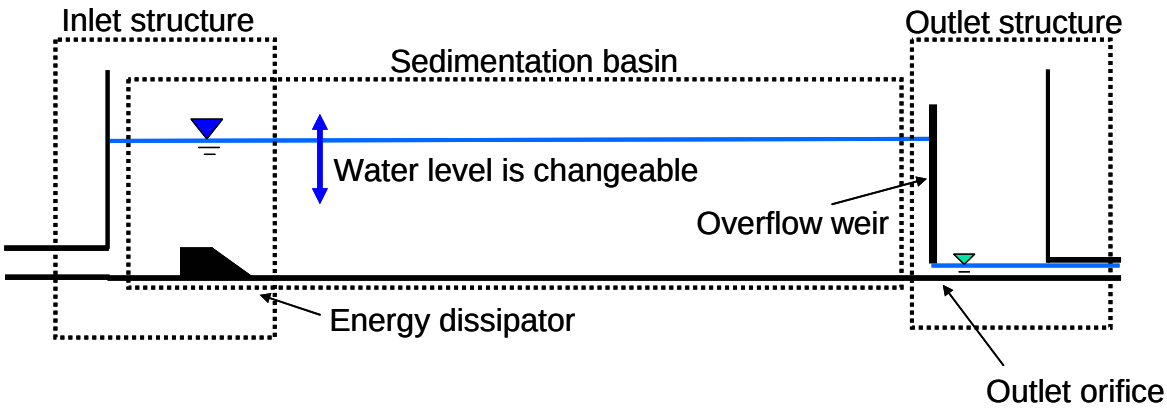

Figure 1.2. Design schematic for box culvert type stormwater sedimentation basin

"Inlet structure" refers to the inlet pipe system and the energy dissipation system. In a water treatment device, the inlet structure is important because a strong jet from the inlet pipe can cause resuspension of previously deposited sediment near the inlet. Thus the inclusion of an energy dissipator or a diffuser is an important design component so that effective sedimentation is not adversely affected by a strong inflow jet. Also, the inlet pipe system should be carefully designed such that the inlet pipe is large enough to convey roadway runoff caused by design storm (*e.g.*, 15 minute duration and 25 year storm). Sometimes, excessive runoff is bypassed to the outlet in order to avoid flooding so that the inlet pipe doesn't need to account for all the runoff in case of large storms. The design of the inlet structure must account for both water quality and hydraulic considerations.

"Sedimentation basin" refers to a box type culvert section that is used for settling and retaining sediments. Use of highway right-of-way for subsurface placement of box-culvert type structures may be the most cost effective stormwater management strategy. Some manufactured BMPs utilize centrifugal force to promote sedimentation. These products are effective when there is limited space, but the development of such a system takes more time and is more expensive than that of simple box culvert type.

Although very few municipalities have set requirements for the removal of total suspended solids (TSS) from storm water, those that have requirements commonly call for 80% removal of TSS in influent storm water. The Edwards Aquifer Recharge Zone in Austin, Texas, for example, is a sensitive drainage area and state regulations call for the removal of 80% TSS in influent storm water. Practically all storm water BMP manufacturers claim their products provide 80% removal of TSS in storm water but do not have proper documentation (lab and field studies) to back up these claims (Bartosh

2004). A box type culvert structure might be more cost effective than a centrifugal storm water treatment system to achieve the required 80% removal.

While TSS (total suspended solids) is commonly used as the measure of suspended sediment concentration, some authors claim that SSC (suspended sediment concentration) should be used. The difference between TSS and SSC is in the measurement methods. For TSS, a sub-sample is taken from the suspension with a pipette and then is dispensed onto filter paper to gather the sediment. For SSC, the whole sample is poured onto the filter paper to catch the sediment (Minton, 2002). The reason that the SSC technique is considered by many to be the preferred method for runoff samples is that it is difficult to get a representative sample into a pipette. The stormwater runoff samples have particles with high settling velocities. These particles settle rapidly to the bottom of the container, so it is difficult for them to be pulled up by the pipette (Karamalegos, 2006). Therefore, SSC was used instead of TSS in this research.

The design shape of the sedimentation basin in this research is a rectangular box culvert. Parameters for sedimentation basin design are volume and the ratios between width, length, and height. The physical model for the sedimentation basin was designed as an open-topped tank. Tank performance can be measured by physical experiments; however, it is difficult to test different size and length ratios because a new tank is required for each scenario. A mathematical model was used to help evaluate different sizing scenarios as part of the design process.

"Outlet structure" refers to a simple overflow weir with an orifice placed at the bottom and the outlet pipe system. Storm runoff, once stored in the tank, slowly exits the system through the orifice; in situations when the volume of runoff exceeds the holding capacity of the tank, water flows over the weir to the outlet pipe system to prevent

surcharge of the system and roadway flooding. Drainage time of stored stormwater through the orifice depends on the initial depth of the water and the size of the orifice.

1.2.3 Need for Physical Models

Physical models are indispensable in testing pollutant removal ratio for a given stormwater detention basin and allow for the variation of input variables such as flow rate and initial SSCs of stormwater runoff. Also, performance results for each physical model should be used to check if the model design meets required criteria such as the particle removal ratio.

In the physical model testing, two conditions can be considered; no overflow conditions and over flow conditions. “No overflow” describes the condition that runoff volume is within the capacity of sedimentation basin and all runoff water is drained by the outlet orifice. Outlet SSCs are measured with time, and then event mean concentration (EMC) and particle removal ratio are estimated for each runoff event. “Overflow” describes the condition in which runoff volume exceeds the capacity of the sedimentation basin and excess water overflows to the other side of the overflow weir. Once overflow starts, flow in the tank becomes more dynamic because outflow rate is dramatically increased. In such dynamic flow conditions, flow and the sedimentation pattern in the sedimentation basin are expected to be very different from the condition of no overflow. However, the overflow case was not studied in this research.

According to a simple methodology for estimating solids removal fraction in detention ponds (Urbonas and Stahre 1993), volume, residence time, and average depth of a detention pond are used as the major parameters when flow conditions are ideal. In a simple box type culvert sedimentation basin, these three parameters can be translated into detention time, depth, and the area of detention basin. Detention time, determined by

outlet orifice size and water depth, can be controlled by using different orifice sizes. The relationship between detention time and particle removal ratio was studied in evaluation of the no overflow condition.

1.2.4 Need for a Conceptual Model

Small-scale modifications of the physical model, such as different orifice sizes or different energy dissipaters, can be easily done. However, large-scale modifications to the physical model design are more difficult; testing alternate tank sizes may require a new tank for each scenario. A mathematical model can be a useful tool in estimating tank performance and can help evaluate different sizing scenarios in the designing process.

According to Ford and Hamilton (1996), a mathematical model can be categorized either as empirical or conceptual. According to the definition, an empirical model is formulated from observation of input and output without seeking to represent explicitly the process of conversion. A conceptual model, by definition, is formulated from consideration of physical, chemical, and biological processes acting on the system.

The modeling for stormwater treatment performance requires a large number of variables such as inflow rate, runoff duration, inflow SSC, particle sizes, etc. Taking this into account, formulation of a conceptual model is more feasible than an empirical model since there are too many variables associated with empirical modeling. Therefore, the strategy for this research includes creating a conceptual model and verifying it through use of physical model results.

Numerical modeling using computational fluid dynamics (CFD) has been popular in the stormwater area. However, such a numerical model was not developed for the same reason that the empirical model was not pursued. The system cannot be at steady state due to the natural variation of inflow rate and the variation of outflow rate governed by

orifice size and water level. Parameters such as fluid velocity are a function of time and space, which requires enormous amount of data collection to calibrate velocity profile over time and space.

The conceptual model for this research was not designed to include the overflow conditions since an overflow event should be less frequent than no overflow conditions in real sites. Also it was considered that flow during overflow is more dynamic and makes the sedimentation phenomena more complicated. Thus the conceptual model is designed only for no overflow conditions in this research.

1.2.5 Need for Prototype Scale Testing

An operational design prototype, which can be tested with actual storm runoff, is the final component of this project. A prototype scale stormwater sedimentation basin was installed at College Station, Texas and has been tested by Texas A&M University project team members. Data have been collected from synthetic storms. Their measurement results can be compared with the physical and conceptual modeling results of this research using scaling techniques.

1.3 RESEARCH OBJECTIVES

The main scope of this research is physical and conceptual modeling of a rectangular stormwater sedimentation basin and evaluation of performance tests of candidate designs. Specific objectives to achieve this overall research objective are listed below.

1. Build a rectangular sedimentation basin as a physical model, which can reproduce and vary input conditions such as inflow rate and suspended

sediment concentration (SSC), and can be used to take samples at any time from inlet and outlet to measure SSC.

2. Build a conceptual model, which can estimate time series outflow SSC, event mean concentration (EMC), and particle removal ratio, and verify the conceptual model using physical model results.
3. Test different lengths of the basin and outlet orifice sizes in the physical model to evaluate how overflow rate and detention time affect the particle removal ratio.
4. Study how geometric and hydraulic parameters should be scaled to have identical particle removal efficiency in the physical model and prototype using conceptual and physical model results.

1.4 DISSERTATION ORGANIZATION

This dissertation consists of six chapters. A literature review is presented in Chapter 2. Chapter 3 describes the details of the conceptual model and the methodology of the model application. Chapter 4 describes the physical model including how it was designed and built and how measurements were made. Chapter 5 includes results and analysis of both the conceptual and the physical model. A CSTR (Continuous Stirring Tank Reactor) model to estimate time series outflow SSC and particle removal ratio using empirically determined parameter is also shown in this chapter. In Chapter 6, conclusions and future work are discussed.

Chapter 2 Literature Review

A literature review is presented to provide a background relating to the issues of stormwater and its treatment by gravitational separation. This chapter includes 1) characteristics of stormwater, 2) modeling of treatment systems, and 3) physical model scaling.

2.1 CHARACTERISTICS OF STORMWATER

Pollutants in stormwater

Many different constituents are found in stormwater runoff. The EPA (Environmental Protection Agency) adopted for their Nationwide Urban Runoff Program (NURP) several constituents as standard pollutants characterizing urban runoff shown. For these constituents, the NURP evaluated data collected between 1978 and 1983 from 81 sites in 22 cities and presented the recommendations for concentration estimates. Table 2.1 shows these major constituents in urban runoff and the NURP recommendations for load estimates (ASCE, 1992).

Table 2.1. Major constituents in urban runoff and NURP recommendations for load estimates (EPA 1983)

Constituent	Concentration estimates
TSS	180-548 mg/L
BOD	12-19 mg/L
COD	82-178 mg/L
Total P	0.42-0.88 mg/L
Dissolved P	0.15-0.28 mg/L
TKN (Total Kjeldahl Nitrogen)	1.90-4.18 mg/L
Nitrite (NO_2^-) and Nitrate (NO_3^-)	0.86-2.2 mg/L
Total Cu	43-118 µg/L
Total Pb	182-443 µg/L
Total Zn	202-633 µg/L

In Texas, the Lower Colorado River Authority (LCRA) and the Texas Commission on Environmental Quality (TCEQ) added oil and grease as important stormwater runoff constituents (TTI Research Report, 2000). These organics usually contain polyaromatic hydrocarbons (PAHs) such as pyrene, phyenanthrene, and chrysene.

Some pollutants are attached to particles rather than being dissolved in the runoff. For example, phosphorus is primarily sorbed on the soil surface or precipitated through chemical reaction, forming calcium phosphate, aluminum oxide-phosphate, iron oxide-phosphate, and ferric phosphate (Minton, 2002). Metals are also sorbed on the soil surface, and the degree of sorption depends on metal species, ionic strength, pH, redox potential of the soil, and so on. Most organics such as PAHs and petroleum hydrocarbons are hydrophobic and sorbed to the soil. The sorption correlates strongly with the organic content of the soil, f_{oc}, and organic-carbon partition coefficient, K_{oc}. The significance of sorption processes implies that particle removal from stormwater could realize the removal of other pollutants from stormwater runoff to some extent.

Particle size distribution

Particle size distribution (PSD) is also one of the most important characteristics of stormwater runoff since the diameter and density of a particle determines particle settling velocity, and surface area of a particle affects the capacity of sorption in soil in addition to surface charge, and organic contents of a particle.

There are several methodologies to measure particle size distribution, which are dry/wet sieving, electrical sensing zone (ESZ) instrument, and a laser diffraction particle size analyzer. Dry/wet sieving method can measure the mass distribution directly, but it is only useful for larger particles since fine sieves are easily clogged with fine particles. The ESZ instrument determines the number distribution of particles by measuring the voltage flux between two electrodes caused by the particles. The laser diffraction particle analyzer determines relative volume distribution by measuring diffraction pattern and intensity (Shimazu 2006). Each of these methodologies determines the size distribution by measuring either number, mass, or volume. However, there is no clear protocol for accurately determining particle size distribution (Karamalegos, 2006).

Also, particle size distribution of stormwater runoff is very different from place to place or time to time even in a single storm event. Minton (2002) pointed out several possible reasons for the particle size difference.

- Particle mass distribution may be affected by the runoff rate. In general, larger material is resuspended with increasing flow rate.
- Sampling location affects results. Samples taken immediately at the edge of pavement may find a greater fraction of large particles than those taken within a drainage system where the large particles may have already settled. Furthermore, very small particles aggregate while traveling through drainage

pipes (1-5 microns to 30-40 microns) by precipitation with silica leachate from concrete.

- Site conditions: In temperate climates with winter snow and ice, the application of sand affects the particle size. Snow causes small particles to aggregate.

In general, street sediment is larger than stormwater sediment and its particle size ranges from 10 μm to 10 mm, while the particle size of stormwater sediment ranges from 1 μm to 1 mm. Many studies have found that the majority of particles are less than 50 to 75 μm (Minton, 2002).

Density of particles

Particle density affects particle settling velocity. Frequently, 2.65 g/cm^3, which is equivalent to the density of quartz and sand, is used to estimate particle settling velocity. However, the density of smaller particles is sometimes much less than the density of sand. This is because of organic matter, which is lighter than sand, tends to be absorbed onto the smaller particles which have larger specific surface area per mass than to the larger particles, and a small particle is sometimes wholly or intrinsically organic as condensed organic material or fragmentary plant material (Lee, *et al*. 2005). Karamalegos (2006) summarized previous measurements of density of suspended solid particles and performed additional measurements of stormwater runoff from highway in Austin, TX using an ESZ instrument. Karamalegos reported that the density, from thirteen papers and reports, ranges from 1.1 to 2.86 g/cm^3, snowmelt density was slightly higher than the density of road sediment, and smaller particles had a lower density compared to bulk samples. The measurements by Karamalegos shows that the density of particles smaller than 75 μm ranged from 1.4 to 2.4 g/cm^3 with the mean of 1.8 g/cm^3 for four different

storm samples from a highway, and 1.4 to 2.8 g/cm^3 with the mean of 1.8 g/cm^3 for three different storm samples from the inlet of an extended detention basin. These measurement data show that density of suspended solid particles from stormwater runoff are much lighter than the density of sand. Therefore, this should be taken into account when removal efficiency of any detention basin is designed.

2.2 MATHEMATICAL MODELING OF TREATMENT SYSTEMS

2.2.1 Modeling of particle settling velocity

Particle settling velocity has been measured, calculated, and discussed in the environmental engineering field for a long time as the settling velocity affects gravity separation systems. Stokes (1851) was the first to derive the terminal settling velocity of a spherical particle. Terminal settling velocity, v_s, occurs when gravitational force, F_g, minus buoyancy force, F_b, equals drag force, F_d. This relationship can be extended using the spherical assumptions:

$$\begin{aligned} & F_g - F_b = F_d \\ & \text{LHS} = F_{g-b} = \pi(\rho_p - \rho_f) g \frac{{d_p}^3}{6} \\ & \text{RHS} = F_d = \frac{1}{8} C_D \pi {d_p}^2 \rho_f {v_s}^2 \end{aligned} \tag{2.1}$$

Where d_p is the diameter of a particle, ρ_p and ρ_f are the density of a particle and a fluid, and C_D is the drag coefficient of a particle. By solving Equation (2.1), the drag coefficient C_D can be described as follows:

$$C_D = \frac{4}{3} \frac{\rho_p - \rho_f}{\rho_f} g \frac{d_p}{{v_s}^2} \tag{2.2}$$

For creeping flow conditions where inertial effects are negligible, Stokes derived the following equation for drag force:

$$F_d = 3\pi\mu d_p v_s \tag{2.3}$$

where μ is viscosity. C_D can be simplified by substituting Eq. (2.3) for Eq. (2.1):

$$C_D = \frac{24\mu}{\rho_f v_s d_p} = \frac{24}{Re} \tag{2.4}$$

where the Reynolds Number, Re, is defined as

$$Re = \frac{\rho_f v_s d_p}{\mu} \tag{2.5}$$

The terminal settling velocity of a sphere particle for the creeping flow conditions can be finally obtained by substituting drag coefficient equation, (2.4), for the force balance equation (2.1) as follows:

$$v_s = \frac{g}{18\mu}(\rho_p - \rho_f){d_p}^2 \tag{2.6}$$

When inertial effects cannot be neglected, the drag coefficient cannot be predicted theoretically. Experimental data have been correlated to estimate C_D and v_s to develop predictive tools. The drag coefficient has different values depending on whether the flow surrounding the particle is laminar or turbulent (*i.e.,* depending on the value of Re). For smooth, spherical particles with $Re < 10^4$, the drag coefficient can be approximated by (Fair and Geyer, 1954):

$$C_D = \frac{24}{Re} + \frac{3}{\sqrt{Re}} + 0.34 \tag{2.7}$$

This equation also includes Eq. (2.4) for Re<0.3. Recently, more empirical equations have been suggested to estimate the drag coefficient C_D more precisely (Clift et al 1978, Turton and Levenspiel 1986). For example, Khan and Richardson (1987) suggested

$$C_D = (2.25\,\mathrm{Re}^{-0.31} + 0.36\,\mathrm{Re}^{0.06})^{3.45} \tag{2.8}$$

Haider and Levenspiel (1989) proposed

$$C_D = \frac{24}{\mathrm{Re}}(1 + 0.1806\,\mathrm{Re}^{0.6459}) + \frac{0.4251}{1 + \frac{6880.95}{\mathrm{Re}}} \tag{2.9}$$

Brown and Lawler (2003) suggested revising Eq. (2.9) since this equation might include wall effect errors. They took the general form of (2.9) with parameters determined by a local minimization of the sum of squared errors, Q, defined in Eq. (2.10)

$$Q = \sum_{1}^{n} (\log C_{D,\mathrm{exp}} - \log C_{D,\mathrm{cal}})^2 \tag{2.10}$$

They found Eq. (2.11)

$$C_D = \frac{24}{\mathrm{Re}}(1 + 0.150\,\mathrm{Re}^{0.681}) + \frac{0.407}{1 + \frac{8710}{\mathrm{Re}}} \tag{2.11}$$

Figure 2.1 shows the good fit of experimental data and Eq. (2.11).

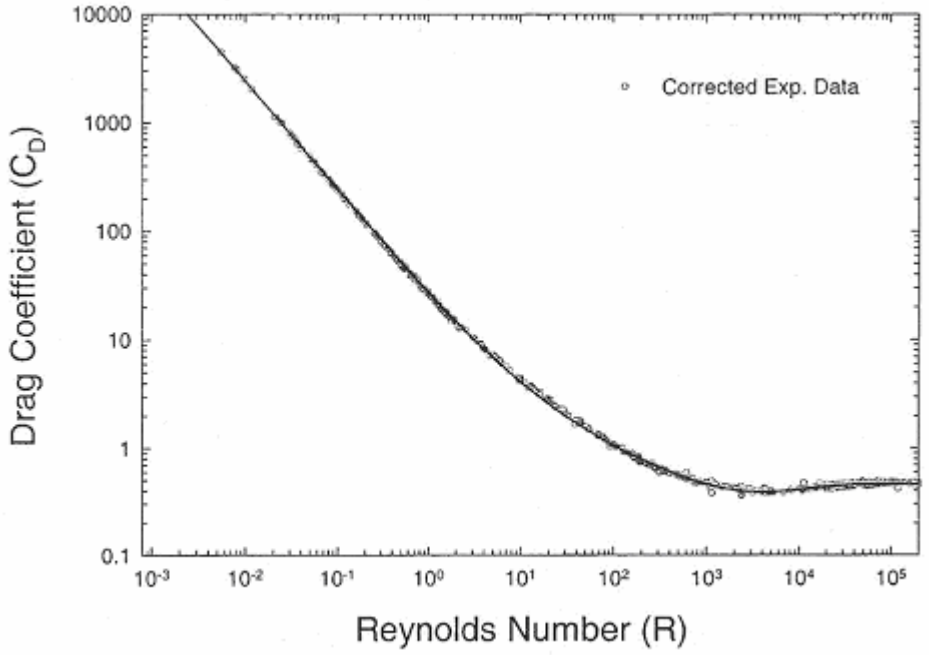

Figure 2.1. Competition of recommended drag correlation (Eq. 2.16) to experimental data (Brown and Lawler 2003)

These results show that the drag coefficient, $C_{D,}$ could be estimated satisfactorily and implies that terminal settling velocity also could be estimated by these revised empirical equations.

2.2.2 Modeling of primary settling tank

An ideal horizontal flow reactor, or a Class I settling tank, is one of the oldest and most fundamental conceptual models for modeling gravitational settling, developed by Camp (1946). The following figure is a schematic of a rectangular, continuous flow settling tank, with horizontal flow.

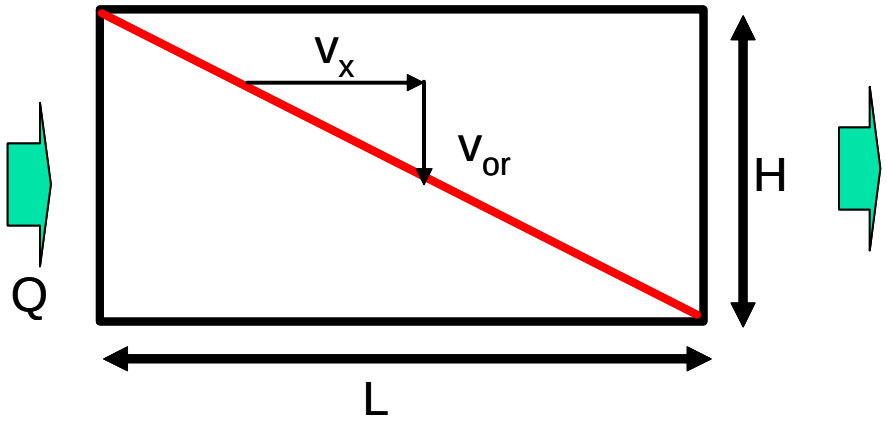

Figure 2.2. Schematic view of ideal horizontal flow reactor

Overflow rate, v_{or}, is defined by

$$v_{or} = \frac{\text{Flow rate}}{\text{Surface area}} = \frac{Q}{B \cdot L} \tag{2.12}$$

where B is the width and L is the length of the reactor.

Camp (1946) developed the following equation for removal efficiency, R, expressed as a function:

$$R = 1 - f_0 + \int_0^{f_0} \frac{v_s}{v_{or}} df \tag{2.13}$$

where v_s is Stokes settling velocity (2.6), f is the fraction of the particles with $v_s < v_{or}$, and f_0 is the fraction with $v_s = v_{or}$.

The ideal horizontal flow reactor model has been modified both conceptually and numerically. Swamee and Tyagi (1996) added a scour effect for the model and developed modified removal efficiency. The sedimentation performance was also calculated with advection and diffusion equation with settling velocity term. Takamatsu, *et al*. (1974) estimated the diffusion coefficient and scouring coefficient experimentally and analytically solved the system. Hydrodynamics of the sedimentation tank have been

analyzed numerically. Zhou and McCorquodale (1993) calculated the velocity field and suspended solid transport numerically to investigate the effects of density stratification on the hydrodynamics. Turbulence modeling, using k- ε model, has been applied by several researchers (Adams and Rodi, 1990; and Zhou, et al., 1994). Sediment concentration and bed depth in the sedimentation basin were modeled numerically by Jin and Guo (2000).

As shown above, research in the modeling of settling basins is extensive since such basins are common to drinking water and waste water treatment. However, these findings may not be directly applied to the modeling of stormwater sedimentation basin. This is because stormwater detention basins are not steady state systems; inflow rate from runoff always fluctuates and outflow rate is not always the same as inflow rate especially when outflow is controlled by an orifice and the shape of the detention basin, which, in most cases, is not simply rectangular. In the following section, how sedimentation has been modeled in the stormwater detention basins is described.

2.2.3 Modeling of gravitational treatment systems for stormwater runoff

Modeling of particle removal efficiency in gravitational treatment systems for stormwater runoff has been more empirical and statistical rather than conceptual or numerical because the system is far from steady state during a storm and the runoff characteristics (*e.g.*, inflow rate, volume, and sediment concentration) are different from storm to storm. To deal with these non-ideal problems and their effects on long term performance, a methodology was suggested by EPA in 1986 for the analysis of detention basins for the control of urban runoff pollution (Urbonas and Stahre, 1993). The methodology combines probability concept with theoretical removal efficiency modeling concepts. The calculation method is different for dynamic conditions and quiescent conditions and the calculation should be done for different particle size fractions. The

bases of the probability concept using the methodology was developed by Di Toro and Small (1979). This methodology can be applied when there are non ideal situations such as turbulent condition or flow short circuiting in the basin by applying non-ideality parameter. However water level change is not considered in this model.

For wetland, Su and Mitchell (2006) presented a removal efficiency model using plug flow reactor (PFR) and CSTR (continuous stirred tank reactor) model to estimate the characteristics of first flush effect reduction. In a single storm event, initial concentrations of most pollutants including sediment are generally much higher than the concentration during the latter part of the storm because the initial flush of water washes off the accumulated contaminants in air and ground. This is called first flush phenomena. The flush effect was modeled by the first order concentration reduction using the measured inflow concentration decline. Their model results show that PFR has more significant effects on first flush reduction than CSTR. However, the simulation results of constituent concentrations were not validated with measured data in Su and Mitchell's research. For combined sewer overflow (CSO), removal of sewer solids by treatment facilities such as storage sedimentation tank, high side weir overflow, and vortex overflow is modeled with Hazen number, which is the ratio of particle settling velocity to the overflow rate. Luyckx, et al. (2005) proposed a normalized particle efficiency and showed its strong relationship with the Hazen number for several CSO treatment facilities. This research provides insight in terms of how the Hazen number is effective on the removal efficiency of stormwater treatment systems. Jensen (2005) modeled the CSO system using a 1-D advection-diffusion equation and estimated the dispersion coefficient and depositional velocity by comparison with laboratory data. However Jensen's model deals with only steady state conditions.

For the purpose at the present work, no existing model was found which could be applied to this research. This is mainly because existing models do not incorporate water level change, which affects the unsteady outflow rate and therefore the particle settling too in the proposed stormwater BMP design.

2.3 PHYSICAL MODEL SCALING

Physical models are often employed in hydraulic studies. The full-scale object of interest is called the "prototype" while the scaled down experimental object is called the "model". The length ratio of the prototype to the model is called the geometric length ratio (L_R). This length ratio should be kept constant throughout the model except for distorted models that use a different length ratio in the vertical compared with horizontal. This consistency is called geometric similarity. In the same manner, to make two flow patterns similar, velocity ratio (v_r) and force ratio (FC_r) must be kept the same throughout the model. These consistencies are called kinematic similarity and dynamic similarity, respectively. To maintain the dynamic similarity, an appropriate dimensionless number must be given the same value in the model as in the prototype.

In hydraulic models, the Froude number is used to maintain dynamic similarity if inertial force and gravity force are significant, such as in open channel flow. The Froude number is specified as follows:

$$Fr = \sqrt{\frac{v^2}{gL}} \tag{2.14}$$

Where v is flow velocity, g is gravitational acceleration, and L is characteristic length.

On the other hand, if inertial force and viscous forces are significant, such as in pipe flow the Reynolds Number (Re) may be important (Henderson, 1966):

$$Re = \frac{vL\rho}{\mu} \tag{2.15}$$

However, a different scaling methodology is proposed for the particle settling system. This scaling method is called Hazen number scaling. Hazen number is the ratio of particle settling velocity, v_s, to overflow velocity, v_{or}.

$$H_a = \frac{v_S}{v_{or}} \tag{2.16}$$

Some researchers show the validity of Hazen number scaling. For primary settling basin, Thompson (1969) proved by using two geometrically similar models that the same removal efficiency of a rectangular sedimentation tank can be reproduced using the same powder if the overflow rates are the equal in model and prototype even though the removal efficiencies in the model and prototype were around 10% worse than theoretical estimation using ideal horizontal flow reactor theory.

For CSO structures, physical scaling problems have been much discussed (Luyckx, et al., 1998, 2002, Fenner and Tyack, 1998). Luyckx, et al. (2002) did a comprehensive research in removal efficiency of CSOs, including high side weir overflows, hydrodynamic separator, and vortex separator, with many physical model results. The research indicated that the same removal ratio could be achieved with identical Hazen number and geometrically scaled model if Reynolds number is less than 200,000.

However, not much research has been done to deal with the scaling problem in the area of stormwater detention basin. One of the reasons is that wet basin is usually not

only for sediment treatment but also for other pollutants removal by biological activity (Urbonas and Stahre, 1993), which is no longer just a physical process. In this research, the only target pollutant was particles, and the treatment method was purely gravitational separation. Also, the rectangular detention basin had a simple shape, which was easy to be scaled down geometrically and reproducible in a laboratory.

Chapter 3 Conceptual Model and Application

The removal efficiency of particles with a known settling velocity in a primary settling basin can be simply calculated by ideal horizontal flow reactor theory. A conceptual model to calculate particle removal efficiency was developed in the same manner of the ideal horizontal flow reactor theory by employing similar assumptions used in the theory. This chapter covers 1) how the conceptual model was developed to calculate removal efficiency of particles and 2) how the model can be applied in example problems such as constant inflow runoff rate and a triangular hydrograph inflow.

3.1 CONCEPTUAL MODEL

3.1.1 Model description

This section describes how a rectangular detention basin was modeled and how the modeling process was similar and/or different from the ideal horizontal flow reactor theory. Figure 3.1 shows the schematic of the detention basin. Stormwater runoff from a roadway surface flows into the basin through inlet pipes and drains out of the basin through the outlet orifice. Water level increases when the inflow rate is larger than the outflow rate and decreases when the opposite occurs. This flow process is different from a primary settling tank because inflow and outflow rates are not always constant and they are not equal and therefore water level varies depending on the inflow rate and the volume of water in the basin.

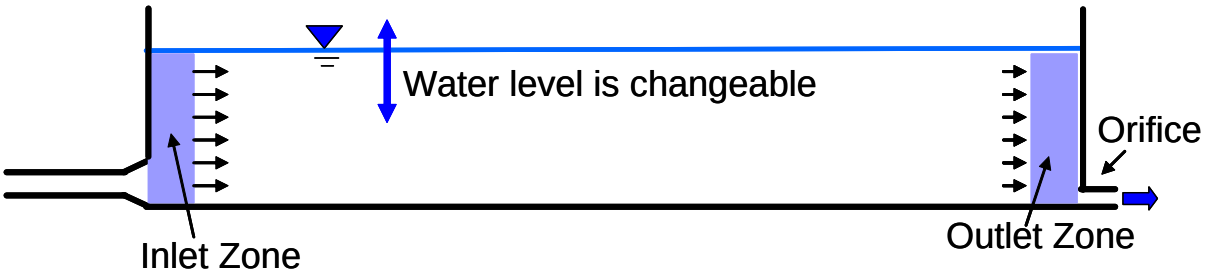

Figure 3.1. Schematic of rectangular stormwater detention basin

Next, assumptions used for modeling are explained here. The water level was assumed to be zero when a runoff starts. Inflow was assumed to be well distributed over the submerged depth of the basin. Also, flow in the basin was assumed to be plug flow and resuspension effects were assumed to be negligible as in the ideal horizontal flow reactor theory. Outflow rate was controlled by an orifice set at the bottom of the end wall. Particles that did not reach the outlet zone would be removed. Water was overflowed in the case that runoff volume was larger than the basin capacity. However, the overflow condition was not studied in this research.

The critical settling velocity is the velocity where all the particles with higher settling velocities will settle out in a reactor. In the ideal horizontal flow reactor, critical settling velocity is simply the overflow velocity, which is a constant flow rate divided by the surface area. However, in this rectangular detention basin, calculating critical settling velocity was not as simple because of unsteady inflow and outflow rates and variable water level. Figure 3.2 shows the schematic of trajectories of water molecules and a particle which has a critical settling velocity in an ideal horizontal flow reactor and the rectangular detention basin. Trajectories of a water molecule and a particle are curved while the trajectory of a particle in an ideal horizontal flow reactor is straight. Here,

methodologies to calculate the curved particle trajectory and critical settling velocity for a rectangular detention basin are developed within the stated model assumptions.

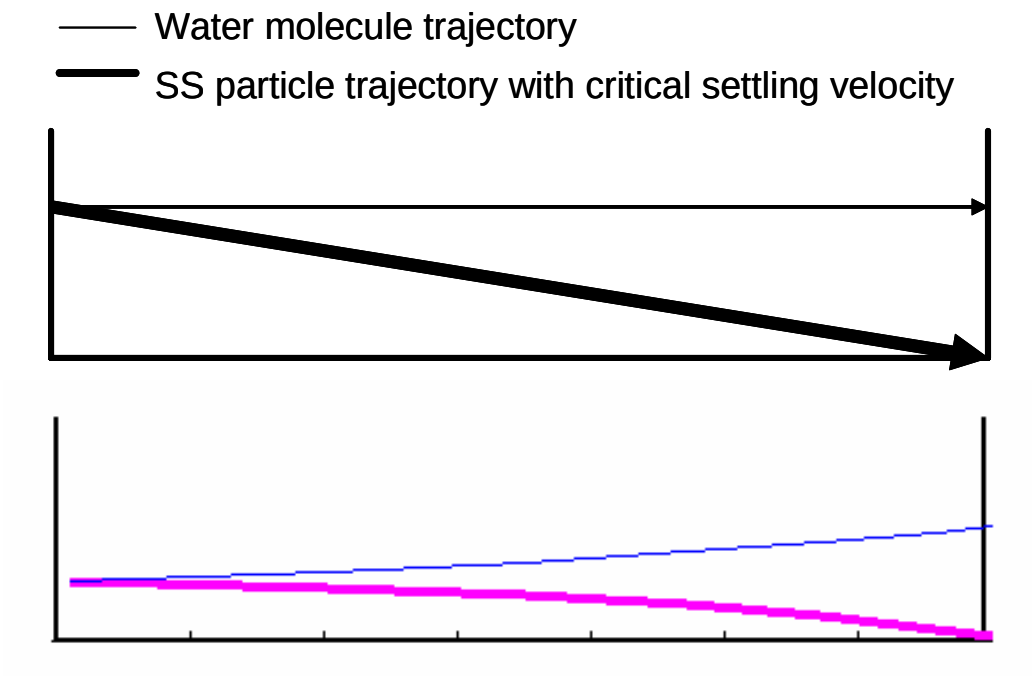

Figure 3.2. Trajectory of water molecules and a particle with critical settling velocity in an ideal horizontal flow reactor (above) and rectangular stormwater detention basin (below) during filling period

3.1.2 Hydraulics of the basin

Water level keeps changing from the start of runoff to the end of drainage which makes the system unsteady. Water level change can be determined as follows from mass balance if both the inflow rate, $Q_{in}(t)$, and outflow rate, $Q_{out}(t)$, are known. h(t) is the water level as a function of time, B is width, L is the length of the basin, and t represents time.

$$\frac{dh(t)}{dt} = \frac{1}{B \cdot L}\left(Q_{in}(t) - Q_{out}(t)\right) \tag{3.1}$$

It was assumed that there is no horizontal or vertical mixing in the sedimentation basin. Numerical simulation would be required if mixing is significant. This assumption implies that longitudinal velocity is uniform over the vertical cross section and vertical velocity is uniform over the horizontal cross section.

Mass balance was considered in a control volume at the right hand side of the detention basin including the outlet orifice as shown in Figure 3.3. The local flow rate at x and t, Q(x,t), is equal to the sum of the outflow rate, $Q_{out}(t)$, and upflow rate (or downflow rate when the tank is emptying) within the control volume as shown in Equation 3.2.

$$Q(x,t) = (L - x) \cdot B \cdot \frac{dh(t)}{dt} + Q_{out}(t) \tag{3.2}$$

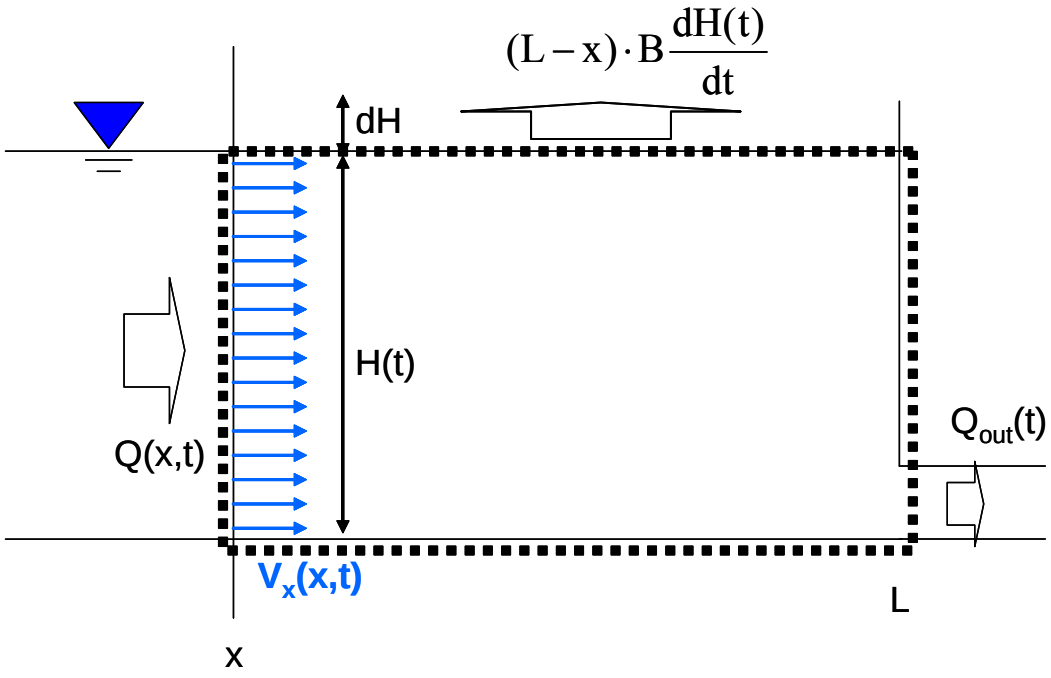

Figure 3.3. Local convectional velocity at storm runoff period

The corresponding local horizontal flow velocity at x and t, u(x,t), is Q(x,t) divided by the submerged cross sectional area at t as shown in Equation (3.3).

$$u(x,t) = \frac{Q(x,t)}{B \cdot h(t)} \tag{3.3}$$

Vertical flow velocity at the water surface is the velocity of water level change, $\frac{dh(t)}{dt}$, and 0 at bottom. Vertical velocity in between, v(z,t), is linearly distributed over depth;

$$v(z,t) = \frac{dz}{dt} = \frac{dh(t)}{dt} \cdot \frac{z}{h(t)} \tag{3.4}$$

3.1.3 Critical Settling Velocity

As mentioned in the model description section, the particle path is not straight as seen in the ideal horizontal flow reactor, but is curved. Therefore, trajectories of particles should be calculated first in order to calculate critical settling velocity. Trajectories, or pathlines, of particles were calculated from the velocity field. A pathline is a line which is traced out in time by a given fluid particle as it flows, while a streamline is an instantaneous line whose tangents are everywhere parallel to the velocity vector (Currie, 1974). A pathline is calculated using the following equation.

$$\begin{aligned} \frac{dx}{dt} &= u(x,t) \\ \frac{dz}{dt} &= v(z,t) \end{aligned} \tag{3.5}$$

The benefit of using the pathline concept in this study is the position of a particle can be traced with time. In this section, both water molecules and particle pathlines are described. Pathlines for a water molecule can be derived in (3.6) from local flow rate (3.2), local flow velocity (3.3) and pathline equation (3.5) as follows;

$$\frac{dx_w}{dt} = \frac{(L - x_w)}{h(t)} \cdot \frac{dh}{dt} + \frac{Q_{out}(t)}{B \cdot h(t)} \tag{3.6}$$

where x_w means the position of the traced water molecules. Equation (3.6) was analytically solved with the initial condition that the longitudinal position of a water molecule at time t_{in}, $x_w(t_{in}; t_{in})$, is 0. $x_w(t; t_{in})$ means the longitudinal position at time t of a traced water molecule that flowed into the tank at time t_{in}. Equation (3.7) is the solution of (3.6).

$$x_w(t;t_{in}) = \frac{1}{B \cdot h(t)} \int_{t_{in}}^{t} Q_{in}(t)dt \tag{3.7}$$

Vertical position of water molecules can be determined by the integration of Equation (3.4) from t_{in} to t and $h(t_{in})$ to h(t) as follows depending on initial height, $z(t_{in}; t_{in})$;

$$z_w(t;t_{in}) = \frac{h(t)}{H(t_{in})} z_w(t_{in};t_{in}) \tag{3.8}$$

The combination of (3.7) and (3.8) shows the position of water molecules.

Next, the pathline of a particle is derived. The velocity vector of a particle can be determined as follows using the velocity vector of water and settling velocity of the particle, v_s. Settling velocity was assumed to be independent of the ambient flow field.

$$\begin{aligned} u_p(t;t_{in}) &= u(t;t_{in}) \\ v_p(t;t_{in}) &= v(t;t_{in}) - v_s \end{aligned} \tag{3.9}$$

where $u_p(t;t_{in})$ is the x component of particle velocity and $v_p(t;t_{in})$ is the z component of particle velocity. Longitudinal position of a suspended solid particle at t with given t_{in}, $x_p(t;t_{in})$, is the same as the position of water particle, $x_w(t;t_{in})$ since longitudinal velocity of water molecules and particles are assumed to be the same;

$$x_p(t;t_{in}) = \frac{1}{B \cdot h(t)} \int_{t_{in}}^{t} Q_{in}(t)dt \tag{3.10}$$

Substitution of the vertical flow velocity equation (3.4) and (3.9) for the pathline equation (3.5) yields vertical velocity vector equation of a particle;

$$\frac{dz_p(t;t_{in})}{dt} = \frac{z_p(t;t_{in})}{H(t)} \cdot \frac{dh(t)}{dt} - v_s \tag{3.11}$$

Equation (3.11) was analytically solved with the initial position of the particle at $t=t_{in}$., which is $z_p(t;t_{in})=z_p(t_{in};t_{in})$.

$$z_p(t;t_{in}) = H(t)\left\{ - v_s \int_{t_{in}}^{t} \frac{1}{h(t)} dt + \frac{z_p(t_{in};t_{in})}{h(t_{in})} \right\} \tag{3.12}$$

Finally, detention time of the particle is calculated here. Since the position of the suspended solid particle, $(x_p(t;t_{in}), z_p(t;t_{in}))$, is known, time to reach the end of the tank, t_{out}, for the particle can be calculated by substituting $x_p(t;t_{in})=L$ in (3.10) and solving for t. Detention time of a particle can be simply calculated from t_{out}- t_{in}. As shown in Figure 3.2, a particle with critical settling velocity, which enters the basin at the very top of the water column, will settle to the bottom on the right hand side when reaching the outlet. Therefore, the focus was on a particle released from the water surface at the inlet. Initial vertical position of such a particle is the same as the water level at t_{in}, or simply $h(t_{in})$. Therefore, vertical position of the particle is shown in equation (3.13) by substituting $z_p(t_{in};t_{in})=h(t_{in})$ in (3.12), the pathline equation of a particle.

$$z_{p,top}(t;t_{in}) = h(t)\left\{ - v_s \cdot \int_{t_{in}}^{t} \frac{1}{h(t)} dt + 1 \right\} \tag{3.13}$$

Then, the minimum particle which meets $z_{p,top}(t_{out};t_{in}) > 0$ establishes the critical settling velocity, $v_{s,c}(t_{in})$ as shown in equation (3.14).

$$v_{s,c}(t_{in}) = \frac{1}{\int_{t}^{t_{out}} \frac{1}{h(t)} dt} \tag{3.14}$$

3.1.4 Overall Removal Ratio of Particles

Some particles settle out, but some don't settle if the settling velocity of a particle is smaller than critical velocity. Figure 3.4 shows the trajectories of a particle with lower

settling velocities. The figure shows a particle released from the water surface that didn't settle out, but the other particle, released from the middle of the water level, just settles out at the outlet orifice. This exact particle (solid line in Figure 3.4) has the initial height of $z_p1(t_{in};t_{in})$ at inlet, which is the maximum initial height for particles to settle out. This implies that particles with higher initial position than this particle will all flow out and those with lower initial position will all settle out. The ratio of settling is exactly same as the height ratio, $\frac{z_p(t_{in};t_{in})}{h(t_{in})}$, at inlet since it is assumed that particles are uniformly distributed at inlet.

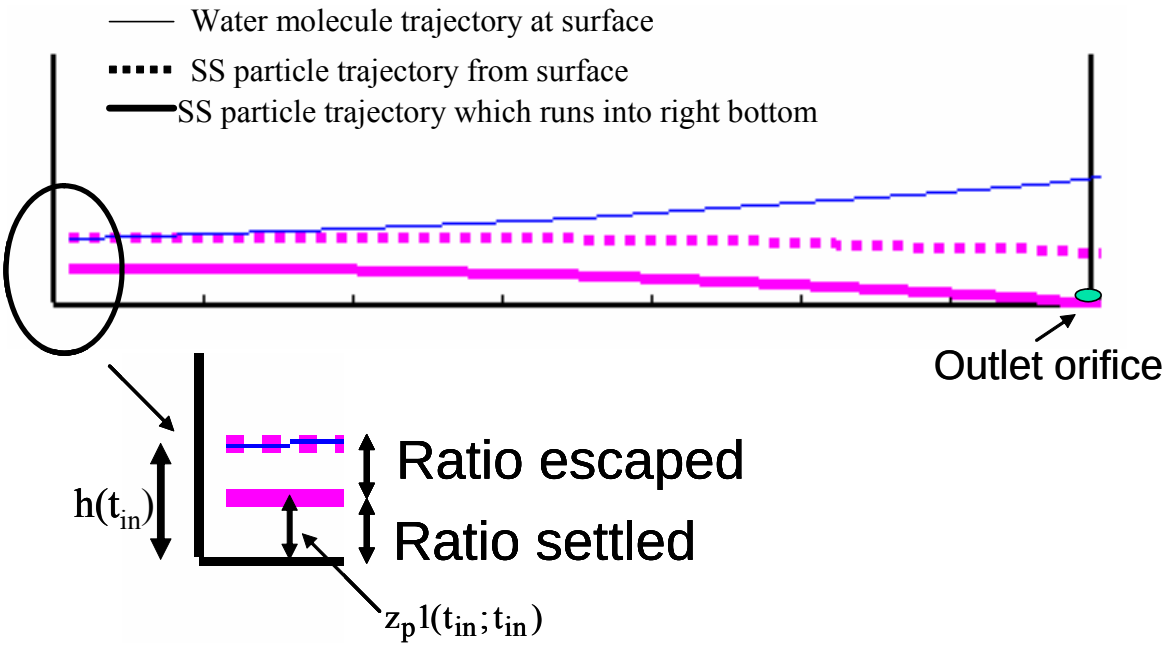

Figure 3.4. Trajectory of a particle with lower settling velocity than critical settling velocity and the particle ratio of captured and escaped

The ratio of settling can be calculated as described below. First, solve the pathline equation for a particle which exactly runs into the bottom orifice. Mathematically, put

$(t,z_p)=(t_{out},0)$ into the particle pathline equation (3.12) and solve for the term $\frac{z_p(t_{in};t_{in})}{h(t_{in})}$.

The settled mass ratio, which is the settled number ratio with the same size particles, can be simplified as the ratio of settling velocity to the critical settling velocity.

$$\frac{z_p(t_{in};t_{in})}{h(t_{in})} = v_s \cdot \int_{t_{in}}^{t_{out}} \frac{1}{h(t)} dt = \frac{v_s}{v_{s,c}(t_{in})} \tag{3.15}$$

The settled mass ratio, $F(v_s,t_{in})$, also called reactor settling potential function (Lawler, 2006), is shown in equation (3.16), and this equation suggests that all particles with settling velocity larger than critical settling velocity will settle out and the fraction $\frac{v_s}{v_{s,c}(t_{in})}$ will settle out for particles with settling velocity smaller than critical settling velocity.

$$F(v_s, t_{in}) = \begin{cases} 1 \text{ for } v_s > v_{s,c}(t_{in}) \\ \dfrac{v_s}{v_{s,c}(t_{in})} \text{ for } v_s < v_{s,c}(t_{in}) \end{cases} \tag{3.16}$$

Assume the settling velocity of inflow particles has its own probability density function, $E(v_s)$. Then, mass removal ratio can be calculated as a function of inflow time.

$$\begin{aligned} R_{out}(t_{in}) &= \int_0^{\infty} F(v_s) \cdot E(v_s) dv_s \\ &= \int_{v_{s,c(tin)}}^{\infty} 1 \cdot E(v_s) dv_s + \int_0^{v_{s,c(tin)}} \frac{v_s}{v_{s,c}(t_{in})} \cdot E(v_s) dv_s \end{aligned} \tag{3.17}$$

Overall mass removal ratio of suspended solids can be calculated by the total mass of particles flowing out divided by total mass of particles flowing in the basin as follows:

$$R = \frac{\int_0^{Ts} Q(t_{in}) \cdot C(t_{in}) \cdot R_{out}(t_{in}) dt_{in}}{\int_0^{Ts} Q(t_{in}) \cdot C(t_{in}) dt_{in}} \tag{3.18}$$

where T_s represents duration of storm runoff.

Time series outflow SSC can be estimated by equation (3.19).

$$C(t_{out}; t_{in}) = C(t_{in}) \cdot \left(1 - R_{out}(t_{in})\right) \tag{3.19}$$

3.2 CONCEPTUAL MODEL APPLICATION

Two example problems and their solutions using the developed conceptual model are shown in this section to illustrate how the conceptual model could be applied. The first is a simple example which has a constant inflow rate and SSC so that it is reproducible using the physical model. The second example employs a triangular hydrograph as inflow, which makes the inflow condition more realistic than the first example.

3.2.1 First Application Example: Constant Inflow Case

Assume that there is constant inflow of Q_{in}=0.53 L/s for the duration of T_s=40 min and the inflow SSC is C_{in}=202 mg/L. Outflow is governed by a small orifice installed at the bottom of the end wall. The effective area of the orifice is $A_e = C_d \cdot A_p = 0.43\,cm^2$, the multiplication of orifice coefficient, C_d, and the area of orifice, A_p. Assume the particle size distribution of inflow suspended solid can be properly described by lognormal distribution and the mean of $\ln(d_p)$, λ_p, is 2.286 (dp (μm)) and the standard deviation of $\ln(d_p)$, ζ_p, is 0.908 (d_p (μm)) where d_p is the diameter of a particle. Several articles (Campbell, 1985; Buchan, 1989) suggested that soil particle size distribution can be well described by lognormal distribution. Table 3.1 summarizes the input parameter values used in the example.

Table 3.1. Input parameters, their units, and values

Parameters	Unit	Value
Ae	cm^2	0.43
L	m	6.96
B	m	0.62
Q_{in}	L/s	0.53
T_s	min	40
C_{in}	mg/L	202
λ_p		0.908
ζ_p		2.286
ρ_p	g/cm^3	2.65
ρ_w	g/cm^3	1
μ	g/cm-s	0.01

Inflow suspended solid particles

Stokes law, shown in Equation (2.6), was applied to calculate particle settling velocity, v_s (m/hr), from the diameter of a particle, d_p (μm).

$$\begin{aligned} v_s &= \frac{g\cdot(\rho_p-\rho_w)}{18\mu}\cdot\left(d_p * 10^{-6}\left[\frac{m}{\mu m}\right]\right)^2\cdot\frac{3600}{100}\left[\frac{s}{hr}\right] \\ &= \frac{g\cdot(\rho_p-\rho_w)}{18\mu}\cdot\left(3.6*10^{-7}\right)\cdot {d_p}^2 \\ &= 3.24*10^{-3}\cdot {d_p}^2 \end{aligned} \tag{3.20}$$

For the parameter values in this equation, gravitational acceleration, g, is $981 cm/s^2$, density of particles, ρ_p, is 2.65 g/cm^3, density of water, ρ_w, is 1.00 g/cm^3, and viscosity of water is 10^{-2} g/cm-s, which are shown in Table 3.1. Particle Reynolds number, defined in the equation (2.5), for the particle with the diameter of 50 μm is approximately 0.1 for the silica particle. This is within the range of particle Reynolds

number where the Stokes law can be applied. Figure 3.5 shows the relationship between diameter of the silica particles and their settling velocity using the Stokes law.

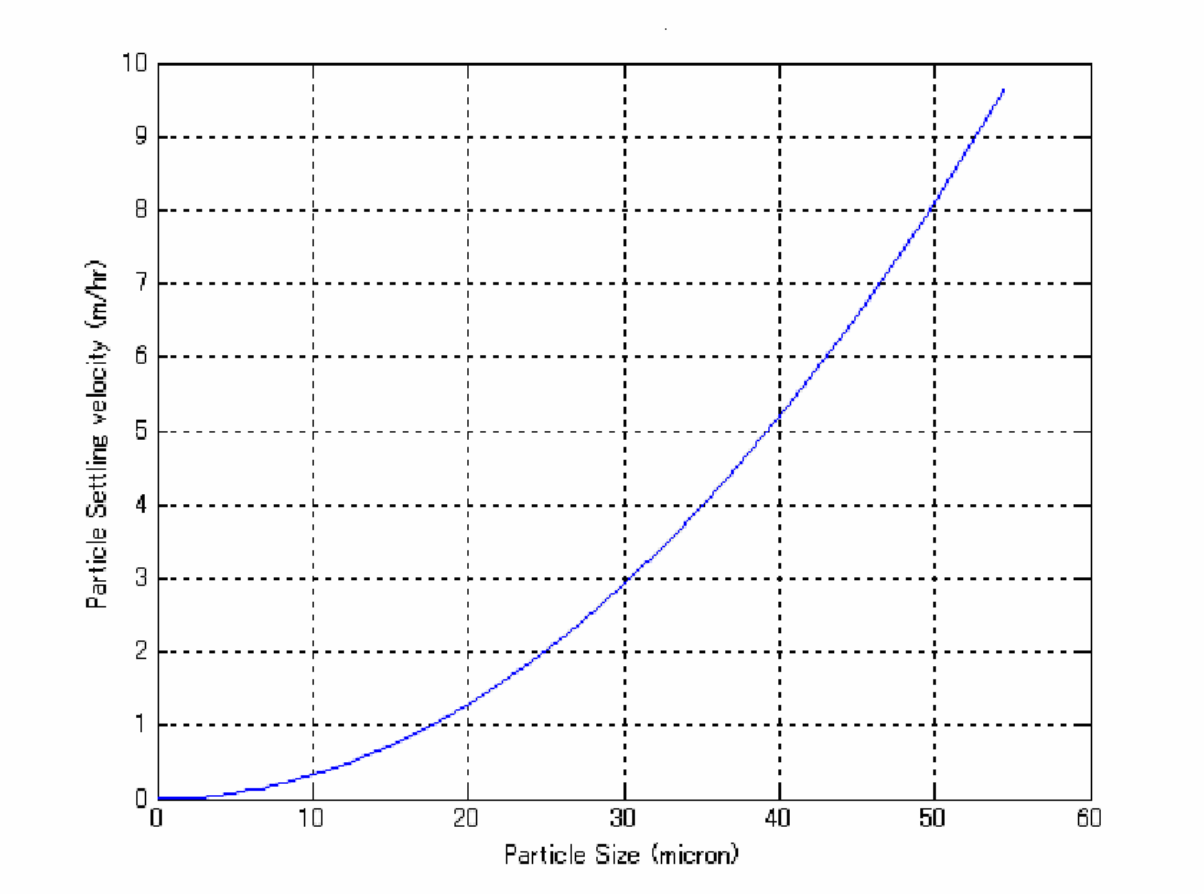

Figure 3.5. Relationship between particle diameter and settling velocity

Equation form in (3.20) implies suspensions settling velocities will have a lognormal distribution (v_s=LN($\lambda_{v,}$ ζ_v)) if particle size assumes to have a lognormal distribution (d_p=LN($\lambda_{p,}$ ζ_p)) with the random variable transformation. The validity of the assumption will be shown in the section 4.2.3. The relationship of lognormal mean and lognormal standard deviation of particle diameter and settling velocity is as follows using the relationship (3.20).

$$\lambda_v = 2 \cdot \lambda_p + \ln\left(3.24 * 10^{-3}\right)$$
$$\zeta_v = 2 \cdot \zeta_p \tag{3.21}$$

Then, the mean of lognormal settling velocity, λ_v, is -1.186 (v_s (m/hr)) and the standard deviation of lognormal settling velocity, ζ_v, is 1.816 (v_s (m/hr)) from the calculation of equation (3.21). Figure 3.6 shows Particle Size Distribution (PSD) and settling velocity distribution of inflow runoff in the forms of a Probability Density Function (PDF) and Cumulative Density Function (CDF).

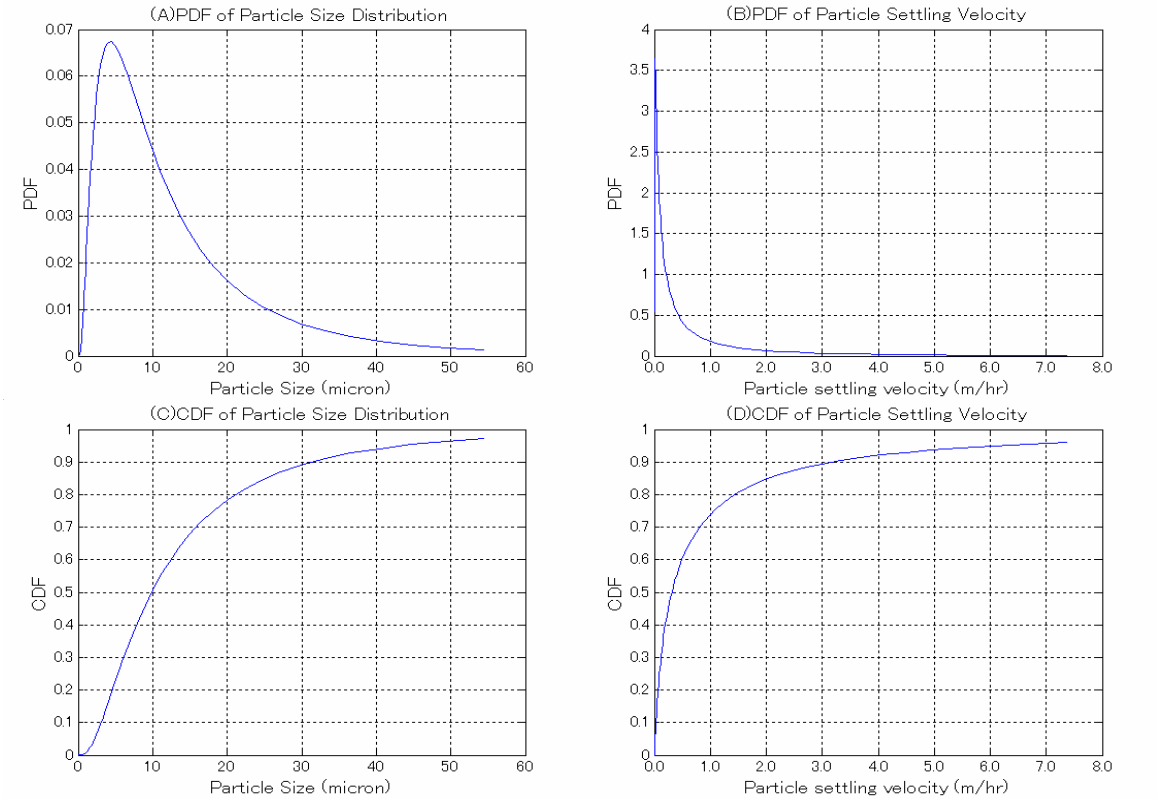

Figure 3.6. (A) PDF of mass base Particle Size Distribution, (B) CDF of mass base particle size distribution, (C) PDF of theoretical settling velocity, and (D) CDF of theoretical settling velocity

The PDF of the particle size distribution graph shows the majority of the particle sizes are less than 20 μm, and the PDF of the particle settling velocity graph shows the majority of the particle settling velocities are less than 1 m/hr. That can be confirmed in the graphs of CDFs with actual numbers. The CDF of particle size distribution graph shows that about 50% of particles on mass base are smaller than 10 μm which correspond to the settling velocity smaller than 0.32 m/hr, and 80% of particles are smaller than 20 μm which correspond to the settling velocity smaller than 1.3 m/hr. The CDF of the settling velocity distribution graph shows that more than 70% of particles have settling velocities less than 1m/hr.

Model application

The example problem was solved by writing a code in MATLAB. How the MATLAB code was built is shown in this section. The code is provided in Appendix A.

1) Water level and flow rate calculation

Mass balance equation (3.1) was rewritten by substituting an orifice equation for outflow rate.

$$\frac{dh(t)}{dt} = \frac{1}{B \cdot L}\left(Q_{in}(t) - A_e\sqrt{2gh(t)}\right) \tag{3.22}$$

This nonlinear differential equation was solved numerically. Equation (3.22) was discretized as Equation (3.23) and water level was solved explicitly by using previous time step water level values with an initial condition of water level (H^0=0).

$$\frac{h^{n+1} - h^n}{dt} = \frac{1}{B \cdot L}\left({Q_{in}}^n - {Q_{out}}^n\right)$$
$$h^{n+1} = h^n + \frac{dt}{B \cdot L}\left({Q_{in}}^n - {Q_{out}}^n\right) \tag{3.23}$$

Where

$$Q_{in}{}^{n} = Q_{in} \qquad \text{for } 0 < n \le \frac{T_s}{dt}$$

$$Q_{in}{}^{n} = 0 \qquad \text{for } \frac{T_s}{dt} < n$$

$$Q_{out}{}^{n} = A_e\sqrt{2gh^{n}} \quad \text{for any } n$$

Calculated water level change, given inflow rate, and calculated outflow rate are shown in the Figure 3.7. As the graph shows, it takes about 6 hours to drain all the water after runoff stops and the drainage time is about as 9 times long as the 40 minute runoff period.

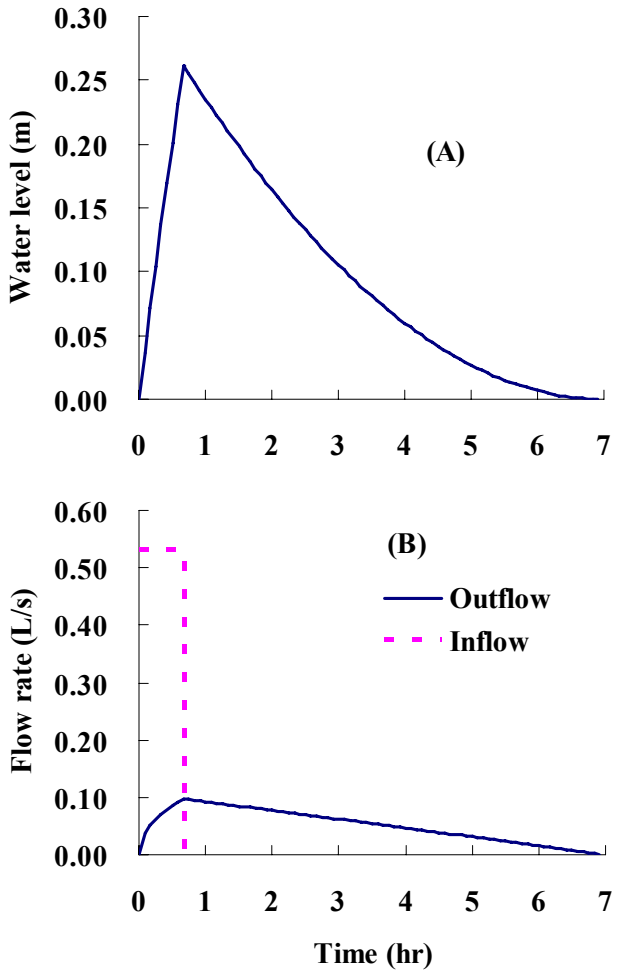

Figure 3.7. (A) Calculated water level change in the sedimentation basin and (B) Inflow and outflow rate

2) Critical settling velocity calculation

Think about an imaginary water column which is traveling from inlet to outlet without exchanging water with surrounding water because no mixing is assumed. Each imaginary water column is released from the inlet every time step, dt, from the beginning to the end of the runoff. The water column travels through the sedimentation basin and eventually reaches the outlet. Time to reach outlet, t_{out}^{n}, corresponding to each inflow time, t_{in}^{n}, was calculated by substituting $x_p(t_{out};t_{in})=L$ in Equation (3.10).

$$L = \frac{1}{B \cdot h(t_{out}^{n})} \int_{t_{in,n}}^{t_{out,n}} Q_{in}\,dt = \frac{\left(t_{out}^{n} - t_{in}^{n}\right) \cdot Q_{in}}{B \cdot h(t_{out}^{n})} \tag{3.24}$$

End of the travel time, t_{out}^{n}, of a water column which started traveling at t_{in}^{n}, can be calculated iteratively from the equation (3.24). Figure 3.8 shows the calculated detention time, t_{out}^{n}-t_{in}^{n} of water columns released at t_{in}^{n}. In the graph, traveling time, or detention time, of the first quarter (0 to 10 minutes) is less than an hour while detention time of the last quarter (30-40 minutes) is around 4 hours. Therefore, initial part of a runoff, sometimes it is the dirtiest, won't stay in the basin longer compared to the latter part of the runoff.

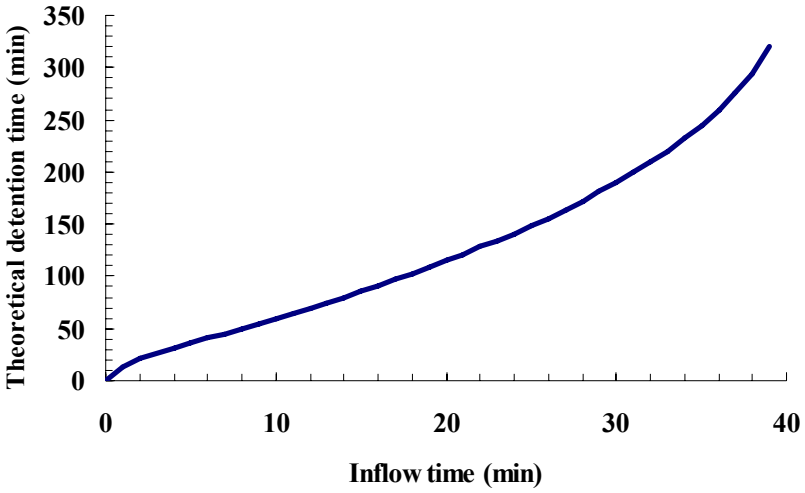

Figure 3.8. Theoretical detention time of water columns with respect to their inflow time.

Critical settling velocity, $v_{p,c}(t_{in})$, was calculated from equation (3.14). The integral, in the denominator of equation (3.14), was calculated using the MATLAB function "trapz", which conducts a trapezoidal numerical integration. Figure 3.9 shows the critical particle size change with respect to the inflow time, t_{in}. This implies that particles larger than 8 μm would all settle throughout the runoff-drainage process.

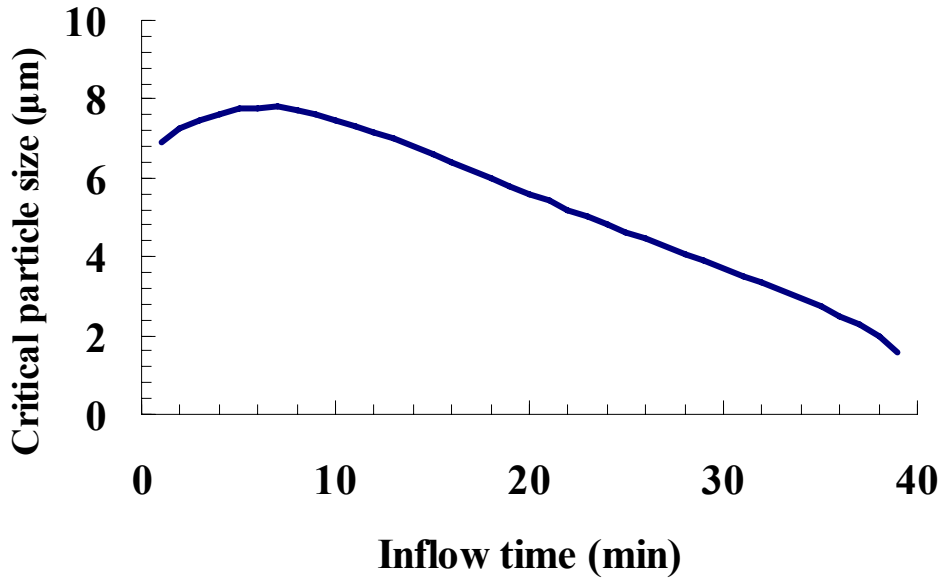

Figure 3.9. Critical particle size change with respect to inflow time

3) Overall particle removal ratio calculation

As shown in Equation (3.17), PDF of settling velocity, $E(v_s)$, and potential settling function, $F(v_s)$, should be known to calculate the overall particle removal ratio. PDF of settling velocity, $E(v_s)$, shown in Figure 3.6 (b) can be described as follows using the calculated mean and standard deviation value of natural logarithm of particle settling velocity, $\ln(v_s)$:

$$E(v_S) = \frac{1}{v_S \cdot \zeta_v \sqrt{2\pi}} e^{\frac{-1}{2}\left(\frac{\ln(v_s)-\lambda_v}{\zeta_v}\right)^2} \tag{3.25}$$

Settling potential function, $F(v_s)$, can be calculated from the calculated critical particle velocity. For this application case, Stokes velocity, equation (3.20), can be put into (3.16) and can be further transformed as follows:

$$F(v_s) = \begin{cases} 1 \text{ for } v_s > v_{s,c} \\ \dfrac{v_s}{v_{s,c}} = \left(\dfrac{d_p}{d_{p,c}}\right)^2 \text{ for } v_s < v_{s,c} \end{cases} \tag{3.26}$$

This settling potential function varies depending on inflow time. This function can be visually understood by Figure 3.10. This graph shows the particle size distribution of inflow and the fraction removed in the form of Probability Density Function (PDF). The group of particles shown in the graph flowed into the detention basin at t_{in}=5 min and flowed out at t_{out}=40 min. Calculated critical particle settling velocity, $v_{s,c}$, is 0.195 m/hr and the corresponding critical particle size, $d_{p,c}$, is 7.8 μm. The area surrounded by the solid and dotted lines corresponds to the fraction flowing out, and the area under the dotted line is the fraction settled out.

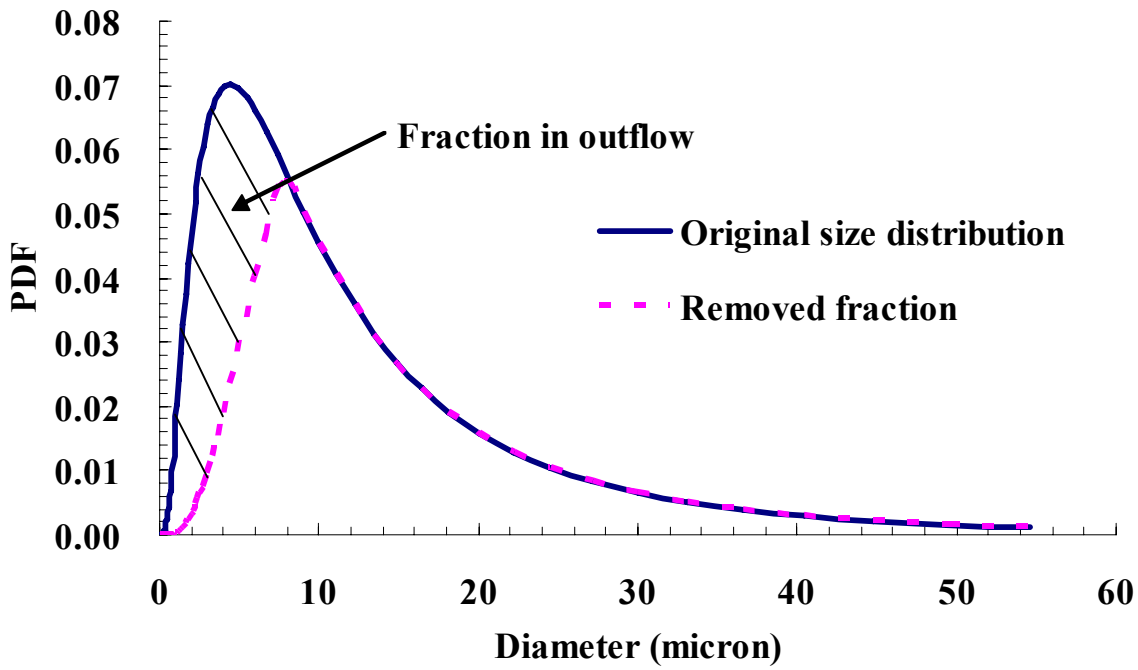

Figure 3.10. Particle size distribution of inflow suspended solid and the fraction removed.

Given the particle settling velocity distribution, $E(v_s)$ in Equation (3.25), and calculated reactor potential settling function, (3.26), these can be plugged into (3.17) to calculate the removal ratio of particles flowing into the tank at t_{in}. The first term, called $R_1(t_{in})$, of the right hand side of (3.17) is the ratio of particles larger than critical particle size and the second term, $R_2(t_{in})$, is the ratio of captured particles smaller than critical particle size. Each term was transformed as follows and calculated separately using the numerical integration function "trapz" in MATLAB. Figure 3.11 shows the calculation results of $R_1(t_{in})$ and $R_2(t_{in})$. The graph shows the $R_1(t_{in})$ is much greater than the $R_2(t_{in})$, which is surrounded by the $R_1(t_{in})$ lines and $R_1(t_{in})+ R_2(t_{in})$ lines. This implies most of inflow particles will be removed because the particle size is larger than the critical particle size.

$$
\begin{aligned}
R_1(t_{in}) &= \int_{vs,c(tin)}^{\infty} 1 \cdot E(v_s)\,dv_s \\
&= \int_{vs,c(tin)}^{\infty} \frac{1}{v_s \cdot \zeta_v \sqrt{2\pi}} e^{\frac{-1}{2}\left(\frac{\ln(v_s)-\lambda_v}{\zeta_v}\right)^2} dv_s \\
&= 1 - \int_{0}^{vs,c(tin)} \frac{1}{v_s \cdot \zeta_v \sqrt{2\pi}} e^{\frac{-1}{2}\left(\frac{\ln(v_s)-\lambda_v}{\zeta_v}\right)^2} dv_s
\end{aligned}
\tag{3.27}
$$

$$
\begin{aligned}
R_2(t_{in}) &= \int_{0}^{vs,c(tin)} \frac{v_s}{v_{s,c}(t_{in})} \cdot E(v_s)\,dv_s \\
&= \frac{1}{v_{s,c}(t_{in})} \int_{0}^{vs,c(tin)} \frac{1}{\zeta_v \sqrt{2\pi}} e^{\frac{-1}{2}\left(\frac{\ln(v_s)-\lambda_v}{\zeta_v}\right)^2} dv_s
\end{aligned}
$$

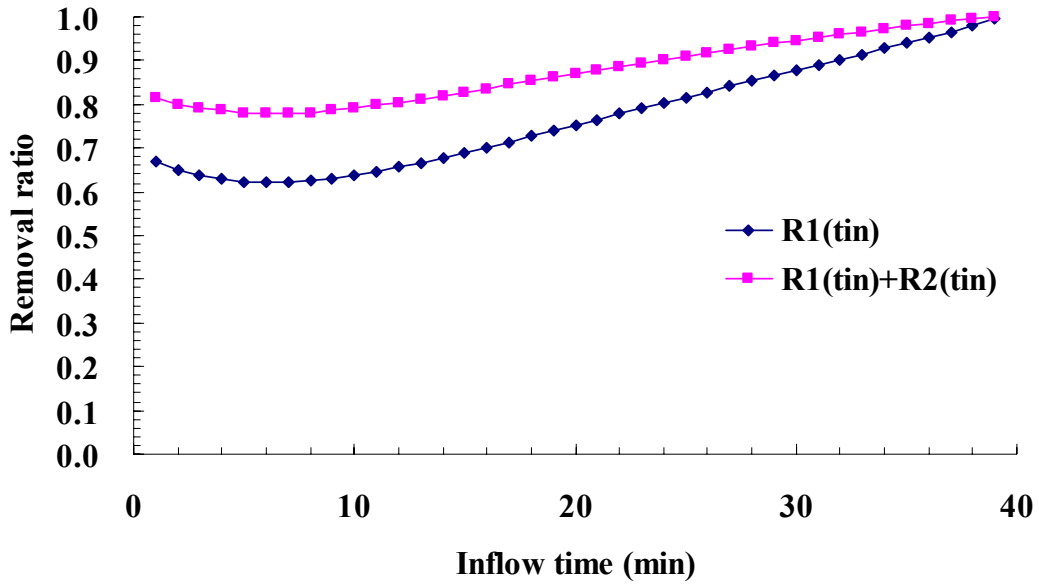

Figure 3.11. Removal ratio of Particles as a function of inflow time

Finally, total removal ratio of suspended solid and time series outlet SSC were calculated by substituting the calculated (3.17) for (3.18) and (3.19). Figure 3.12 shows the calculated time series outflow SSC. This graph shows the outflow SSC gradually increased until approximately 50 min, which is 10 minutes after runoff stopped. Then, the concentration dropped steadily with increasing time until water was completely drained. The calculated total particle removal ratio was 0.875.

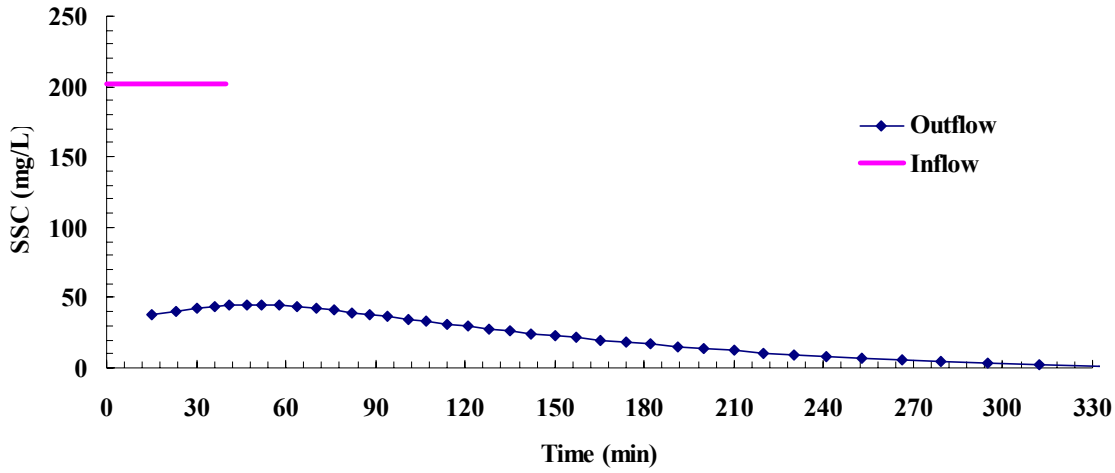

Figure 3.12. Time series SSC change in inflow and outflow

Time series outflow SSC from the outlet may not be necessary to be estimated for stormwater management purpose since the total particle removal ratio is more important in the general case. However this model can determine the particle size distribution change in the outflow. This implies that this study could be extended for estimating removal ratio of other important pollutants in stormwater such as nutrients, heavy metals, and organic materials in particulate form since hydrophobic pollutants are likely to attach to the surface of suspended solids. Adsorption is usually highly dependent on the surface area of sediment, which can be estimated from the particle size distribution.

3.2.2 An Example with Triangular Hydrograph inflow

The conceptual model was applied to deal with the SCS triangular hydrograph as an inflow rate. The SCS triangular hydrograph is a synthetic unit hydrograph, which relates direct runoff to a unit depth of excess rainfall. The benefit of applying a synthetic hydrograph, such as this triangular hydrograph, is that it is more realistic than a constant

runoff (inflow) rate since a hydrograph tends to have a skewed bell shape rather than a rectangular shape. A drawback, on the other hand, is these bell shaped hydrographs are very difficult to reproduce experimentally. The triangular hydrograph can be determined by specifying the peak flow rate, Q_p, and peak time, T_p, as shown in Figure 3.13.

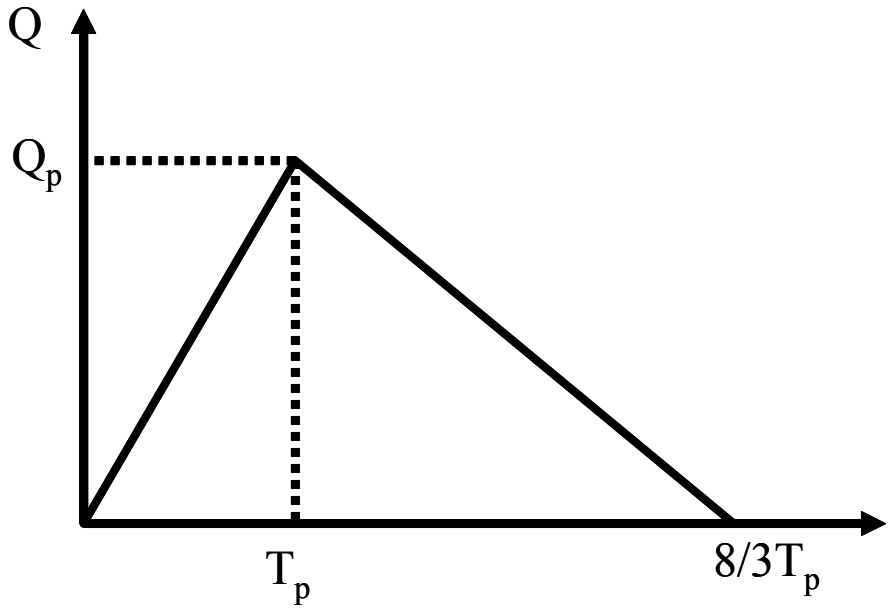

Figure 3.13. SCS triangular hydrograph

Water level and flow rates calculation

Water level in the detention basin and corresponding outflow rate were calculated based on the mass balance equation (3.28).

$$\begin{aligned}\frac{dh(t)}{dt} &= \frac{1}{B \cdot L}\left(Q_{in}(t) - Q_{out}(t)\right) \\ &= \frac{1}{B \cdot L}\left(Q_{in}(t) - A_e\sqrt{2gh(t)}\right)\end{aligned} \tag{3.28}$$

Water level was solved numerically since mass balance is a nonlinear differential equation. Equation (3.28) was discretized as follows. Water level was solved explicitly using the previous time step water level value.

$$\frac{h^{n+1}-h^{n}}{dt}=\frac{1}{B\cdot L}\left(Q_{in}(t^{n})-A_{e}\sqrt{2gh^{n}}\right)$$
$$h^{n+1}=h^{n}+\frac{dt}{B\cdot L}\left(Q_{in}(t^{n})-A_{e}\sqrt{2gh^{n}}\right) \tag{3.29}$$

where

$$Q_{in}(t)=\frac{t}{T_p}Q_p \qquad \text{for } 0<t<T_p$$
$$Q_{in}(t)=\left(\frac{8}{5}-\frac{3}{5}\frac{t}{T_p}\right)Q_p \quad \text{for } T_p<t<\frac{8}{3}T_p$$
$$Q_{in}(t)=0 \qquad \text{for} \frac{8}{3}T_p<t$$

An example problem

The MATLAB program was modified to have an unsteady state inflow and run with a triangular hydrograph. As an example, the inflow condition was set with Q_p=1 L/s and T_p=30 min at the model scale. Inflow and outflow rate are snown in Figure 3.14 and the calculated time series SSC is shown in Figure 3.15. The calculated removal ratio was 84.1%. The outflow peak occured at 70 min and the outlet SSC peak was at 77 min.

Table 3.2. Input parameters, their units, and values

Parameters	Unit	Value
Ae	cm^2	0.43
L	m	6.96
B	m	0.62
Q_p	L/s	1
T_p	min	30
C_{in}	mg/L	202
λ_p		0.908
ζ_p		2.286
ρ_p	g/cm^3	2.65
ρ_w	g/cm^3	1
μ	g/cm-s	0.01

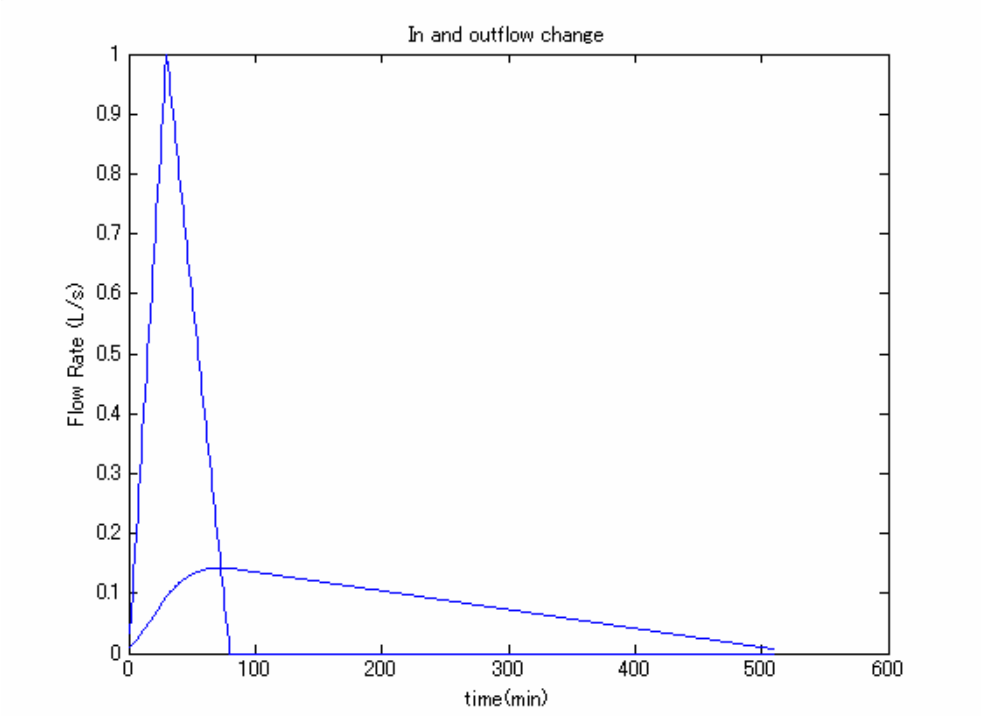

Figure 3.14. Inflow and outflow rate

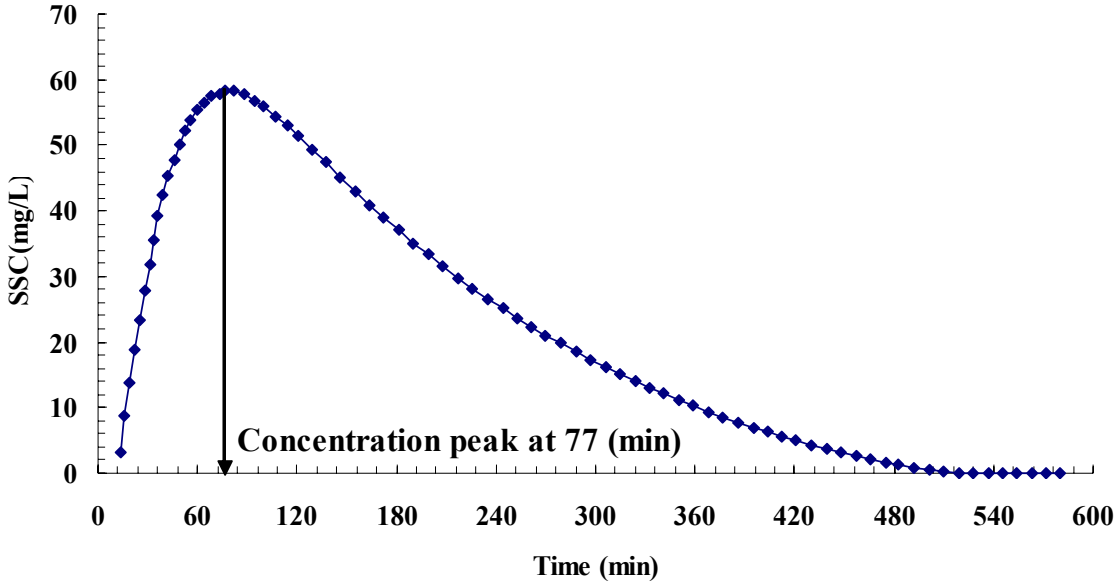

Figure 3.15. Time series outflow SSC

Application and comparison

A) Three different triangular hydrographs

The conceptual model was run in the model scale with three different triangular hydrographs (Figure 3.16) and the same runoff volume of 2400 L to see how removal ratio will be different for different runoff intensity. Table 3.2 shows the inflow conditions and resulting particle removal ratio. This table shows that the removal ratio for the slowest runoff, C, is approximately 5% higher than the most intense runoff, A. Figure 3.17 shows outflow SSC change for run A, B, and C. This graph shows that the peak SSC in a short and intense storm is higher than that in a slower storm.

Table 3.3. Inflow condition and calculated removal ratio

Run	Peak time (min)	Duration (min)	Peak flow rate (L/s)	Runoff Volume (L)	Removal ratio
A	20	53	1.5	2400	0.828
B	40	107	0.75	2400	0.852
C	80	213	0.375	2400	0.879

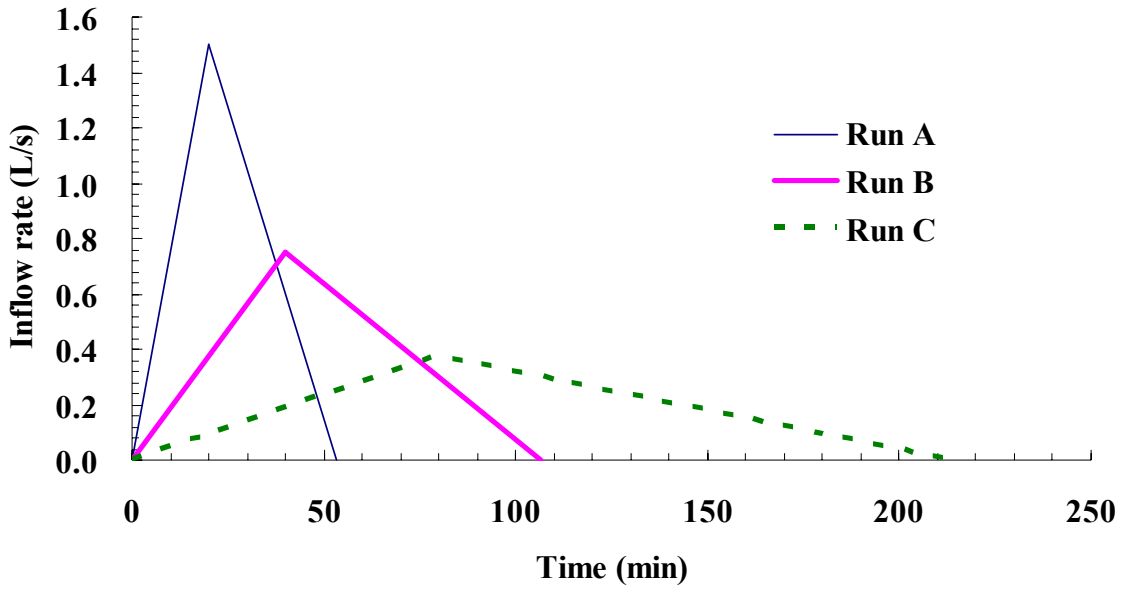

Figure 3.16. Inflow hydrographs of three tested examples

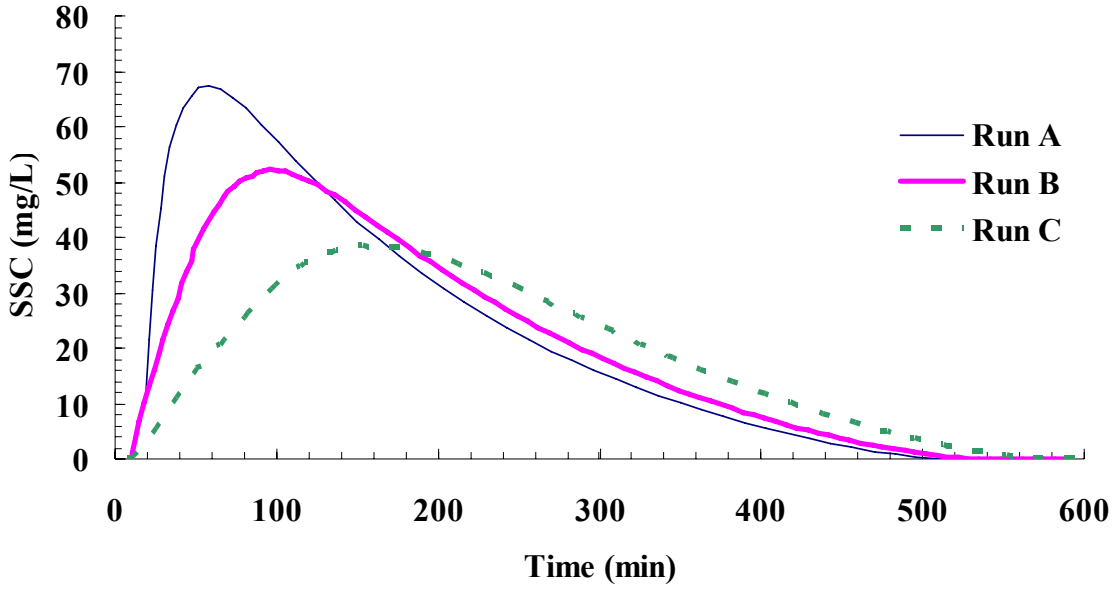

Figure 3.17. Timeseries outlet concentrations for the three different hydrographs

B) Triangular hydrograph vs flat hydrograph

It is of interest to see how performance would be different between a triangular hydrograph and a flat hydrograph. Three runoff values with flat hydrographs, each of which corresponds to the triangular hydrograph show in Table 3.2, were tested to compare their removal ratios. These three flat hydrographs were made to have the same durations and runoff volumes from their corresponding triangular hydrographs. Table 3.4 shows the inflow conditions and Figure 3.18 shows the tested inflow hydrographs of both the triangular and flat hydrographs.

Table 3.4. Inflow conditions and resulting particle removal ratios for flat hydrographs (A', B', and C') and particle removal ratio of corresponding triangular hydrograph (A, B, and C)

Run	Duration (min)	Inflow rate (L/s)	Runoff Volume (L)	Removal ratio	Removal ratio of corresponding triangular hydrograph (A, B, and C)
A'	53	0.750	2400	0.837	0.828
B'	107	0.375	2400	0.863	0.852
C'	213	0.188	2400	0.893	0.879

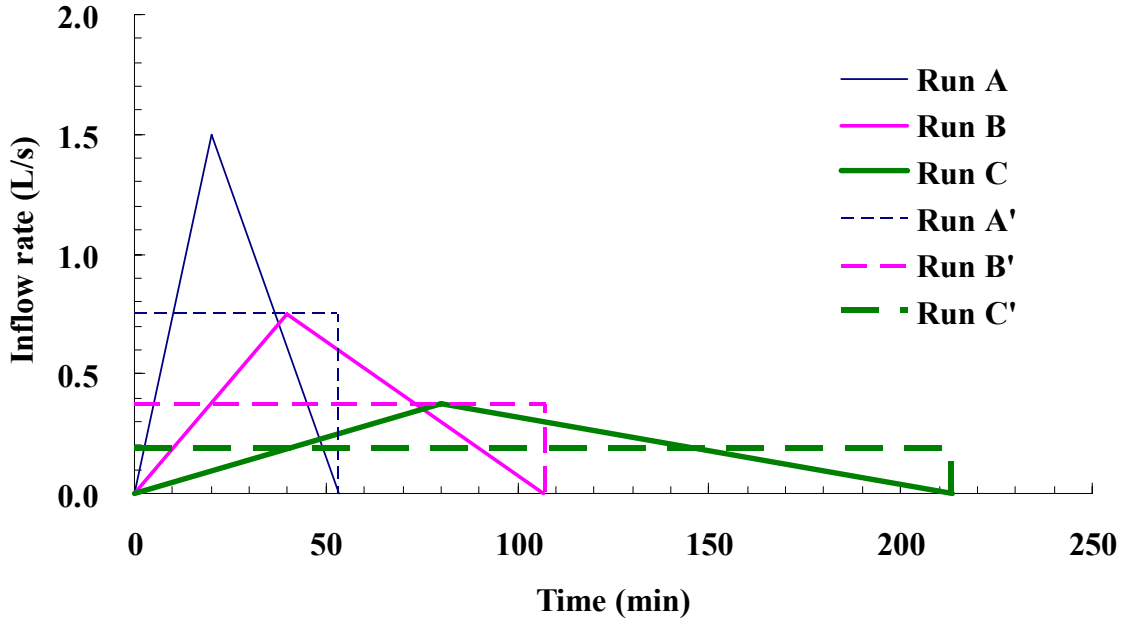

Figure 3.18. Triangular and flat inflow hydrograph

Table 3.4 also shows the results of the removal ratio calculation for both triangular and flat hydrographs. The removal ratio results from corresponding hydrographs are very close (around 1% difference), while removal ratio of triangular hydrograph is always a little less than that of flat hydrograph. However, the peak SSCs

are different. Figure 3.19 shows the calculated SSC change of runoff B for both triangular and flat hydrograph. The graphs shows that the peak SSC of the triangular hydrograph is much higher than that of the flat hydrograph. These simulation results imply that particle removal efficiency results from physical models with constant inflow would not be very different from the results with the corresponding actual stormwater runoffs such as bell shape inflows.

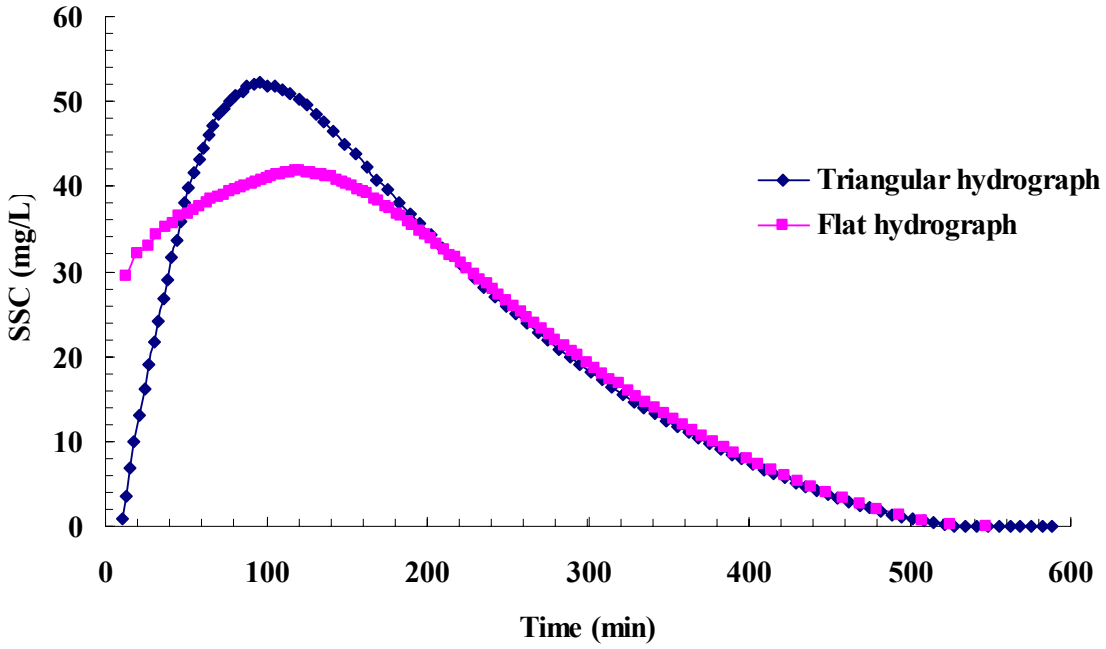

Figure 3.19. Outflow SSC for triangular and flat hydrograph

Chapter 4 Physical Model

A physical model was built in a smaller scale of the prototype rectangular detention basin to conduct performance tests of particle removal efficiency. By using a physical model, it is possible to see the validity of the developed conceptual model and see what parameters will strongly affect particle removal ratio. To cover these subjects, this chapter includes 1) physical model design; 2) detailed description about physical model; and 3) data acquisition and processing.

4.1 PHYSICAL MODEL DESIGN

The physical model was designed based on the design of a prototype scale rectangular stormwater detention basin. The prototype is assumed to have a 1 acre (4047 m^2) watershed. The basin volume is equivalent to the water quality volume, where the water quality volume is typically taken as the first 25.4 mm (=1 inch) of runoff from the impervious areas of the watershed (Young, et al., 1996). Based on the criteria, the dimensions were determined to be 34.8 m long, 3.1 m wide, and 1.7 m high to be able to fit in the right of way area along a highway. Drainage time was assumed to be 24 hours.

A physical model, geometrically similar to the prototype, was built with length scaling ratio, L_R, of 1:5. However, issues were raised when kinematic similarity was set up as to whether Froude number scaling, Hazen number scaling, or other scaling methods should be considered. If Froude number scaling was chosen, which is used when gravitational force and inertial force are dominant such as in open channel flow problems (Hwang and Houghtalen, 1996), both the time ratio and velocity ratios are $\sqrt{L_R}$. However, this doesn't take sedimentation processes into account. If Hazen number

scaling is chosen, the ratio of settling velocity to overflow velocity should be identical for both model and prototype and overflow velocity should be identical if the same particles are used for both. Then the time ratio is set to L_R since the length ratio is L_R and velocity ratio is 1.

Here, Hazen value scaling was chosen for kinematic similarity since it was experimentally proved by Thompson (1969) that Hazen value scaling would work for an ideal horizontal tank, which is similar to the rectangular stormwater detention basin in the aspect of shape and function. Accordingly, the drainage time was determined to be 4.8 hours, or 24 hours divided by time ratio of 5. Then, time is nondimensionalized by runoff duration, T_s, as follows;

$$t^* = \frac{t}{T_s} \tag{4.1}$$

This is necessary because the water level and inflow and outflow rates are a function of time and they should be scaled on the same time frame. With the nondimensionalized time, the scaling ratio of water level, $\frac{h(t^*)^P}{h(t^*)^M}$, should be equal to L_R because water level has the length scale. The ratio of flow rate, $\frac{Q(t^*)^P}{Q(t^*)^M}$, should be the multiplication of velocity ratio and area ratio which is equal to L_R^2. Orifice area ratio was calculated to be $L_R^{3/2}$ to have a properly scaled outflow rate at the orifice as follows:

$$\frac{A_e{}^P}{A_e{}^M} = \frac{\dfrac{Q_{out}(t^*)^P}{\sqrt{2*g*H(t^*)^P}}}{\dfrac{Q_{out}(t^*)^M}{\sqrt{2*g*H(t^*)^M}}} = \frac{Q_{out}(t^*)^P}{Q_{out}(t^*)^M} \Bigg/ \frac{\sqrt{H(t^*)^P}}{\sqrt{H(t^*)^M}} = L_R{}^{3/2} \tag{4.2}$$

This assumption on scaling is verified in chapter 5 using the conceptual model. Table 4.1 has the summary of scaling ratio of each parameter. The physical model dimensions were calculated based on design dimensions of the prototype and scaling down using this table.

Table 4.1. Scaling ratio of each parameter

Variable	Description	Ratio
L	Length of the detention basin	L_R
B	Width of the detention basin	L_R
h	Water level of the detention basin	L_R
Ts	Storm duration	L_R
v	Velocity	1
Q_{in} and $Q_{out}(t^*)$	Flow rate	$L_R^{\ 2}$
A_e	Effective Area of orifice	$L_R^{\ 3/2}$

4.2 PHYSICAL MODEL DESCRIPTION

Two similar (L=20 ft) sedimentation basins were built at Center for Research in Water Resources (CRWR). The first, built in fall 2003, did not provide consistency of experimental conditions while the second, built in summer 2004, worked better since it was modified to overcome drawbacks of the first. How the first sedimentation basin was built and why it did not work well are explained below, followed by the details of the successful second basin.

4.2.1 The first built sedimentation basin – an unsuccessful example

The first sedimentation basin, shown in Figure 4.1, was built with several 3/4 inch plywood sheets and was set on several wooden supports.

Figure 4.1. The first sedimentation basin, built in 2003, caused a lot of problems (Top-Left: Sedimentation basin set on wooden supports (view from inlet to outlet), Top-Right: mixing box, 3-inch pipe connecting mixing box and sedimentation basin, and Bottom-Left: mixing box)

Water, taken from the outside reservoir through a pump, was conveyed to a wooden mixing box by flowing on a roadway surface. Then the water was mixed in the box, shown in the bottom left of Figure 4.1, with an introduced mixture of silica particles. Silica particles were introduced to the mixing box with a peristaltic pump with a flow rate controller. The water with silica particles was conveyed to the sedimentation basin through 10 ft long, 3-inch diameter pipe. Then the water was drained to the return

channel which brought water back to the reservoir. This basin was not successful, and the data taken from the structure were not reliable enough to be used for several reasons:

- Mixing of water and particles in a rectangular mixing box by a propeller type mixer was neither efficient nor constant and resulted in too much sedimentation in the mixing box. Therefore, the box couldn't achieve a constant inflow SSC.
- The 3-inch diameter pipe connecting the mixing box to the basin for approximately 10ft was too long and too wide. This caused sedimentation and resuspension to occur in the pipe, which made experimental conditions more uncontrolled.
- Water proofing which was done by silicone caulking couldn't hold water well; leakage from the basin was significant, especially from the seams of plywood and the connection between the pipe and the basin.

4.2.2 The second sedimentation basin – a successful example

The second basin was built after the careful consideration of solutions for the problems encountered in the first sedimentation basin. This section covers details of the sedimentation basin including construction, water proofing, pipe networking, characteristics of structures, and particle mixing and the delivery system.

- Construction and water proofing

The sedimentation basin was made of 3/4 inch plywood. Prior to construction, nine cutout boards, three each for both sides and bottom, were painted with a polycrylic waterproofing medium, followed by primer paint and a tinted water-based latex paint. The nine boards were carefully connected to each other with screws and put on cinder blocks. Pieces of wood boards were attached to support connections between longitudinally connected boards, and 1 by 1 inch boards surround several cross sections of the basin to firmly support the hydraulic pressure (Figure 4.2). The seams were then sealed with silicone caulking. To complete the water proofing of the model basin, resin

was applied in a multiple-coat thickness throughout the whole inside surface of the model basin. This resulted in excellent water proofing.

Figure 4.2. Whole structure of the physical model

- Pipe network

Inflow to the model basin was taken either from the indoor reservoir via a pump system or from tap water. Figure 4.3 shows the schematic of the pipe network used for the physical model. Tap water was preferred to pump water because the reservoir water contains a few mg/L of SSC, and this might affect the particle size distribution of inflow particles. Therefore, the pump system was used only when tap water couldn't achieve the required flow rate. Water, taken either from pump or tap water, was circulated back to the indoor reservoir when the water was clean and was drained out when the water contained a certain SSC. Once the pump was switched on, the flow rate was regulated by valve V_B, while valve V_C is open for bypass and valve V_D is closed, blocking inflow to the model

basin. V_A was always widely open when water was taken from the indoor reservoir during an experimental run to prevent pump impairment because the required inflow to the model basin is very small relative to the pump capacity and too little flow through a large pump can easily impair the pump.

The flow rate was roughly measured at the outfall, following valve V_C, by measuring the time needed to fill a bucket of known volume. When multiple measurements showed the flow rate to be steady, this rate was noted, then V_C was closed and V_D was opened. Flow was lead to bypass through V_E by closing V_F until the silica slurry was prepared in the mixing tank, delivered via the peristaltic pump to the pipe system and stabilized. Finally, runoff with a certain SSC was lead to the model basin.

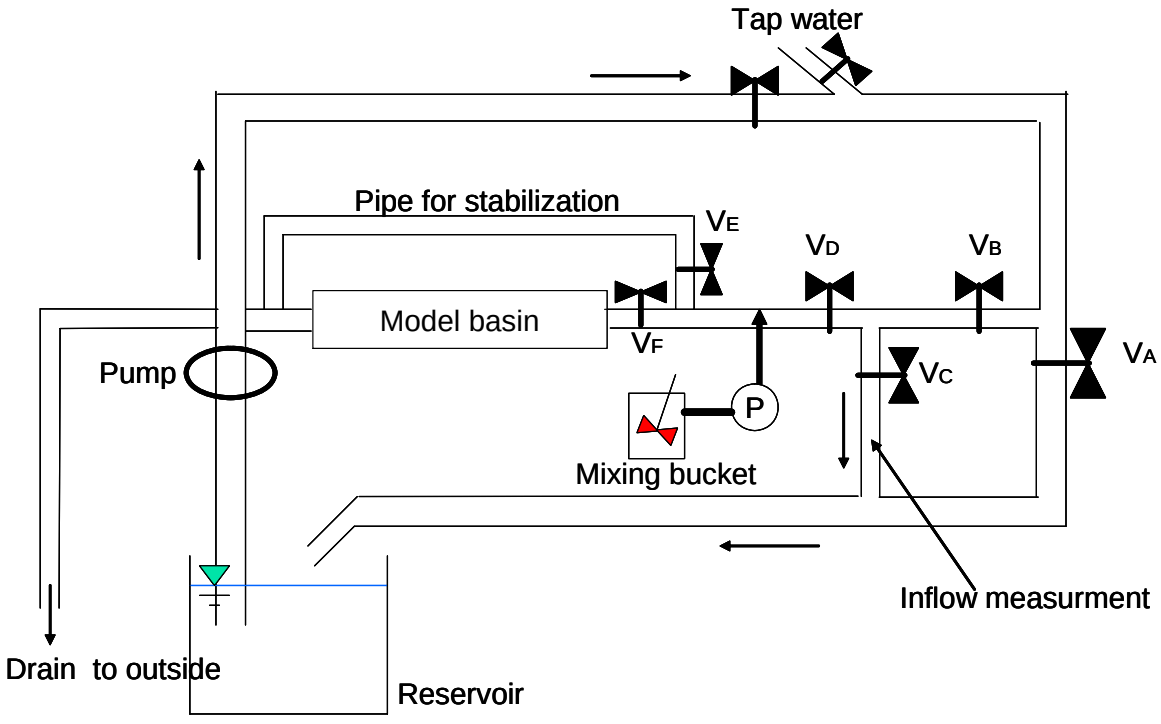

Figure 4.3. Pipe network for the physical model

- Inlet structure

A 1-inch pipe was attached near the center at the bottom of the end piece of the sedimentation basin as the inflow opening. A 3-inch pipe was used in the first basin because a 3-inch pipe is approximately 1/5 diameter of an 18-inch pipe, which is the minimum diameter of stormwater pipes. However, it caused particle accumulation in the pipe due to small flow velocity in the pipe. Therefore, 1-inch pipe was used to pursue experimental consistency and prevent the influence of previous runs.

A small wooden block with a 9 cm by 9 cm square face and streamline tail was attached to the bottom, 13 cm behind the inlet opening as an energy dissipator. The purpose of the energy dissipator is to disperse the strong momentum of the inflow jet and prevent resuspension of sediment around the inlet area. The position and shape of the energy dissipator determine the effect it will have on the flow and sedimentation pattern around it. These effects were not studied intensively in this research because resuspention effect was out of our modeling focus and the existing energy dissipator did effectively disperse the strong momentum of inflow jet to minimize the resuspension effect. Figure 4.4 shows the picture around the inlet including the wooden block used as an energy dissipator.

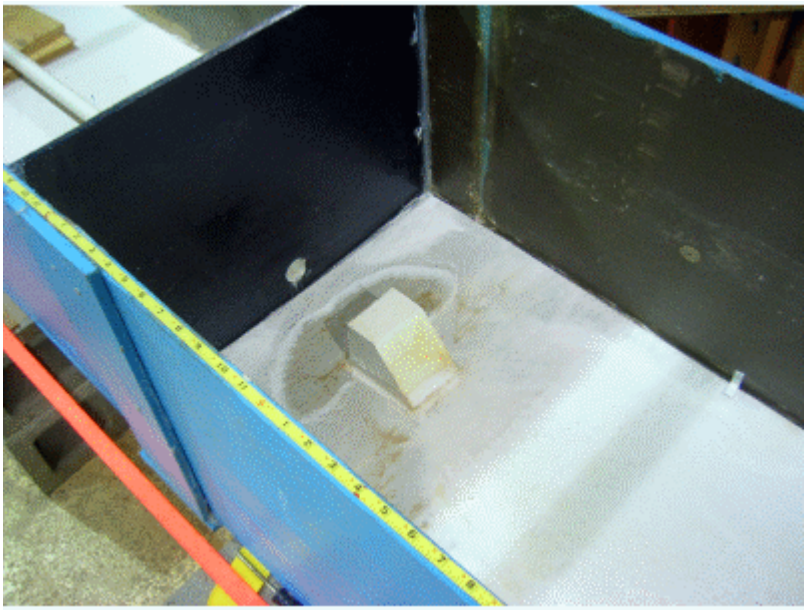

Figure 4.4. Inlet pipe and energy dissipator

- Sedimentation basin

The sedimentation basin has the length of 6.96 m and width of 0.62 m. The bottom of the basin was painted dark blue and the sides were painted gray. At the middle of the basin, a Plexiglas window was attached to view sedimentation pattern or flow pattern using dye. Particles precipitated from previous runs were not removed as is the case for real detention basin. Therefore, each experimental result has some extent of influences such as resuspension from previous runs. Figure 4.5 shows the sedimentation basin with Plexiglas window. After several measurements were taken at the original length basin, the basin was shortened to have 2/3 length of the original length by sliding the inlet wall to the 1/3 of the original sedimentation basin.

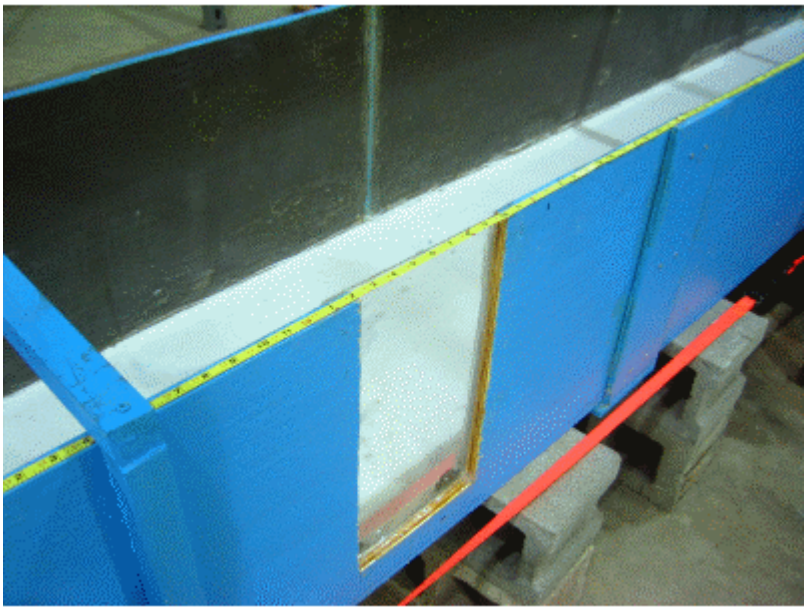

Figure 4.5. Sedimentation basin with view window

- Outlet structure

At the far end of the sedimentation basin, plywood and a small section of metal sheeting made up a composite 0.37 m high overflow weir and outlet orifice (Figure 4.6). The effective area of the orifice, A_e, was calculated as follows to take 4.8 hours to drain completely from the very top of the basin.

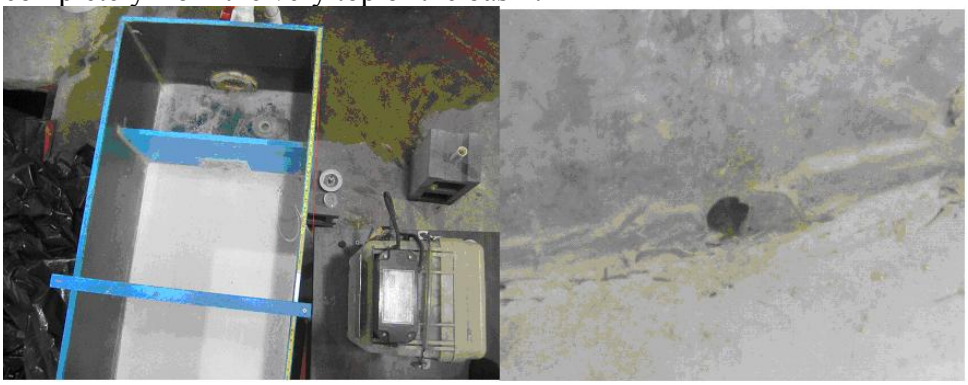

Figure 4.6. Setups around outlet orifice (Left: view from top, Right: orifice)

Mass balance for the emptying period can be expressed using the orifice equation,

$$BL\frac{dh}{dt} = -A_e\sqrt{2gh}$$
$$\frac{dh}{\sqrt{h}} = -\frac{A_e}{BL}\sqrt{2g}dt \tag{4.3}$$

This can be integrated as

$$2\left[\sqrt{h}\right]_{h_{max}}^{h} = -\frac{A_e}{BL}\sqrt{2g}\cdot\left[t\right]_{Ts}^{t}$$
$$\sqrt{h} = \sqrt{h_{max}} - \sqrt{\frac{g}{2}}\frac{A_e}{BL}\left(t - T_s\right) \tag{4.4}$$

Put h_{max}=0.37 m, h= 0 m, and t-T_s=4.8 hr, then A_e is calculated as 0.69 cm^2.

To have this effective orifice area, the diameter of orifice, D_o, was calculated as 1.1 cm assuming the orifice coefficient, C_d, is 0.8.

$$A_e = C_d \cdot A_o = C_d \cdot \frac{\pi {D_o}^2}{4}$$
$$D_o = \sqrt{\frac{4A_e}{\pi \cdot C_d}} = 1.1\text{cm} \tag{4.5}$$

Then the circular orifice with a diameter of 1.1 cm was cut out from metal sheet by metal scissors.

4.2.3 Suspended sediment particle

Synthetic silica was used as the suspended sediment for the physical model instead of using real suspended sediment from the natural environment because the particle size distribution of this commercial synthetic sediment is known. This characteristic made experiments reproducible and made the verification process of conceptual modeling easier. In this section, how the particle size distribution of inflow particles was determined and how particles were introduced to the system are discussed.

- Particle size distribution determination

SIL-CO-SIL®49, a product of US Silica Company, was used for this experiment. According to the information that the manufacturer provides, density of the product is 2.65 g/cm^3, which is very close to the density of quartz, and the particle size distribution was also given. Figure 4.7 shows the provided particle size distribution of the product. As shown in this figure, almost all the particles of SIL-CO-SIL®49 were less than 50 μ m. It seems SIL-CO-SIL®49 is too small to be a representative of suspended solid particles in stormwater since stormwater particle size ranges up to 500 to 1,000 μ m (Minton, 2003). Andral *et al* (1999) reported that the particles with a diameter larger than 100 μm settle out of the suspension easily; however, the particles with a diameter less than 100 μm remain in suspension. Thus, the investigators concluded that particles with a diameter less than 50 μm must be studied in order to effectively treat runoff. That is one reason that using SIL-CO-SIL®49 for experiments are reasonable. The other reason is the removal efficiency of the sedimentation basin. Removal efficiency of SIL-CO-SIL®49 was around 85% and there were small fluctuations with different experimental conditions. This implies removal efficiency would be higher than 85% with bigger particles and this would make comparison of experimental data more difficult.

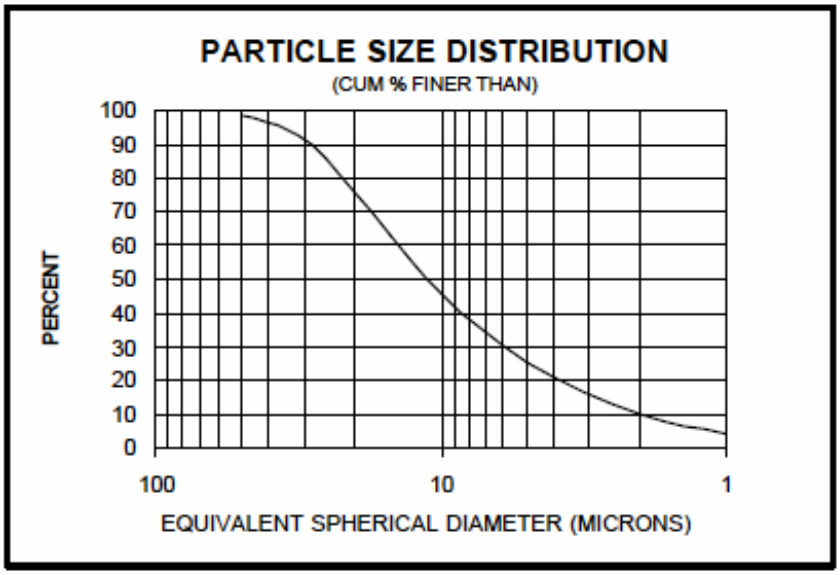

Figure 4.7. Particle size distribution of SIL-CO-SIL®49 (provided by US Silica)

Although the PSD of SIL-CO-SIL®49 is given by the manufacturer, particle size of an inflow sample was also measured. The inflow sample was taken from a nozzle right before the sedimentation basin. The measurement was done using a Coulter Counter operated by an experienced graduate student. Figure 4.8 shows the mass base particle size distribution of SIL-CO-SIL®49 read from the manufacturer data and the PSD of an inflow sample measured by the Coulter Counter in the form of a cumulative density function. A gap is observed between the two, and the gap is approximately 20 % for particles smaller than 15 μm. This gap comes from mixing and the sediment delivery process, which will be explained in the next section. Some or most of the bigger particles might settle in the mixing tank, or they may not be pumped by the peristaltic pump. Therefore, the measured PSD by the coulter counter was used as the PSD of the inflow sample.

The next step is fitting the PSD using a lognormal distribution. This fitting process was done using the solver function in Excel to find the best fit parameters, which are the mean and standard deviation of the logarithm of particle diameter, $\ln(d_p)$, in order to minimize the summation of square errors of percentage for each particle size range. The calculated mean of $\ln(d_p)$, λ, is 2.286 and standard deviation of $\ln(d_p)$, ζ, is 0.908. The equivalent mean particle size is $\exp(\lambda + \zeta^2/2) = 14.9\,\mu m$. These values were used for the PSD of inflow in the conceptual model. Figure 4.8 also shows the fitted lognormal curve. The graph shows the error is very small for particles less than 25 μm and the error is less than 10% for the entire particle size range. As shown in the conceptual model, bigger particle would all settle out in the basin and the interest is more on smaller particles. Therefore, this lognormal fit, better for smaller particles, is useful for this aspect also.

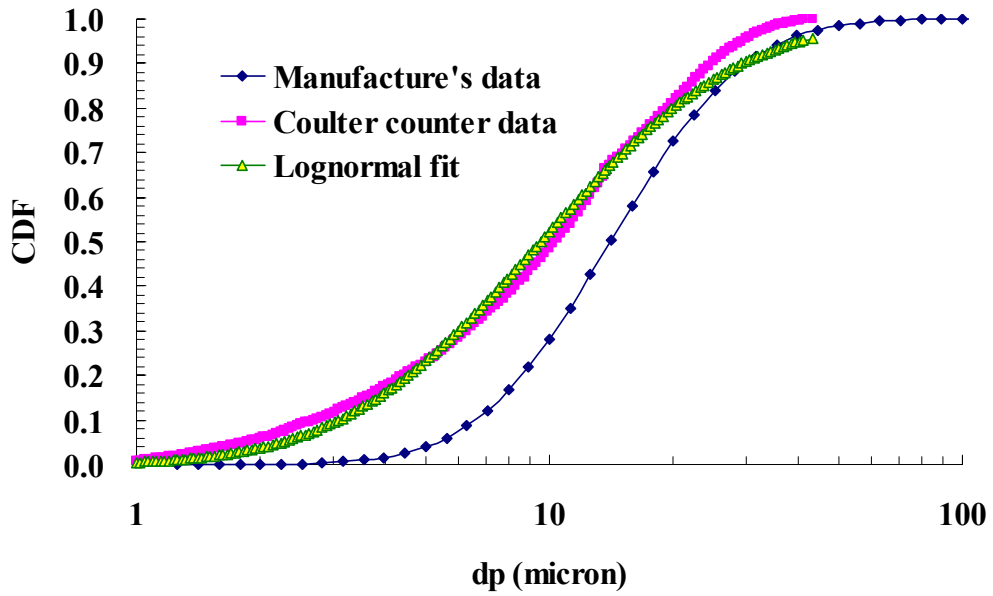

Figure 4.8. Particle size distribution of SIL-CO-SIL®49 (manufacture provided), inflow sample measured by coulter counter, and the best fit lognormal distribution

- Sediment delivery system

Three mixing systems were tried in this research. The first is the mixing box tried in the first built basin, which resulted in failure. The second and the third are explained and compared here. Figure 4.9 shows the second trial system. This system consists of a 4L mixing box, a variable flow peristaltic pump (VWR Vera 4.0-600 mL/min), and tubing. This system worked simply. First, a mixture of particles was prepared in the 4L mixing box and mixed by a propeller. Then, the mixture was sucked from bottom of the box by a peristaltic pump with variable flow rate and pushed into the inflow pipe through the tubing. Unfortunately, this system couldn't achieve a constant inflow SSC due to the following reasons:

- The flow rate of the peristaltic pump was significantly affected by the head drop of the mixing tank.
- The propeller type stirrer created stratification in the mixing box and it prevented uniform mixing.
- Since the volume of the mixing box was too small for a run, a mixture was added to the box 2 or 3 times during a run which made the consistency even worse.

Figure 4.9. Particle delivery system for the second trial

Fortunately, several ideas for mixing were given by professors and a successful system was built. The final design of the sediment delivery system and the mixing box are shown in Figure 4.10. The particle concentrate was prepared in a 22 L bucket and mixed by circulation created by a submersible pump (Rule 1800) placed at the bottom of the mixing bucket. The submersible pump drew water from the bottom of the bucket and pushed water out through 1 inch diameter opening at the rate of 1.8 L/s. The opening angle was set almost parallel to the bottom to enhance scouring and resuspention of silica particles. A large stirrer was also tried for the mixing purpose with the same 22 L bucket, but a constant SSC couldn't be achieved at inlet.

Mixed particle concentrate was delivered using a peristaltic pump (Manostat Vera, 1-3400 mL/s), the flow rate of which can be kept constant. The flow rate of the pump was controlled by a dial, so the relationship between dial indicates and the flow

rates was calibrated beforehand to control inlet SSC. The mixed sediment was introduced with the constant flow rate to the pipe network at right before the inlet opening of the model basin.

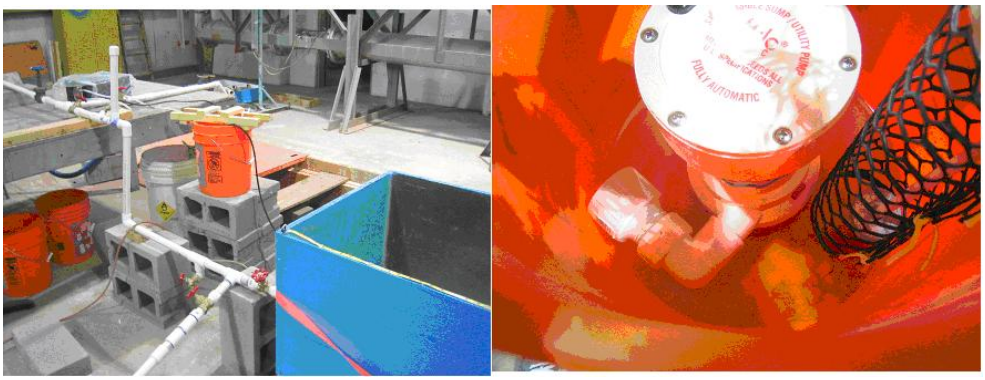

Figure 4.10. Particle delivery system (Left) and inside of the mixing bucket

Next, the experimental process for sediment delivery is shown below:

1. Determine the duration and flow rate of a model runoff
2. Determine the inflow SSC, approximately 200 mg/L is used.
3. Calculate the SSC in slurry, C_{slurry}, and volume of slurry in the mixing basin, V_{slurry}, to be delivered, using the following mass balance;

$$\begin{aligned} &(Q_{pipe} + Q_{tube}) \cdot C_{in} = Q_{tube} \cdot C_{slurry} \\ &\Rightarrow C_{slurry} = \frac{(Q_{pipe} + Q_{tube}) \cdot C_{in}}{Q_{tube}} \\ &\Rightarrow V_{slurry} \geq Q_{tube} \cdot T_s \end{aligned} \tag{4.6}$$

where Q(L/min) is flow rate, C(mg/L) is concentration, and Ts(min) is runoff duration.

Even though the particle delivery system was modified, the inlet SSC was still variable and difficult to control. Therefore a uniformity coefficient parameter was introduced to determine whether inflow SSC was kept constant enough. Uniformity coefficient of inflow SSC was determined by using the following equation.

$$CU(\%) = \left(1 - \frac{\sum_{i=1}^{N} \left| C_{in,i} - \overline{C_{in}} \right|}{N * \overline{C_{in}}} \right) * 100 \qquad (4.7)$$

where N = total number of samples, $C_{in,i}$ represents inflow SSC of i^{th} sample, and $\overline{C_{in}}$ represents average inflow SSC among total samples. A criterion was set at a uniformity of 80%. Then eight runs with the inflow SSC uniformity coefficient larger than the criteria were selected.

4.3 DATA ACQUISITION, EXPERIMENT PROCEDURE, AND POST PROCESSING

Measurable parameters in the physical model are water level of the sedimentation basin and SSC. Inflow and outflow rate, event mean concentration (EMC), and removal ratio are the parameters to be calculated. How values of these parameters were acquired and calculated and how a set of experiments was conducted are explained here.

4.3.1 Data acquisition

A) Water level

Water level in the model basin was measured by an automatic bubbler flow meter (ISCO 3230). A flexible polyurethane tube is fixed to the model basin bottom and then connects to the bubble meter, which sends a slow air stream through the tube allowing the release of air bubbles from the bottom of the model basin. Figure 4.11 shows the pictures of the bubble flow meter and tubing attached to the bottom of the basin adjacent to the orifice. The bubble meter continuously measures the hydrostatic pressure due to the depth of water above the bubbling end of the tube. The meter automatically transfers the pressure into a water height reading. The measurement interval was set for 1 minute for this research.

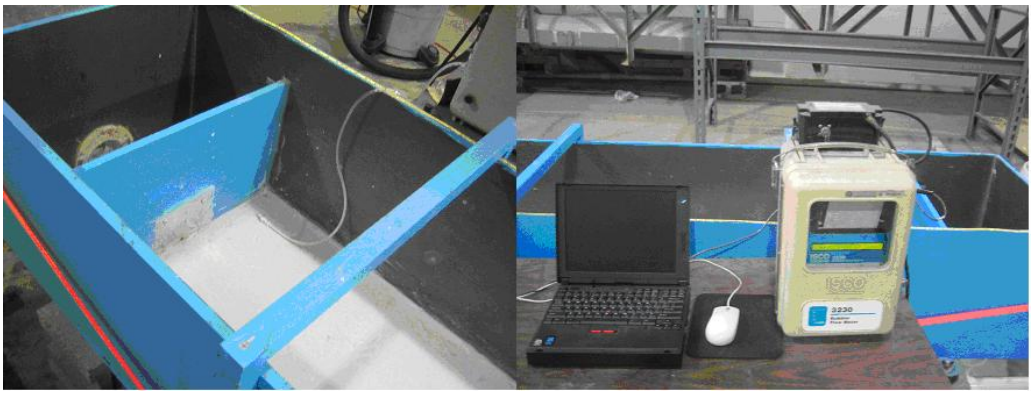

Figure 4.11. Bubble flow meter (right) and tubing attached to the bottom (Left)

B) Suspended sediment concentration (SSC)

Water samples were taken from the inlet and outlet periodically. Inlet samples were taken through a nozzle attached before the sedimentation basin and outlet samples were taken directly from a cascade installed at the bottom of the outlet area. Inflow samples were taken around 5-10 seconds after opening the nozzle to prevent taking particles accumulated in the nozzle. Occasionally, samples were taken from the lengthwise midpoint of the sedimentation basin when necessary. Turkey basters are used to take samples instead of actual pipets since this is much quicker in taking a sample of approximately 200 (mL). Figure 4.12 shows both the inlet sampling nozzle and outlet sampling cascade.

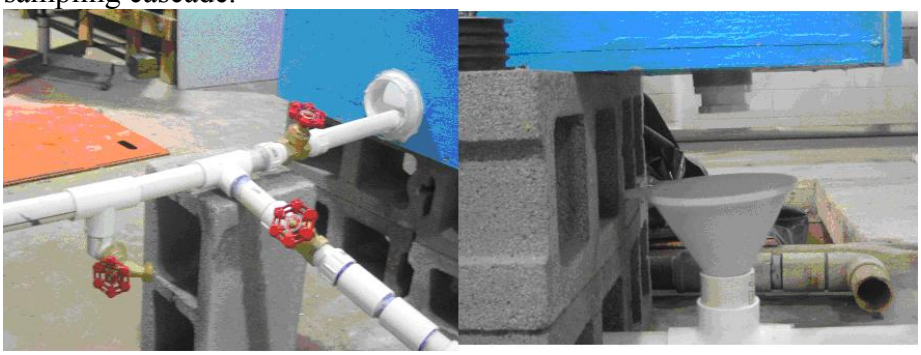

Figure 4.12. Inlet sampling nozzle (Left) and outlet sampling cascade (Right).

Samples were stored in 250 mL polyethylene bottles. Each sample was filtered through a 1.5 μm of particle retention size glass fiber filter (Glass Microfiber Filters 47mm, 934-AH, Whatman) within a few hours after samples are taken. Before use in the measurements, stored filters were washed by reagent-grade water (milli-Q), dried in an oven at 105 °C for 1 hour, stored in a desiccator for at least half an hour, and weighed just before the filtration process. All filters with solid residues were again dried by an oven at 105 °C for 1 hour, kept in the desiccator at least half hour, and weighed. At the time of filtration, sample volume is also measured using a 250 mL graduated cylinder. Then suspended solid concentration (SSC) can be estimated as

$$\mathrm{SSC}(\mathrm{mg/L}) = \frac{(\mathrm{A} - \mathrm{B}) * 1000}{\mathrm{sample\,volume,\,mL}} \tag{4.8}$$

where A is the weight of the dry filter and dried residue in mg, and B is the weight of the dried clean filter in mg.

4.3.2 Experimental procedure

Here is the experimental procedure that took place at each run.

1. Target inflow rate, runoff duration, and inflow SSC were determined prior to each run. Inflow was bypassed to drainage and inflow rate was roughly measured using a stopwatch and bucket of known volume.
2. Detemine SSC in the mixing bucket, C_{slerry}, and the speed of peristaltic pump, Q_{slerry}.
3. Inflow runoff with a given SSC was introduced to the sedimentation basin and maintained for a predetermined duration.
4. Samples were taken periodically from the inlet and outlet by using 250 mL polyethylene bottles. Inflow samples were taken periodically so that at least 4 or 5 samples can be taken. Outflow samples were taken periodically (5 to 10 minutes interval) from the time runoff started until 10 to 20 minutes after the runoff stopped. After that, intervals of taking samples became longer, up to 30 minutes, since the SSC change was small.

5. Water level in the basin was recorded every minute for the entire runoff and drain process using a bubble flow meter (ISCO 3230). Acquired data were used to calculate inflow and outflow rates.
6. SSC of each sample was measured by the filtration method after the entire process was finished.

4.3.3 Data Processing

Variable water level and resulting outflow change made the system unsteady even though inflow rate and inflow SSC were kept constant. However, the hydraulics part concerning the water level and both inflow and outflow rates are fairly easy to estimate, which is a big advantage in consideration of this unsteady system.

(A) Inflow and outflow rate estimation
Effective orifice area

Effective orifice area was measured using time series water level data for the emptying period. This calculation was done using water level change. Equation (4.9) shows that water level change is only a function of time for emptying period and $\sqrt{h}$ is a linear function of time. Figure 4.13 shows the $\sqrt{h}$ change with time for two different orifices which were actually used in experiments. Effective orifice area can be calculated from the gradient of the graph of $\sqrt{h}$ with respect to time.

$$\sqrt{h_1} = \sqrt{h_{max}} - \sqrt{\frac{g}{2}}\frac{A_e}{BL}(t_1 - T_s)$$

$$\sqrt{h_2} = \sqrt{h_{max}} - \sqrt{\frac{g}{2}}\frac{A_e}{BL}(t_2 - T_s)$$

$$A_e = -\frac{\sqrt{h_2} - \sqrt{h_1}}{t_2 - t_1}\frac{BL}{\sqrt{g/2}} \tag{4.9}$$

or with units,

$$A_e\left(cm^2\right) = -\frac{\sqrt{h_2(m)} - \sqrt{h_1(m)}}{(t_2(min) - t_1(min))*60(s/min)} \cdot \frac{BL(m^2)}{\sqrt{g(m/s^2)/2}} \cdot 10^4$$

Where (t_1, h_1) and (t_2, h_2) are two combinations of a time during the emptying period and the corresponding measured water level.

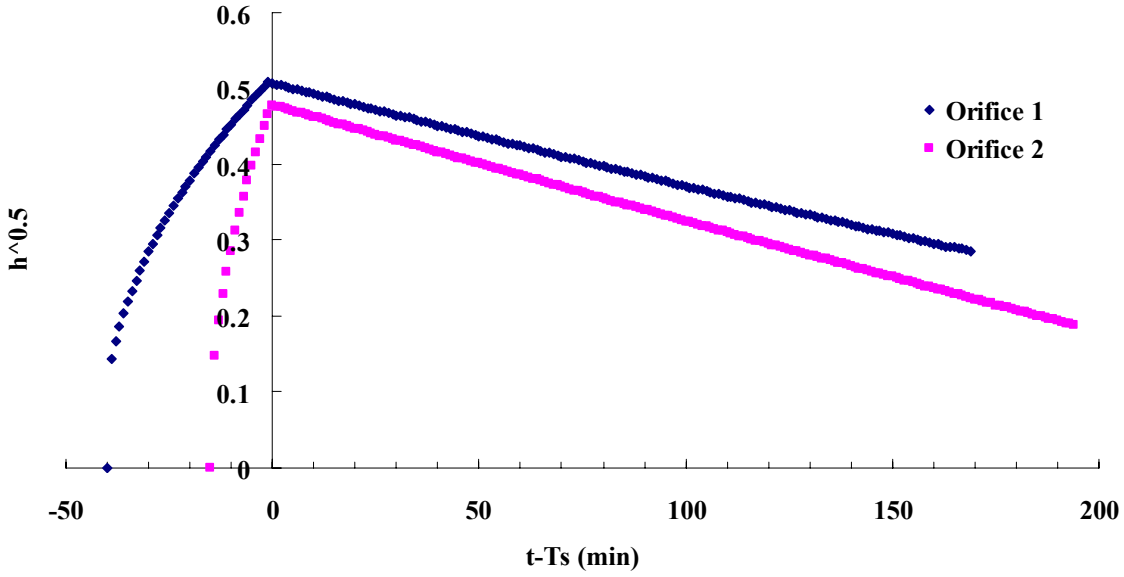

Figure 4.13. $\sqrt{h}$ (square root of water level) change with time

In the experiment, two different size orifices were used and their effective areas were calculated using equation (4.3') as 0.43 cm^2 for orifice 1 and 0.49 cm^2 for orifice 2.

Outflow rate

Outflow rate was calculated by the orifice equation (the RHS of equation (4.3)) with the calculated effective orifice sizes.

Inflow rate

Since the mass balance equation for filling period is non-linear, as shown in (3.22), the inflow rate was adjusted by trial and error until the numerically calculated water level change, fitted with the measured water level change. Figure 4.14 shows an example of water level change comparison between measured and calculated. The figure shows a good fit although there are some errors equal to or less than a centimeter between these two. The errors are mainly because the water level was measured near the outlet and travel time was not considered.

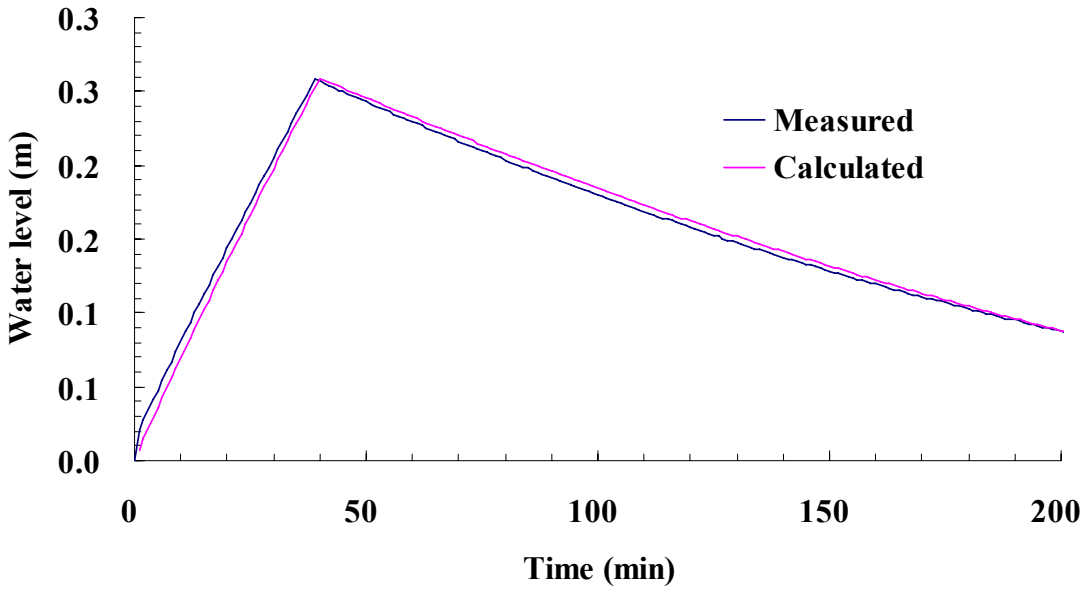

Figure 4.14. Measured and calculated water level change

(B) Event mean concentration, EMC, and particle removal ratio

Samples for measuring SSC can be taken during a storm runoff for only limited times. The interval of taking samples may not be the same through each storm runoff. Specifically, samples should be taken more frequently during a high flow period than during a low flow period because the mass flow rate of particles is greater during a high flow period due to both high flow rate and high particle concentration. The discharged mass of particles in outflow can be estimated by the measured outflow SSC and the estimated outflow rate, as described in the previous section. Figure 4.15 shows a conceptual figure of measured discrete outflow SSC data and continuous estimated outflow data.

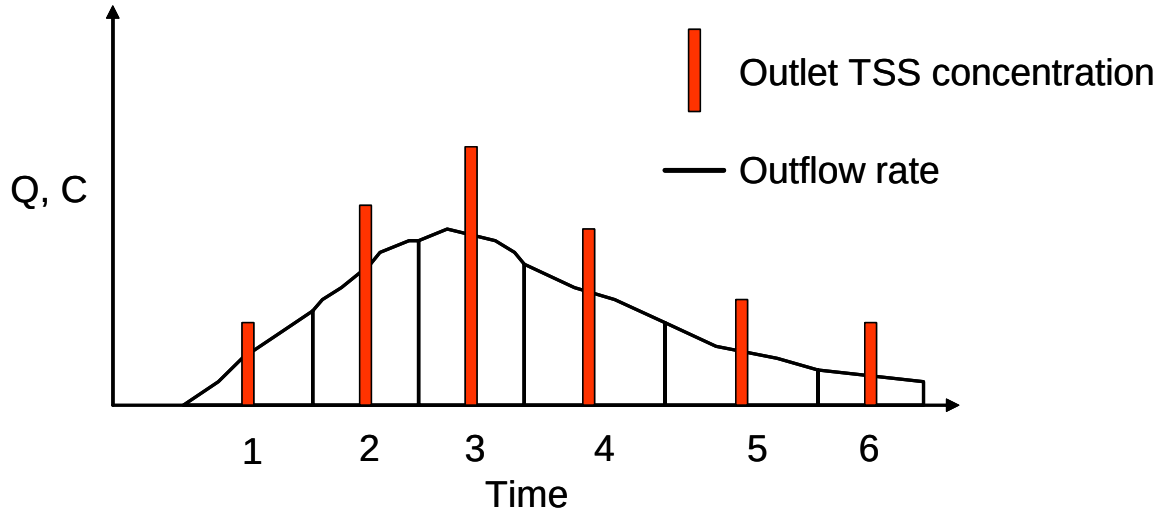

Figure 4.15. Conceptual figure of measured outflow SSC data (discrete) and estimated outflow rate (continuous)

Event Mean Concentration (EMC)

EMC is defined in the following equation;

$$EMC = \frac{M_{out}}{V_{out}} = \frac{\int Q_{out} \cdot C_{out} dt}{\int Q_{out} dt} \tag{4.10}$$

In the case of discrete sampling, the k^{th} value of outflow SSC taken at T_k minutes is the representative value of a group of time which is closer to T_k than T_{k-1} or T_{k+1}. Then, EMC should be estimated as follows:

$$EMC = \frac{\sum_{k=1}^{n} \left\{ C_{out}^{k} \cdot \int Q_{out}^{k} dt \right\}}{\int Q_{out}^{k} dt} \tag{4.11}$$

In the case of Figure 4.15, n=6.

Particle removal ratio

Mass removal ratio of TSS, or simply particle removal ratio, can be defined as follows:

$$R = 1 - \frac{M_{out}}{M_{in}} = 1 - \frac{\int Q_{out} \cdot C_{out} dt}{\int Q_{in} \cdot C_{in} dt} \tag{4.12}$$

In this physical model study, total mass of inflow particles are simply defined as $Q_{in} C_{in} T_s$. Therefore, the mass removal ratio of particle can be estimated as follows:

$$R = 1 - \frac{\sum_{k=1}^{n} \left\{ C_{out}^{k} \cdot \int Q_{out}^{k} dt \right\}}{Q_{in} C_{in} T_s} \tag{4.13}$$

The relationship between EMC and removal ratio is

$$M_{out} = V_{in} \cdot EMC = M_{in}(1 - R)$$

$$\Rightarrow EMC = \frac{M_{in}}{V_{in}}(1 - R) \tag{4.14}$$

Chapter 5 Model Results, Analyses, and Uses

The conceptual model, described in Chapter 3, was developed to explain how sedimentation would occur in a rectangular detention basin under ideal conditions and to estimate removal efficiency of suspended sediment particles. The physical model, explained in Chapter 4, was built to measure the sedimentation performance of a scaled down basin. In this chapter, results from both the physical model and conceptual model are described and compared.

5.1 EXPERIMENTAL RESULTS AND ANALYSIS

5.1.1 Experimental results

(A) Inflow conditions

Hydraulic and setup conditions

Eight experimental runs were conducted with different inflow rates, runoff durations, and inflow SSCs. Table 5.1 shows the summary of inflow conditions including the experimental setups and given hydraulic conditions. Three combinations of setup conditions were tested. Two runs (A and B) were conducted with a smaller orifice area and full length of the basin. The next three (C, D, E) were conducted with a larger orifice area and full length of the basin. The remainder (F, G, H) were conducted with the larger orifice area and 2/3 length of the original sedimentation basin.

Inflow rate, runoff duration, and measured maximum water level are also shown in Table 5.1. Among them, only the inflow rates were calculated values which were fitted to the measured time series water level change based on the method described in section 4.3.3. Inflow volume, V_{in}, and theoretical overflow rate, $Q_{in}/(BL)$, in the table were the calculated values. Theoretical overflow rate is distinguished from overflow rate in this

research. The theoretical overflow rate, the rate of water level increase by ignoring the drainage from outflow is slightly larger than the overflow rate, the rate of water level increase for the filling period. The theoretical overflow rate is often used in this research since outflow rates are negligible compared to inflow rates and easier to calculate. Theoretical overflow rates range from 0.27 m/hr to 1.16 m/hr, which made these eight inflow conditions very different.

Table 5.1. Setup conditions and inflow hydraulic conditions

	Setup conditions		Inflow hydraulic conditions				
	Effective area of orifice, A_e (cm^2)	Basin length, L (m)	Inflow rate, Q_{in} (L/s)	Runoff duration, T_s (min)	Maximum water level, h_{max} (m)	Inflow volume, V_{in} (L)	Theoretical overflow rate, Q_{in}/BL (m/hr)
A	0.43	6.96	0.53	40	0.257	1272	0.44
B	0.43	6.96	0.32	80	0.283	1536	0.27
C	0.48	6.96	0.9	20	0.283	1080	0.75
D	0.48	6.96	1.17	15	0.228	1053	0.98
E	0.48	6.96	0.73	30	0.276	1314	0.61
F	0.48	4.64	0.93	15	0.269	837	1.16
G	0.48	4.64	0.51	30	0.274	918	0.64
H	0.48	4.64	0.32	40	0.212	768	0.40

Inflow SSC

To calculate mean inflow SSC and to check whether or not the inflow particle concentration was uniform enough for each run, 5 to 10 inflow samples were taken from the inlet pipe through the nozzle and SSCs were measured. Figure 5.1 shows measured SSC data with respect to sampling time. The graph shows that all of the inflow SSCs are greater than 150 mg/L and less than approximately 350 mg/L. This inflow SSC range is within the range of TSS in urban runoff recommended by NURP (Table 2.1).

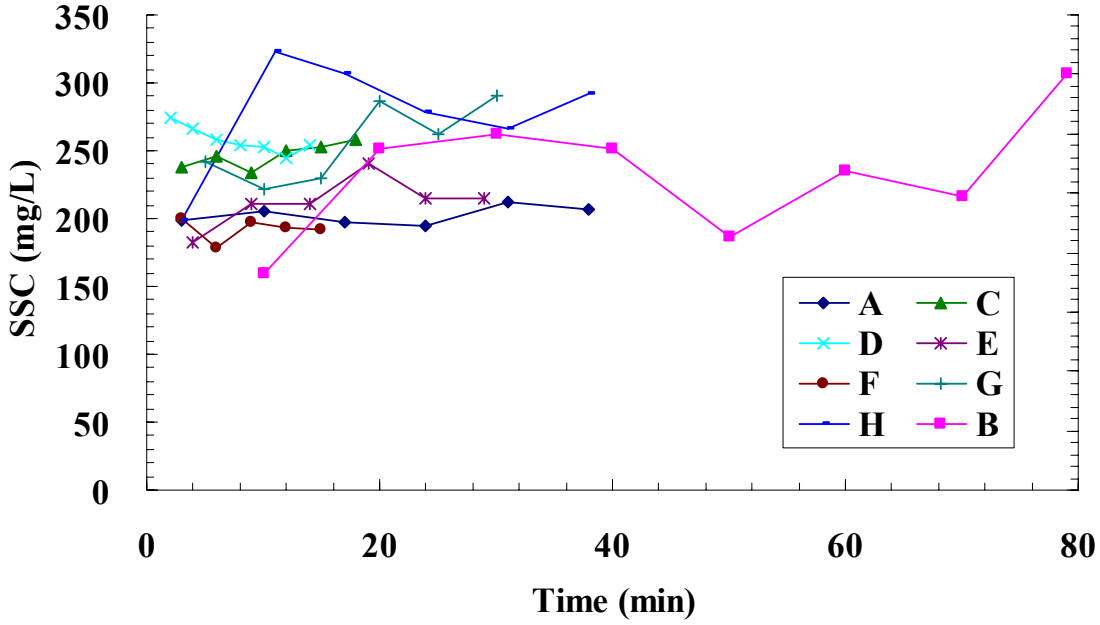

Figure 5.1. Time series inflow SSCs for all eight runs

Mean inflow SSC for each run was calculated by taking an arithmetic average of all the inflow samples SSC because inflow SSC is designed to be constant and samples were taken uniformly over time. Then to check the uniformity of inflow SSCs, a uniformity coefficient was calculated using equation (4.7). Table 5.2 shows mean SSC, total mass of inflow particles, and uniformity coefficient of each run in addition to inflow rate and runoff duration. Overall, uniformity coefficient values are very high, and all of them are much greater than 0.8, which was set as the criteria. Any strong trend such as long term increase or decrease cannot be found from the graph. The table implies that it is difficult to hold inflow SSC uniform when the inflow is very low (*e.g.*, B and H) or duration is very long (*e.g.*, B). Actually, it was very difficult to conduct run B in terms of the uniformity since the flow rate of the peristaltic pump was very low in order to

maintain a certain SSC value for a long time. This might have resulted in sedimentation in the tube.

Table 5.2. Inflow experimental conditions

	Inflow rate, Q_{in} (L/s)	duration, T_s (min)	Mean inflow SSC, C_{in} (mg/L)	Total inflow mass, M_{in} (g)	Uniformity coefficient, CU (-)
A	0.53	40	202	257	0.97
B	0.32	80	267	410	0.85
C	0.9	20	246	266	0.97
D	1.17	15	258	271	0.97
E	0.73	30	212	279	0.95
F	0.93	15	192	161	0.97
G	0.51	30	255	234	0.91
H	0.32	40	277	213	0.89

(B) Outflow SSC and particle removal efficiency

Outflow SSC

Outflow samples were taken periodically for both the filling and emptying periods and their SSCs were measured. Figure 5.2 shows time series SSC change of both inflow and outflow for all the eight runs. Actually, these time series data are difficult to compare since multiple inflow parameters such as inflow rate, runoff duration, and initial SSC are different between runs. Therefore, comparison of time series outflow SSC is done in the next section using the nondimensionalized technique. However, one thing to be noted from the graph is that outflow SSC changes are all very smooth even when the inflow SSC fluctuates significantly such as for run B, G, and H, which implies that the system has the effect of equalization to eliminate the fluctuation of inflow SSC.

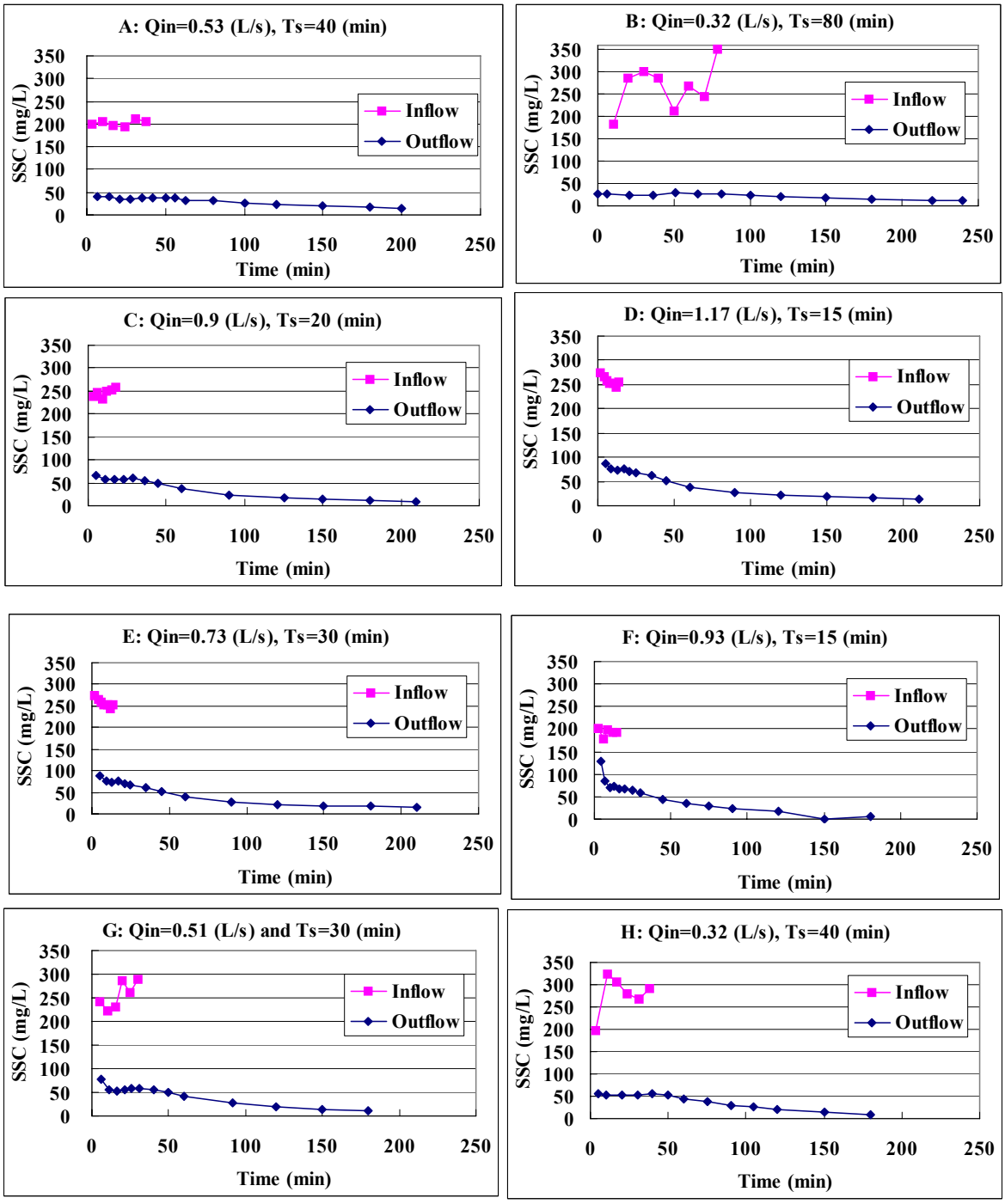

Figure 5.2. Measured inflow and outflow SSC change

Particle Removal efficiency

The calculation method for particle mass removal efficiency was conceptually shown in Chapter 4. Here, the calculation for removal efficiency of each run is shown. Figure 5.3 is a screen shot of the Excel spreadsheet used in the process of removal efficiency calculation for run A.

	A	B	C	D	E	F	G	H	I	J	K
1	Inflow condition (A)	t (min)	h (m)	Q_{out} (L/s)	C_{out} (mg/L)	from (min)	to (min)	v_{out} (L)	m_{out} (g)	Summary	
2	Ts(min)	7	0.06	0.05	40.3	0.0	10.5	29.6	1.2	V_{in} (L)	1272
3	40	14	0.11	0.06	40.3	10.5	17.5	26.1	1.1	V_{out} (L)	932
4	Cin(mg/L)	21	0.15	0.07	34.7	17.5	24.5	31.0	1.1	$V_{residual}$ (L)	340
5	202	28	0.19	0.08	35.8	24.5	31.5	35.1	1.3	M_{in} (g)	257
6	Qin(L/s)	35	0.24	0.09	37.2	31.5	38.5	38.8	1.4	Min M_{out} (g)	26
7	0.53	42	0.25	0.10	37.7	38.5	46.0	43.2	1.6	Max M_{out} (g)	31
8		50	0.24	0.09	37.2	46.0	53.0	39.4	1.5	Max R_{out}	0.90
9		56	0.23	0.09	36.4	53.0	59.5	36.0	1.3	Min R_{out}	0.88
10		63	0.23	0.09	33.0	59.5	71.5	65.1	2.1	Average R_{out}	0.89
11		80	0.20	0.09	31.1	71.5	90.0	95.4	3.0		
12		100	0.18	0.08	26.7	90.0	110.0	97.0	2.6		
13		120	0.16	0.08	21.9	110.0	135.0	113.5	2.5		
14		150	0.13	0.07	21.1	135.0	165.0	122.8	2.6		
15		180	0.10	0.06	18.8	165.0	190.0	91.6	1.7		
16		200	0.09	0.06	14.8	190.0	210.0	67.6	1.0		

Figure 5.3. Excel spreadsheet to calculate removal efficiency

Column A: The inflow conditions consisting of runoff duration, Ts (min), mean inflow SSC, Cin (mg/L), and inflow rate, Qin (L/s), are listed here.

Column B: Time of each sampling (min).

Column C: Measured water level (m) at the time of sampling.

Column D: Calculated outflow rate (L/s) at the time of sampling using the orifice equation.

Column E: Measured SSC (mg/L) at the time of sampling.

Column F and G: Start time (min) and end time (min) during the sampling period. The sampling time is assumed to be in the middle of the range.

Column H: Volume (L) of water discharged from time F to time G, which is calculated by D*(G-F)*60.

Column I: Mass (g) of particles discharged from time F to time G, which is calculated by E*H/1000.

Cell (K2): Total volume of inflow water (L), calculated by A3*A7*60.

Cell (K3): Total outflow volume from the beginning of runoff to the end time represented by the last sampling, calculated by the sum of column H.

Cell (K4): Volume of water that remained in the tank after the end of the last sampling, calculated by Cell (K3)- Cell (K2).

Cell (K5): Total mass of inflow particles (g), calculated by total inflow volume multiplied by mean inflow SSC.

Cell (K6): Minimum mass of discharged particles (g), calculated by the sum of column I.

Cell (K7): Maximum mass of discharged particles (g) assuming all the residual water drained out with the SSC at the last sampling, calculated by Cell(K6)+Cell(K4)*Cell(E16)/1000.

Cell (K8): Minimum removal ratio, calculated by 1-Cell(K6)/Cell(K5).

Cell (K9): Maximum removal ratio, calculated by 1-Cell(K7)/Cell(K5).

Cell(K10): Removal ratio, average value of Cell(K8) and Cell(K9).

Maximum and minimum calculated values of total discharged particle mass, M_{in}, removal efficiency, and EMC are shown in Table 5.3 with the inflow mean SSC, C_{in}, and the total inflow mass, M_{in}. For practical reasons, the average of maximum and minimum removal efficiencies are considered as the removal efficiency of each run, which was calculated in Cell (K10). This is because maximum and minimum values of removal efficiencies are all very close to each other. The table shows removal efficiencies are over 86% except in run F, which was conducted with the highest theoretical overflow rate (1.16 m/hr see Table 5.1) and had the removal ratio of only 82%. Figure 5.4 shows the

relationship between removal ratio and theoretical overflow rate. This figure shows that the larger the overflow rate is, the worse the removal efficiency is, but it is not a very strong relationship. These data are further analyzed in the next section with the assistance of nondimensionalization.

Table 5.3. Removal efficiency and EMC of each run

	Inflow mean SSC, C_{in} (mg/L)	Total mass of inflow particle, M_{in} (g)	Total mass of discharged particle, M_{out} (g)		Removal efficiency		EMC (mg/L)	
			Min	Max	Max	Min	Min	Max
A	202	257	26	31	0.90	0.88	20	24
B	267	410	27	30	0.93	0.93	17	19
C	246	266	29	30	0.89	0.89	27	28
D	258	271	34	36	0.87	0.87	33	34
E	212	279	32	34	0.88	0.88	25	26
F	192	161	28	29	0.82	0.82	34	35
G	255	234	31	32	0.87	0.86	34	35
H	277	213	26	27	0.88	0.88	34	35

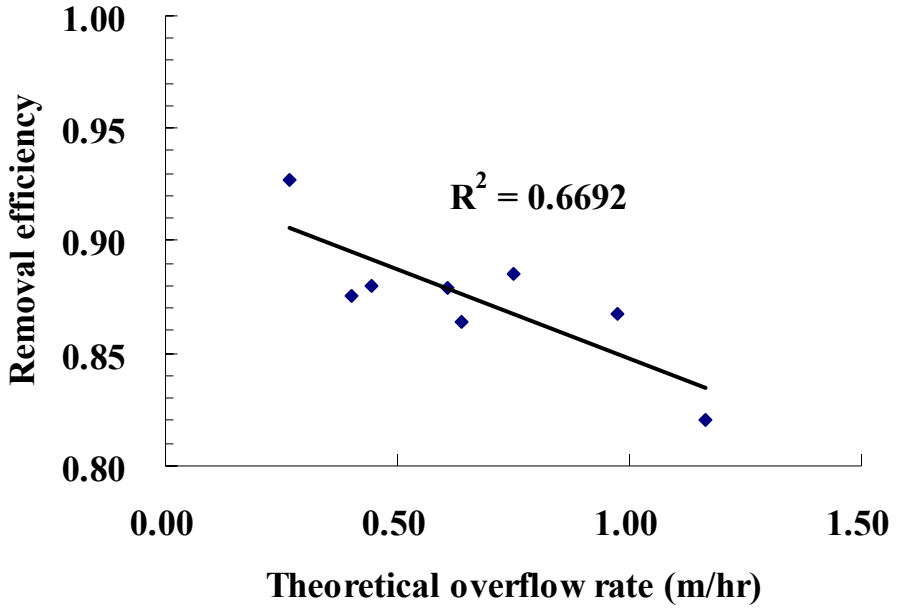

Figure 5.4. Relationship between removal efficiency and theoretical overflow rate

5.1.2 Nondimensionalization of outflow SSC and its analysis

Although time series outflow SSCs and removal efficiencies of all runs were shown in the previous section, they are difficult to compare. For example, all the graphs in Figure 5.2 shouldn't be overlapped since both the concentration and time scale is different. Differences in the concentration scale can be treated by nondimensionalizing the outflow SSC by mean inflow SSC for each run.

$$C^* = \frac{C_{out}}{C_{in}} \tag{5.1}$$

However, differences in time scale are not compared as easily since the time scale for the filling period and emptying period is different. The filling period ends at the end of the runoff duration which is different for each run. The end of the emptying period is governed by the orifice size and maximum water level at the end of filling period, both of which are different for each run. In this section, time nondimensionalization is considered first, and then outflow SSC for each run is compared.

(A) Nondimensionalization of time and outflow SSC

Nondimensionalization of time was done such that all runs have the same filling and emptying period in the nondimensionalized time scale. This allows all the experimental data can be compared in a single graph. First, water level was nondimensionalized simply by the maximum water level. This is because the time scale is dominated by the maximum water level and orifice size during the emptying period.

$$h^* = \frac{h}{h_{max}} \tag{5.2}$$

The nondimensionalization of time is shown here. For the filling period, time was simply nondimensionalized by runoff duration, which is the end time of the filling period so that filling periods of all runs end at the same nondimensionalized time.

$$t_F^* = \frac{t}{T_s} \tag{5.3}$$

For emptying period, water level change is controlled by the outlet orifice. The relationship between water level and time was defined as equation (4.4), and this equation can be modified by nondimensionalized h* as

$$\begin{aligned} &\sqrt{h_{max}} - \sqrt{h} = \frac{A_e}{B \cdot L}\sqrt{\frac{g}{2}}(t - T_s) \\ &\Rightarrow 1 - \sqrt{h^*} = \frac{A_e}{B \cdot L\sqrt{h_{max}}}\sqrt{\frac{g}{2}}(t - T_s) = t_E^* \end{aligned} \tag{5.4}$$

The right hand side of this equation can be defined as the nondimensionalized time for emptying period, t_E^*, so that t_E^* is equal to one when the water is completely drained (h*=0) at the end of the emptying period. Finally, overall nondimensionalized time can be expressed as

$$t^* = \begin{cases} t_F^* = \dfrac{t}{T_s} & \text{for } t \le T_s \\ 1 + t_E^* = 1 + \dfrac{A_e}{B \cdot L\sqrt{h_{max}}}\sqrt{\dfrac{g}{2}}(t - T_s) & \text{for } t > T_s \end{cases} \tag{5.5}$$

The water level change with the defined nondimensionalized time is plotted in Figure 5.5. The nondimensionalized filling period starts from t*=0 and ends at t*=1, then nondimensionalized emptying period starts from t*=1 and ends at t*=2. As shown herein, the scaling method is different between the filling period and the emptying period. While the length of nondimensionalized filling period and the nondimensionalized emptying period are the same, actual filling period is much shorter than the emptying period.

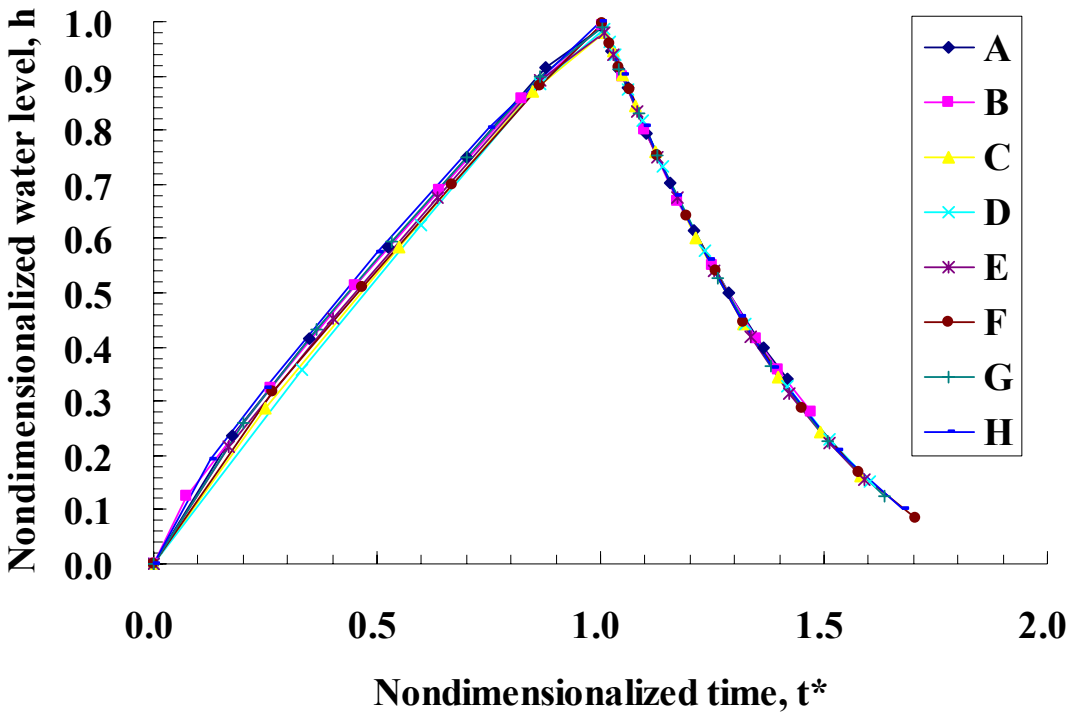

Figure 5.5. Water level change with time in nondimensionalized form

The change in water level can be simplified using the redefined time and water level;

$$h^* \approx t^* \quad \text{for } t^* \le 1$$
$$h^* = (2 - t^*)^2 \quad \text{for } 1 \le t^* \le 2 \tag{5.6}$$

h* cannot be exactly the same as t* for the filling period because there were outflows during this period. h* can be equal to t* only when there is no outflow in the filling period. Next, nondimensionalized outflow SSC, defined by equation (5.1), was plotted on the nondimensionalized scale as shown in Figure 5.6.

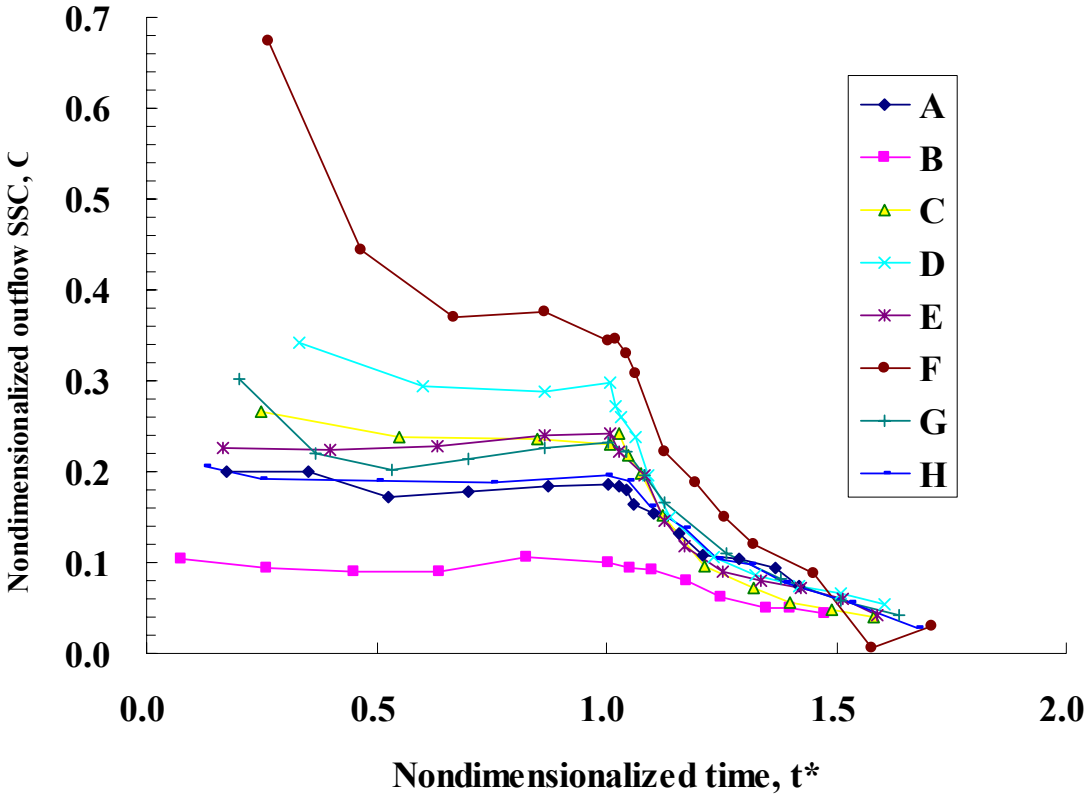

Figure 5.6. Outflow SSC change with time in nondimensionalized form

The graph shows the following three characteristics:

- Some runs have strong initial drops of outflow SSC (*e.g.*, run F and G)
- After the initial drops, SSCs are nearly constant throughout filling period.
- SSCs drop exponentially during the emptying period

The initial SSC drops were considered as the resuspension effect from previous runs and were not considered in depth for this research. The change in SSC data is further analyzed in the next section.

(B) Analysis of nondimensionalized outflow SSC

Filling period

Now it is appropriate to analyze the time series outflow SSC data. Assume outflow SSC is a constant throughout the filling period as seen in Figure 5.6, excluding the initial drop of SSC. The SSC for the filling period, C_F^*, was compared with the theoretical overflow rate, Q_{in}/BL in Figure 5.6. C_F^* was calculated from the arithmetic average of two C* from before t*=1.0 and one from after or exactly at t*=1.0. Figure 5.7 suggests that SSC for the filling period has a strong relationship with theoretical overflow rate. Interestingly, this relationship (R^2=0.94) is slightly better than the relationship between C_F^* and real overflow rate, h_{max}/Ts, which has the R^2=0.92.

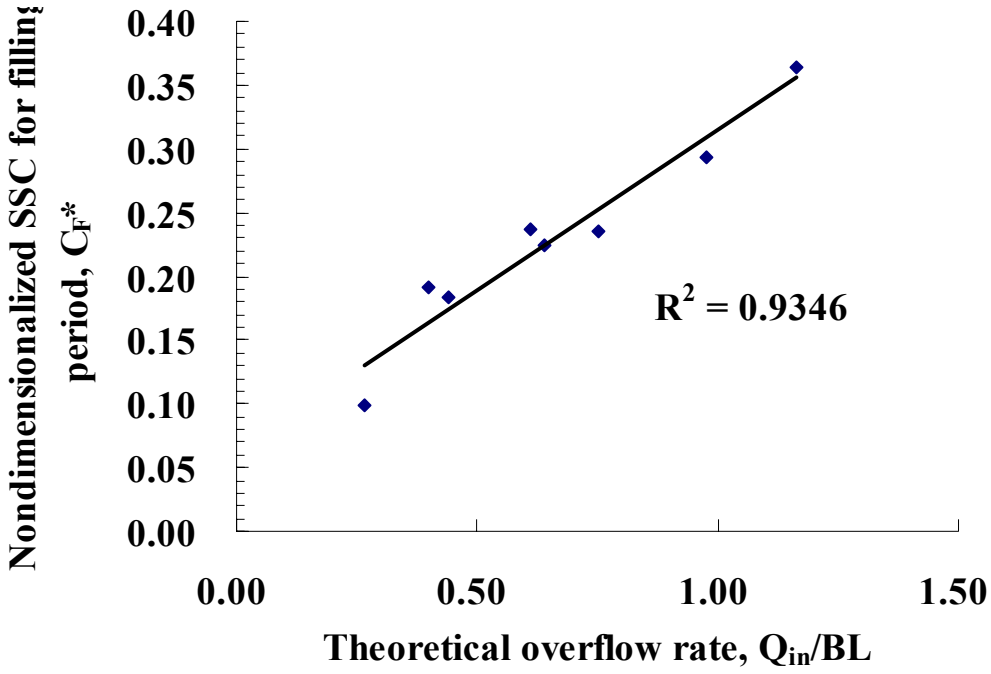

Figure 5.7. Relationship between theoretical overflow rate and average nondimensionalized SSC for filling period

The CSTR (Continuous Stirred Tank Reactor) model with effective particle settling velocity was introduced to understand the relationship between theoretical overflow rate and average nondimensionalized SSC for filling period. The mass balance of water for the filling period is

$$\frac{dh}{dt} = \frac{Q_{in}}{BL} - \frac{Q_{out}}{BL} \tag{5.7}$$

The mass balance of particle, on the other hand, is

$$\frac{dM}{dt} = Q_{in}C_{in} - v_s CBL - Q_{out}C \tag{5.8}$$

Where M is the mass of particles suspended in the basin and v_s is the effective settling velocity and C is the SSC in the basin that is equal to the outflow SSC. LHS of equation (5.8) can be decomposed as follows by setting the concentration in the tank constant throughout the filling period.

$$\frac{dM}{dt} = \frac{d(hBLC)}{dt} = BL\frac{d(hC)}{dt} \approx BLC\frac{dh}{dt} \tag{5.9}$$

Then the mass balance equation for particles can be simplified as

$$\begin{aligned} BLC\frac{dh}{dt} &= Q_{in}C_{in} - v_s CBL - Q_{out}C \\ C\left(BL\frac{dh}{dt} + BLv_s + Q_{out}\right) &= Q_{in}C_{in} \\ \frac{C}{C_{in}} &= \frac{Q_{in}}{BL\frac{dh}{dt} + BLv_s + Q_{out}} \end{aligned} \tag{5.10}$$

This can be simplified using the mass balance of water, equation (5.7), as

$$\begin{aligned} \frac{C}{C_{in}} = C_F^* &= \frac{Q_{in}}{Q_{in} + BLv_s} = \frac{1}{1 + \frac{BLv_s}{Q_{in}}} \\ \Rightarrow \frac{1}{C_F^*} - 1 &= v_s\frac{BL}{Q_{in}} \end{aligned} \tag{5.11}$$

Figure 5.8 plots this relationship. This figure shows the effective settling velocity, v_s, is constant and the value is approximately 2.17 m/hr. In Figure 5.8, the far right point has a

big impact to determine the gradient of the trend line since the gradient will be 1.98 m/hr and the R^2 value is 0.78 without the far right point. Therefore, the accuracy of the gradient should be enhanced by taking more data in the future. However 2.17 m/hr will be used as the gradient value in the dissertation because there is no reason to exclude this far right point.

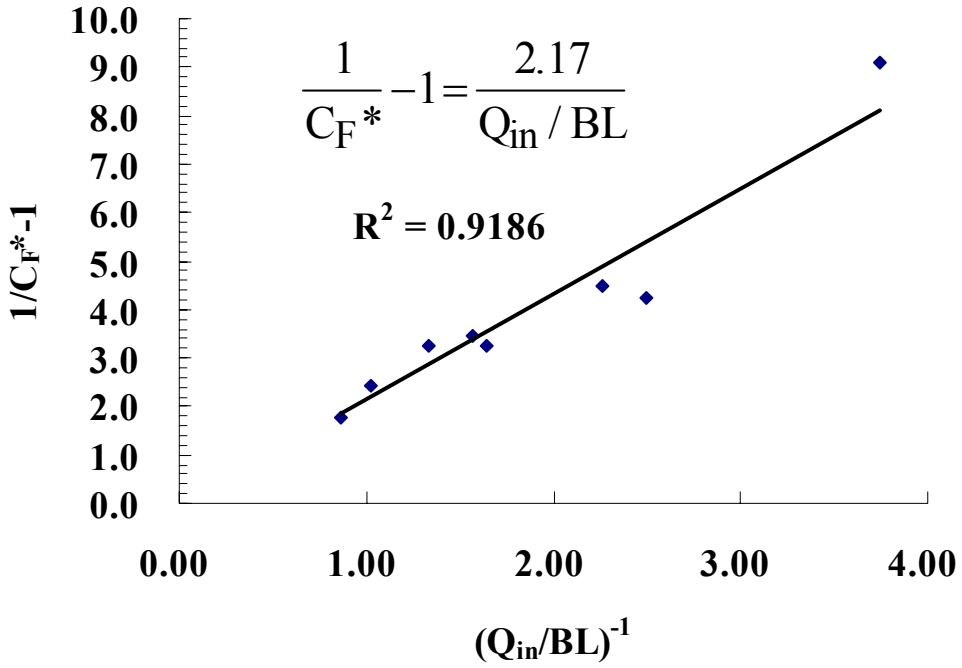

Figure 5.8. Effective particle settling velocity

Here the calculated effective settling velocity, 2.17 m/hr is much higher than mean settling velocity of inflow particles 0.5 m/hr. This difference may be mainly from the assumption that SSC in the basin is equal to the outlet SSC. In reality, the basin cannot be a CSTR and the concentration in the basin is a function of time and location. Therefore, average SSC in the basin should be higher than outlet SSC. However, this CSTR model works well with the calibrated effective settling velocity to estimate the

outflow SSC for the filling period. Finally, nondimensionalized SSC for filling period, C_F^*, can be calculated as follows.

$$C_F^* = \frac{1}{1 + 2.17\dfrac{BL}{Q_{in}}} \tag{5.12}$$

This equation form would work for other rectangular settling basins, although the effective settling velocity, v_s, may change when particle is different or the basin size is very different.

Emptying period

To see the rate of outflow SSC decline, outflow SSC was divided by the SSC at the end of filling period, and the ratio of outflow SSC for the emptying to the average outflow SSC for the filling, C_E^* / C_F^*, was plotted with respect to time in Figure 5.9. This figure shows an interesting feature. There exist two curves; one for A and B, and the other for C through H. The only difference between runs A and B and runs C through H is the effective orifice size as shown in Table 5.1. This suggests sedimentation during the emptying period is highly dominated by the rate of drop in water level.

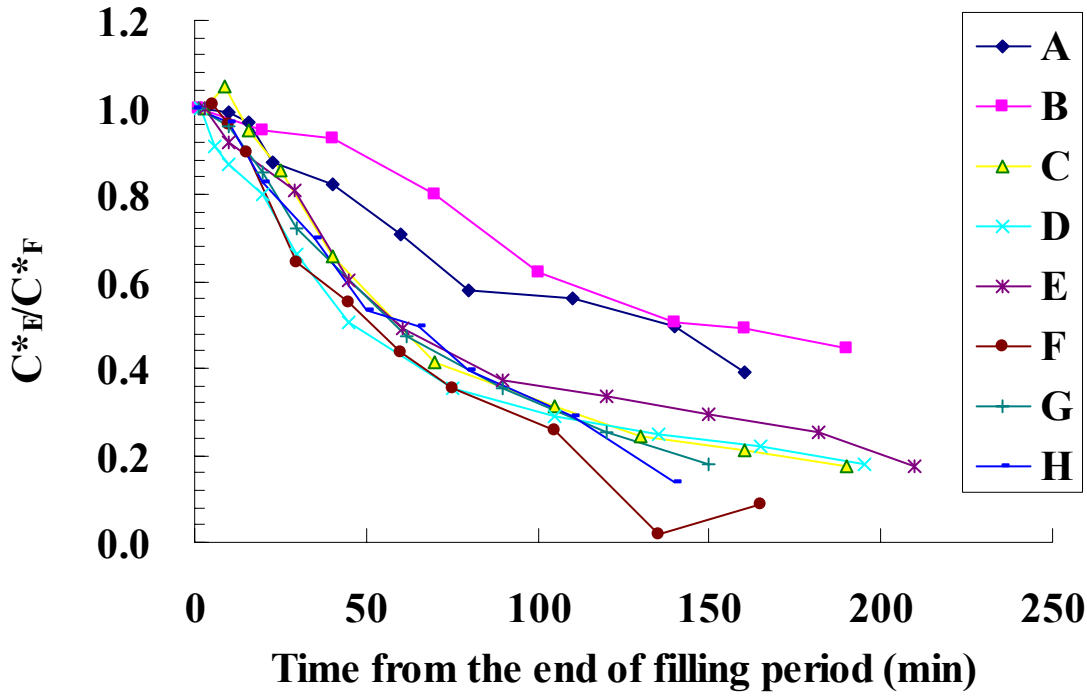

Figure 5.9. Rate of SSC change for emptying period

Mass balance of water in emptying period is

$$\frac{dh}{dt} = -\frac{Q_{out}}{BL} \tag{5.13}$$

Mass balance for particles can be described in the CSTR model with a new effective settling velocity, v_s, for the emptying period as follows and simplified with (5.13).

$$\begin{aligned} \frac{dM}{dt} &= BL\frac{d(Ch)}{dt} = -v_s CBL - Q_{out}C \\ \frac{d(Ch)}{dt} &= -v_s C - \frac{Q_{out}}{BL}C = \left(-v_s + \frac{dh}{dt}\right)C \\ C\frac{dh}{dt} + h\frac{dC}{dt} &= \left(-v_s + \frac{dh}{dt}\right)C \\ \frac{dC}{C} &= \frac{-v_s}{h}dt \end{aligned} \tag{5.14}$$

Here, assume the effective settling velocity is proportional to the change in water level, dh/dt.

$$v_s = -k\frac{dh}{dt} \tag{5.15}$$

Equation (5.14) can be analytically integrated after substituting (5.15) for (5.14) and integrating as follows:

$$\begin{aligned}
&\frac{dC}{C} = k\frac{dh}{h} \\
&\left[\ln(C)\right]_{C_F^*}^{C_E^*} = k\left[\ln(h)\right]_{h_{max}}^{h} \\
&\Rightarrow \ln\left(\frac{C_E^*}{C_F^*}\right) = k\ln\left(\frac{h}{h_{max}}\right) = k\ln(h^*) \\
&\Rightarrow \frac{C_E^*}{C_F^*} = (h^*)^k
\end{aligned} \tag{5.16}$$

Figure 5.10 shows the data follow this relationship when k is 0.98, which is very close to 1.0. k=1.0 in equation (5.15) means the particle settling velocity is the same as the rate of drop in water level for emptying period and the driving force of particle settling is not particle's own settling velocity but the water level drop.

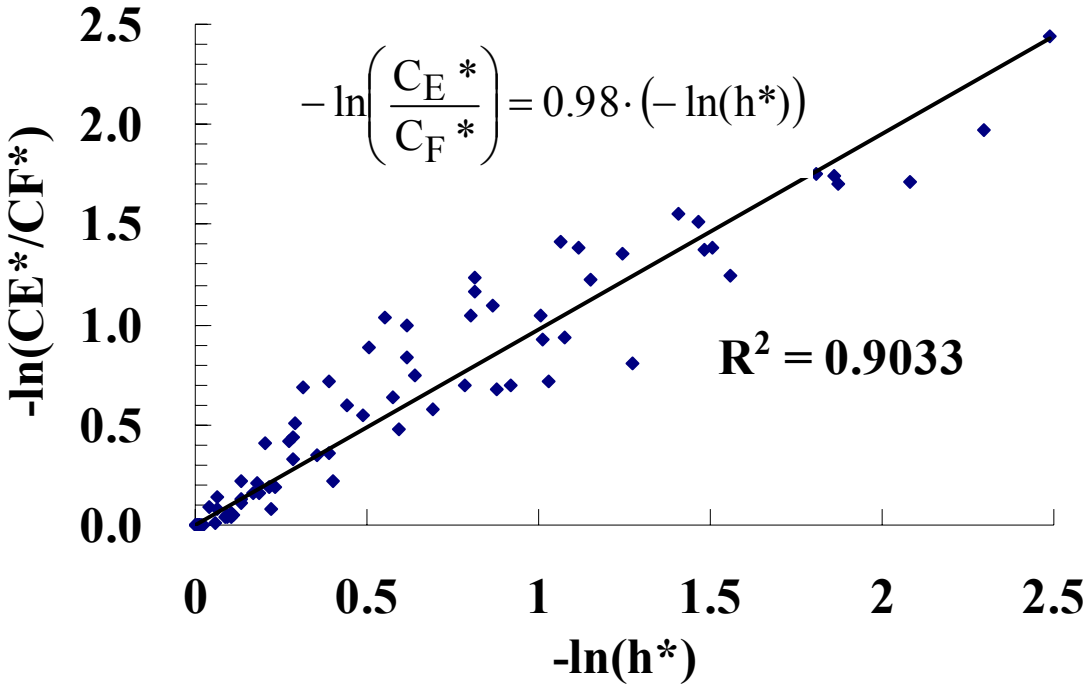

Figure 5.10. Relationship in equation (5.16)

Therefore, nondimensionalized outflow SSC during the emptying period can be simplified by setting k equal to 1.0.

$$\frac{C_E^*}{C_F^*} = h^* = (2 - t^*)^2$$
$$\Rightarrow C_E^* = C_F^* \cdot (2 - t^*)^2 \tag{5.17}$$

Nondimensionalized outflow SSC for the entire period, C*, can be summarized as follows;

$$C^* = \begin{cases} C_F^* = \dfrac{1}{1 + 2.17\dfrac{BL}{Q_{in}}} & \text{for } 0 \le t^* \le 1 \text{ (filling period)} \\ C_E^* = C_F^*(2 - t^*)^2 & \text{for } 1 \le t^* \le 2 \text{ (emptying period)} \end{cases} \tag{5.18}$$

To see how this relationship fits with the measured time series outflow SSC, C^*/C_F^* was calculated as follows and the relationship was compared with measured data in Figure 5.11. The graph shows the equation fits well with measured data.

$$\frac{C^*}{C_F^*} = \begin{cases} 1 & \text{for } 0 \le t^* \le 1 \text{ (filling period)} \\ (2 - t^*)^2 & \text{for } 1 \le t^* \le 2 \text{ (emptying period)} \end{cases} \tag{5.19}$$

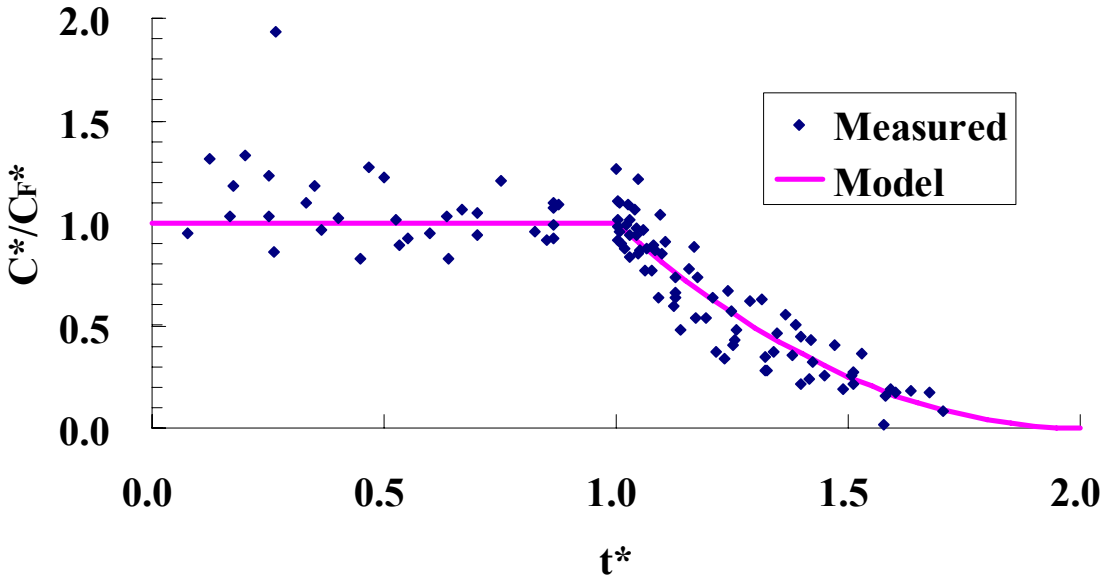

Figure 5.11. Measured and calculated change of C^*/C_F^* with respect to nondimensionalized time

Also, the measured outflow SSC and calculated outflow SSC using equation (5.18) were plotted in Figure 5.12 for the normalized time scale. The figure shows that the decline of measured outflow SSC for the emptying period of run C, D, and F are much steeper than the estimation curve. Actually, Run C, D, and F have the top three highest theoretical overflow rates (see Table 5.1) and three shortest runoff durations,

which implies that the larger overflow rate kept the basin more turbulent during the filling period and didn't allow bigger particles to settle out. However, runs with moderate overflow rates and longer durations had enough time for larger particles to settle out for filling period, and the settling velocity is almost same as the change in water level velocity for the emptying period. So, this empirical model, developed from experimental results, should work better for slower runoff events when compared to rapid runoffs.

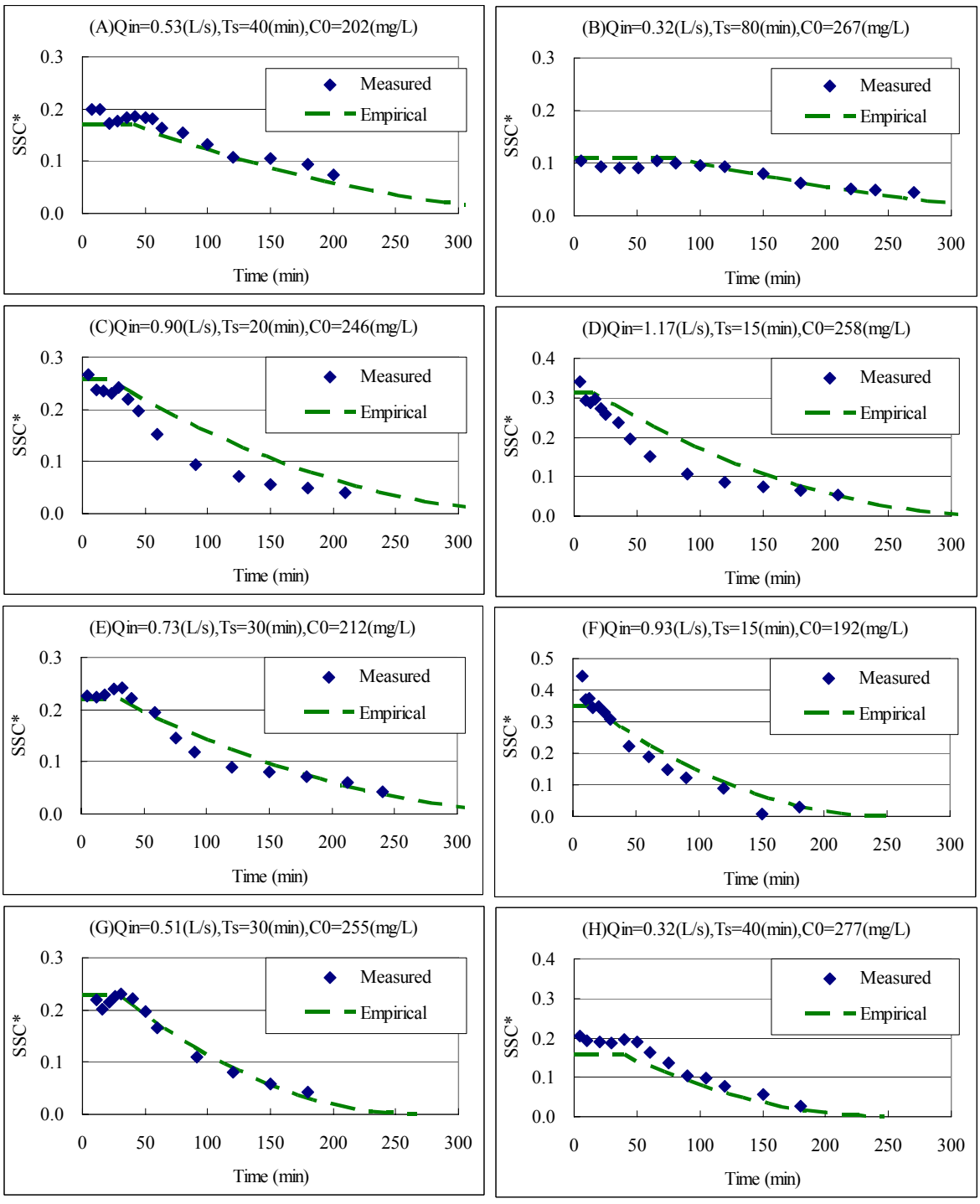

Figure 5.12. Measured and empirically calculated time series outflow SSC

(C) Empirical Model for calculating removal efficiency

Removal ratio can be calculated using the empirically developed CSTR model in the previous sections. The process to calculate removal efficiency from the CSTR model is shown below.

Nondimensionalization of outflow rate and particle mass rate in outflow

Outflow rate can be calculated as a function of nondimensionalized time as follows:

$$Q_{out}(t^*) = A_e\sqrt{2gh(t^*)} \tag{5.20}$$

This outflow rate can be nondimensionalized by the maximum outflow rate as

$$Q^*_{out}(t^*) = \frac{Q_{out}(t^*)}{Q_{out,max}(t^*)} = \frac{A_e\sqrt{2gh(t^*)}}{A_e\sqrt{2gh_{max}}} = \sqrt{\frac{h(t^*)}{h_{max}}} = \sqrt{h^*} \tag{5.21}$$

h* in equation (5.21) can be replaced by t* using (5.6) as

$$\begin{aligned} Q^*_{out}(t^*) &\approx \sqrt{t^*} \quad \text{for } 0 \le t^* \le 1 (\text{filling period}) \\ &= 2 - t^* \quad \text{for } 1 \le t^* \le 2 (\text{emptying period}) \end{aligned} \tag{5.22}$$

Then, the nondimensionalized outflow mass rate of particles can be defined as the multiplication of nondimensionalized SSC and outflow rate as

$$\begin{aligned} M^*(t^*) &= C^*(t^*) \cdot Q^*(t^*) \\ &\approx C^*_F\sqrt{t^*} \quad \text{for } 0 \le t^* \le 1 (\text{filling period}) \\ &= C^*_F(2 - t^*)^3 \quad \text{for } 1 \le t^* \le 2 (\text{emptying period}) \end{aligned} \tag{5.23}$$

Removal efficiency calculation

Here, the process for calculating removal efficiency is presented.

Total particle mass in inflow can be calculated as

$$M_{in} = Q_{in} \cdot C_{in} \cdot T_s \tag{5.24}$$

Total particle mass in outflow is the sum of particle mass for the filling and the emptying period.

For the filling period, particle mass in outflow, $M_{out,F}$, can be calculated as

$$M_{out,F} = \int_0^{T_s} Q_{out}(t)C_{out}(t)dt$$
$$= Q_{out,max}.C_{in} \int_0^{T_s} Q^*_{out}(t)C^*_{out}(t)dt \quad (5.25)$$

This equation can be further transformed by replacing t with t* as follows:

$$t = T_s t^*$$
$$dt = T_s dt^*$$
$$\text{for the range of}$$
$$t : 0 \rightarrow T_s \quad (5.26)$$
$$t^* : 0 \rightarrow 1$$

Therefore, total mass of particles flowing out during the filling period is

$$M_{out,F} = Q_{out,max}.C_{in} \cdot C^*_F \cdot T_s \int_0^1 Q^*_{out}(t^*)C^*_{out}(t^*)dt^*$$
$$= Q_{out,max}.C_{in} \cdot C^*_F \cdot T_s \int_0^1 \sqrt{h^*}dt^*$$
$$\approx Q_{out,max}.C_{in} \cdot C^*_F \cdot T_s \int_0^1 \sqrt{t^*}dt^* \quad (5.27)$$
$$= Q_{out,max}.C_{in} \cdot \frac{2C^*_F \cdot T_s}{3}$$

In this equation, $\int_0^1 \sqrt{h^*}dt^*$ is approximated by $\int_0^1 \sqrt{t^*}dt^*$ using $h^* \approx t^*$ for the filling period. In order to check how much error this approximation has, the most deviated case, which is run H in Figure 5.5 was analyzed. As a result, the real value of $\int_0^1 \sqrt{h^*}dt^*$ was 0.70, while $\int_0^1 \sqrt{t^*}dt^*$ was 0.67, which has approximately 4% error for the worst case, run H. This means equation (5.27) would slightly underestimate particle mass in outflow for the filling period, but with no greater than 4% error.

For the emptying period, in the same manner, total mass of discharged particles is

$$M_{out,E} = \int_{T_s}^{T_{out}} Q_{out}(t)C_{out}(t)dt$$

$$= Q_{out,max}.C_{in} \cdot \int_{T_s}^{T_{out}} Q^*_{out}(t)C^*_{out}(t)dt \tag{5.28}$$

where

$$T_{out} = T_s + \frac{A_e}{BL}\sqrt{\frac{g}{2h_{max}}}$$

Here, t was replaced by t* using equation (5.5) as follows:

$$t^* = 1 + \frac{A_e}{B \cdot L\sqrt{h_{max}}}\sqrt{\frac{g}{2}}(t - T_s)$$

$$\frac{B \cdot L}{A_e}\sqrt{\frac{2h_{max}}{g}}dt^* = dt \tag{5.29}$$

for the range of

$t : T_s \rightarrow T_{out}$

$t^* : 1 \rightarrow 2$

The particle mass in outflow for the emptying period can be calculated by replacing t with t* using equation (5.29) as follows:

$$M_{out,E} = Q_{out,max}.C_{in} \cdot \frac{C^*_F \cdot BL}{A_e}\sqrt{\frac{2h_{max}}{g}}\int_1^2 (2 - t^*)^3 dt^*$$

$$= Q_{out,max}.C_{in} \cdot \frac{C^*_F \cdot BL}{4A_e}\sqrt{\frac{2h_{max}}{g}} \tag{5.30}$$

$$= \frac{1}{2}C_{in}C_F^* BLh_{max}$$

Finally, the total particle mass in outflow can be calculated for the sum of equation (5.27) and (5.30).

$$M_{out} = M_{out,F} + M_{in,E}$$

$$\approx C_{in}C^*_F\left\{\frac{2}{3}T_sQ_{out,max} + \frac{1}{2}BLh_{max}\right\} \tag{5.31}$$

The removal efficiency can be calculated from the particle mass in inflow, equation (5.24), and in outlflow, equation (5.31), as follows:

$$\begin{aligned} R &= 1 - \frac{M_{out}}{M_{in}} \\ &\approx 1 - \frac{C_F^* \left\{ \frac{2}{3} T_s Q_{out,max} + \frac{1}{2} BLh_{max} \right\}}{Q_{in} \cdot T_s} \\ &= 1 - \frac{1}{1 + \frac{2.17}{Q_{in}/BL}} \cdot \left(\frac{2}{3} \frac{A_e \sqrt{2gh_{max}}}{Q_{in}} + \frac{1}{2} \frac{h_{max} BL}{Q_{in} T_s} \right) \end{aligned} \tag{5.32}$$

This equation was used to examine how drainage time affects removal ratio. Inflow and setup conditions of Run A were used for an example. Several different effective orifice areas were used to evaluate the relationship between effective orifice area, A_e, and removal ratio, R. The ratio of particle mass released during the filling period to the total mass is called η_F and the same ratio for emptying period is called η_E. They can be expressed as

$$R = 1 - \eta_F - \eta_E$$

where

$$\begin{aligned} \eta_F &= \frac{1}{1 + \frac{2.17}{Q_{in}/BL}} \cdot \frac{2}{3} \frac{A_e \sqrt{2gh_{max}}}{Q_{in}} \\ \eta_E &= \frac{1}{1 + \frac{2.17}{Q_{in}/BL}} \cdot \frac{1}{2} \frac{h_{max} BL}{Q_{in} T_s} \end{aligned} \tag{5.33}$$

The particle mass ratios released during the filling, η_F, and during the emptying, η_E, were calculated and the results were plotted in Figure 5.13. This figure shows that overall removal efficiency, $R = 1 - \eta_F - \eta_E$, will decrease if drainage time is longer, but the ratio of released mass during the emptying period is decreased if the drainage time is shorter.

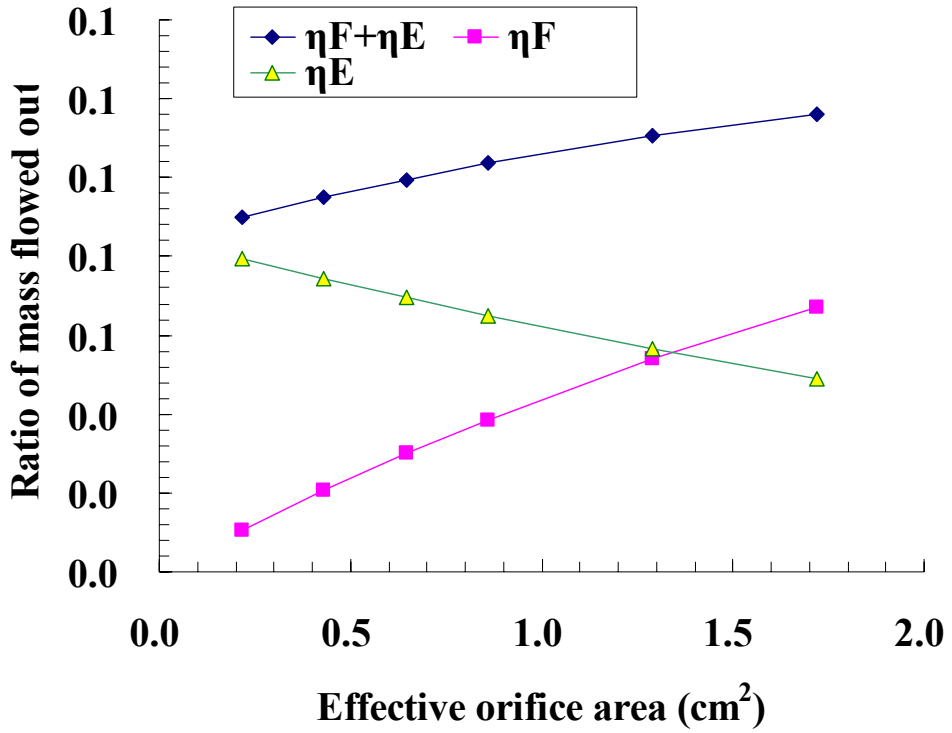

Figure 5.13. Ratio of mass flowed out during filling and emptying and their sum with respect to effective orifice area

Table 5.4 shows the measured and calculated removal ratio using equation (5.32) for all eight runs, as well as the calculated error, which is the calculated removal efficiency minus measured removal efficiency. Calculated removal efficiencies should be greater than the measured values since the calculated values don't take resuspension into account, thereby overestimating the results. However, runs C, D, and F have large negative errors, which means the deviation of outflow SSC calculated for the emptying period, shown in Figure 5.12, affected the removal efficiency calculation by this amount.

Table 5.4. Calculated and measured ratio of outflow SSC to inflow SSC for filling period, C^*_F, and removal efficiency

	Measured CF*	Modeled CF*	Calculated R	Measured removal efficiency	Error (calculated-measured) (%)
A	0.18	0.17	0.91	0.89	1.6
B	0.10	0.11	0.93	0.93	0.2
C	0.23	0.26	0.83	0.89	-5.5
D	0.29	0.31	0.84	0.87	-3.4
E	0.24	0.22	0.88	0.88	-0.3
F	0.36	0.35	0.81	0.82	-1.1
G	0.22	0.23	0.87	0.87	0.4
H	0.19	0.16	0.91	0.88	3.0

The CSTR model was developed to pursue simplicity and make the best use of experimental results. The CSTR model is accurate in estimating both outflow SSC and removal efficiency, especially for slower storms. Also, the particle removal efficiency can be easily calculated if effective settling velocity is known for the filling period. The effective settling velocity might be a function of both the size and shape of the detention basin, and inflow particle settling velocities. Therefore, more data should be taken with different shapes and sizes of basins including prototype to see if the model equation works well. If so, methods to determine the effective settling velocity should be determined and studied more.

5.2 CONCEPTUAL MODEL AND ANALYSIS

5.2.1 Conceptual model results

In the previous section, experimental results were nondimensionalized so that they could be easily compared, and the behavior of time series outflow SSC was explained using the CSTR model with effective particle settling velocity. In this section, the developed conceptual model is examined by comparison with experimental results.

Conceptual model results were compared with experimental results using three parameters: change in water level, outflow SSC, and particle removal efficiency.

Water level change

Water level change was measured every minute during the run. The water level change was used for the conceptual model to determine water balance in the basin. Water level change was explicitly calculated numerically using equation (3.23) for the entire period. Figure 5.14 shows experimental and calculated results of water level change. This figure shows that the water level was accurately calculated by the numerical calculation.

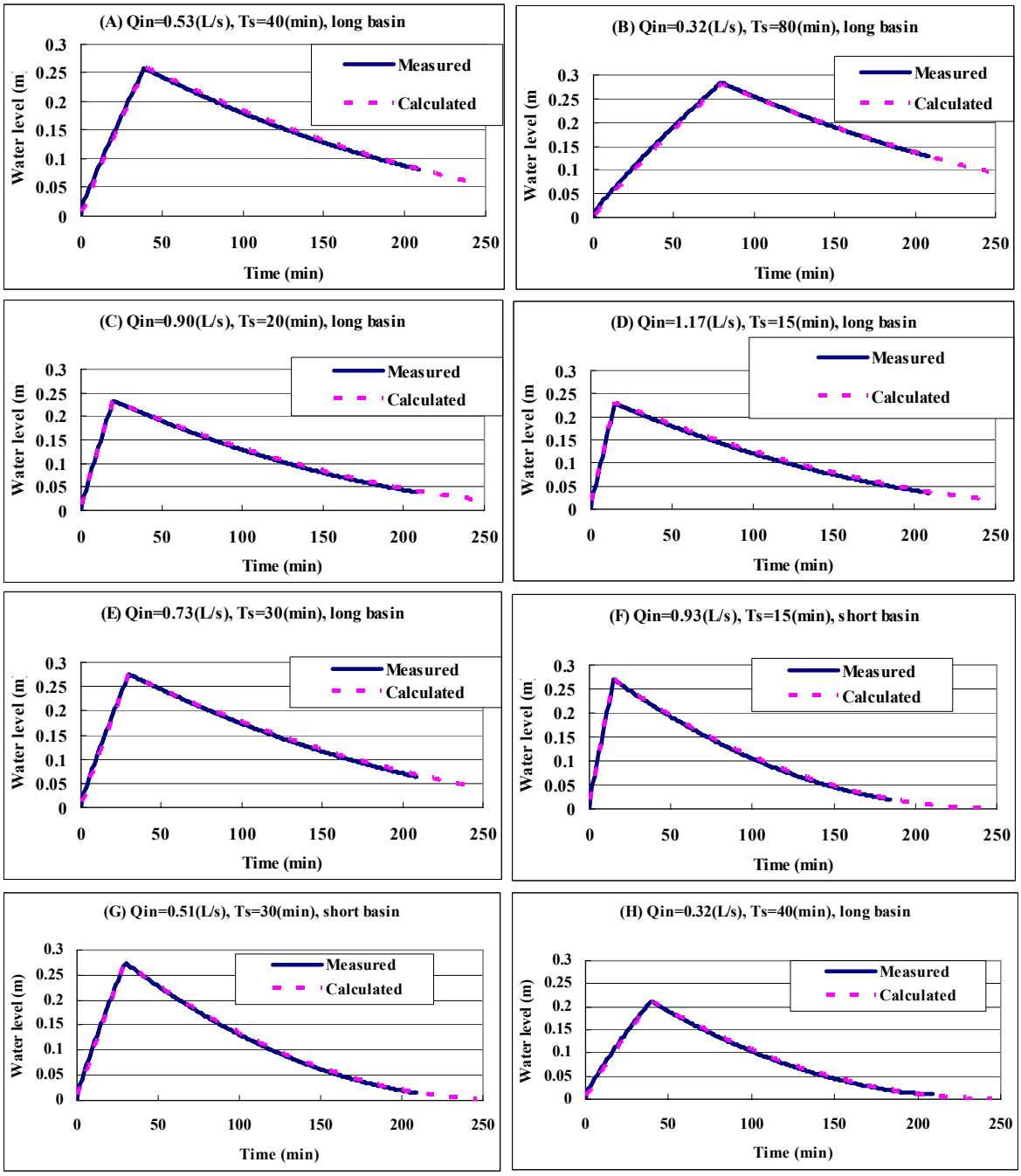

Figure 5.14. Measured and calculated water level change

Outflow SSC change

The outflow SSC was calculated using the calculated water level change. Figure 5.14 shows the calculated and measured outflow SSC for all eight runs. Calculation error for peak concentration is smaller than 15 (mg/L) except for Run B and G shown in Table 5.5. Interestingly, inflow conditions of run B and G are quite different since run B has the longest duration and the slowest theoretical overflow rate, but run G has medium duration and medium overflow rate.

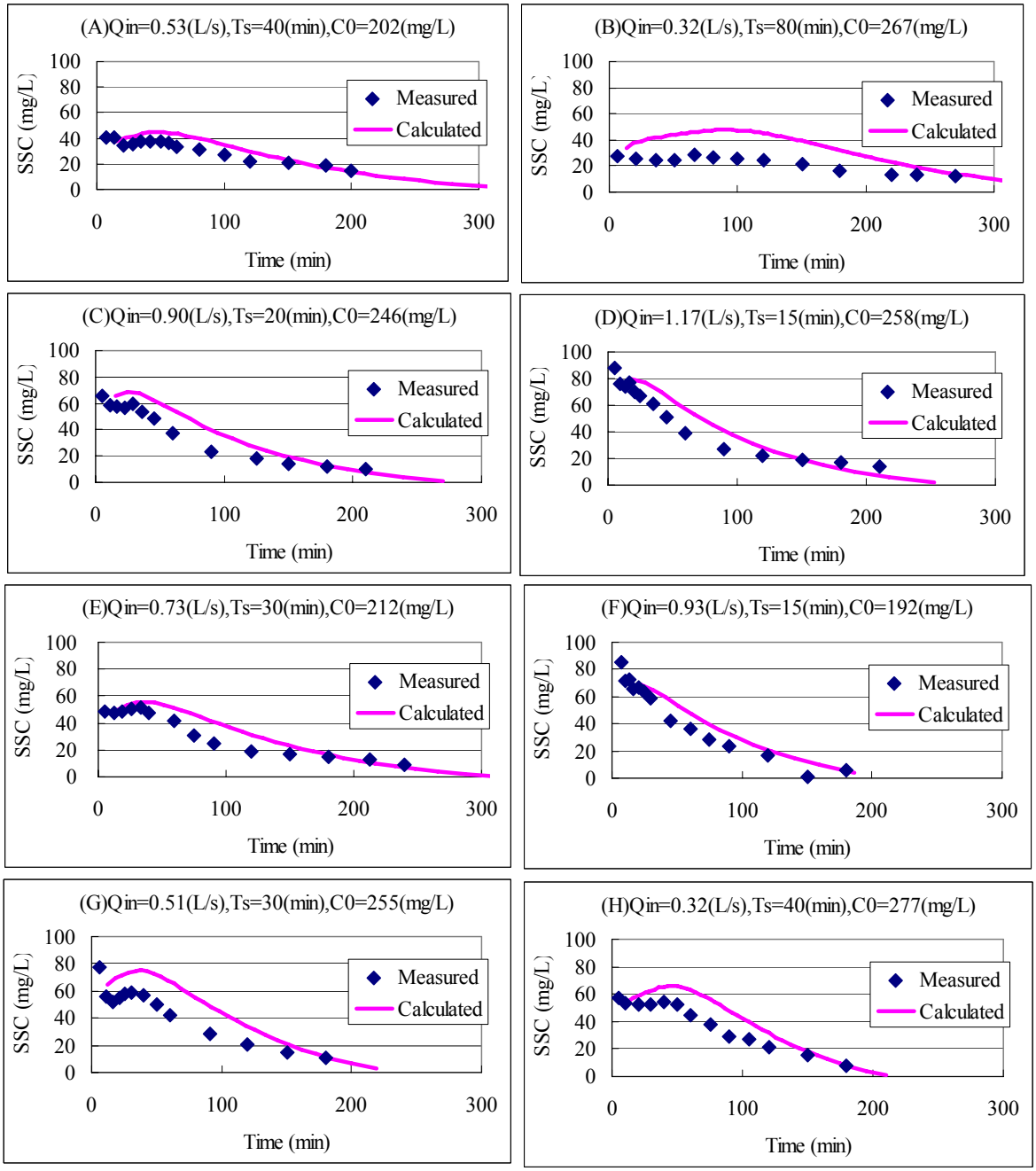

Figure 5.15. Measured and calculated outflow SSC

One possible reason to guess why these two estimations are worse than others is seen in the inflow SSC graph, shown in Figure 5.1. To determine if the inflow SSC increases or decreases with time, a trend line was drawn for each run to check if the gradient of trend lines are significant. In Table 5.5, the gradient of the trend line for time series inflow SSC shown in Figure 5.1 is shown. Then, runoff duration was multiplied by the gradient in order to know how much the difference in inflow SSC for each run is between the beginning and the end of each runoff. This table shows that runs B and G had the greatest inflow SSC differences, which could result in the large deviations of these two cases. Figure 5.16 supports the speculation. In Figure 5.16, the relationship between error in peak outflow SSC and inflow SSC difference at the beginning and ending, which corresponds the 3rd and 4th column in Table 5.5, is plotted. The figure shows the peak concentration error depends on the magnitude of outflow SSC difference at the beginning and ending. Less inflow SSC at the initial stage of a runoff would make peak outflow SSC lower, and a greater inflow SSC at end of runoff would not reach the outlet until a later time when the basin is considered as a plug flow reactor. This implies that fluctuation and stability of inflow SSC are one of the error sources for the conceptual model prediction. If more accurate results are necessary, discrete SSC should be used for input data instead of using mean inflow SSC.

Table 5.5. Gradient and calculated inflow SSC difference between the start and the end of runoff duration

Run	Gradient of inflow SSC (mg/min)	Calculated difference of inflow SSC between at the beginning and end of the runoff (mg)	Peak concentration difference between conceptual model prediction and experimental results (mg/L)
A	0.2	8.1	7
B	1.0	77.4	21
C	1.4	27.1	8
D	-1.9	-28.3	2
E	1.1	34.0	5
F	-0.1	-1.9	3
G	2.4	71.5	16
H	1.2	47.2	12

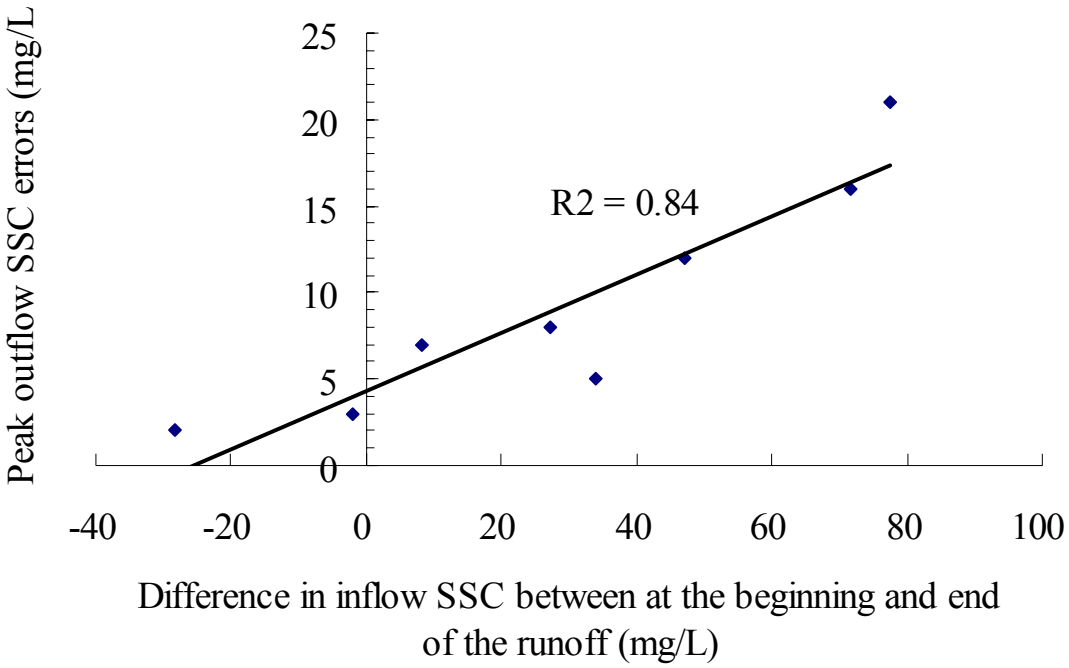

Figure 5.16. Relationship between error in peak SSC and inflow SSC difference between at the beginning and end of the runoff

Particle removal ratio

Table 5.6 shows the calculated and measured particle removal efficiency, as well as the error which is the calculated minus measured removal efficiency for each run. Figure 5.17 shows the resulting and measured removal efficiencies. The figure shows that calculated results underestimated the removal efficiency for a few %, but the trend is consistent.

Table 5.6. Measured and calculated removal efficiencies

Run	Calculated removal efficiency	Measured removal efficiency	Error (calculated-measured) (%)
A	0.88	0.89	-1.4
B	0.89	0.93	-4.6
C	0.86	0.89	-3.2
D	0.85	0.87	-1.8
E	0.85	0.88	-2.8
F	0.80	0.82	-2.4
G	0.81	0.87	-5.2
H	0.84	0.88	-3.6

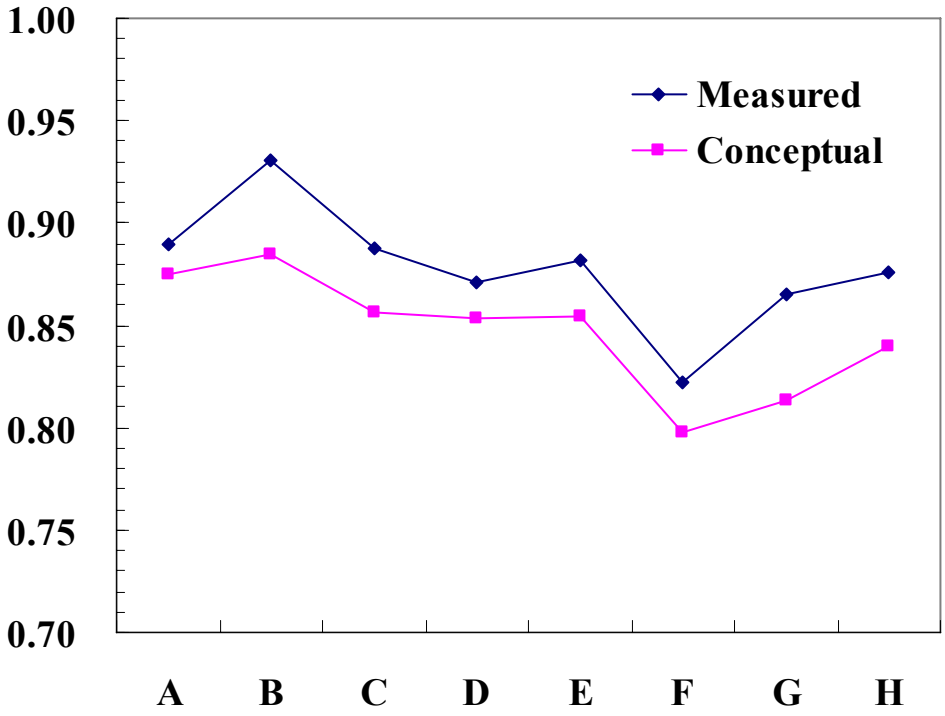

Figure 5.17. Measured and calculated (using conceptual model) removal efficiencies

Here, the conceptual model results are briefly summarized. The conceptual model was developed to treat the sedimentation basin as a plug flow reactor since the basin has a long path and narrow cross sectional area, which is similar to channel flow. The model works well to estimate time series outflow SSC, although the model always underestimated the removal efficiency by a few percent. If a storm runoff is evaluated by only average inflow rate and SSC, the conceptual model may overestimate the removal efficiency because the high inflow SSC, called first flush, will result in higher outflow SSC and lower removal efficiency.

The conceptual model has no calibration parameter, which means the model results cannot be modified by experimental results. This is a desirable characteristic when designing because the conceptual model requires basin dimensions (*e.g.*, Length, width, height, and drainage time) and inflow particle characteristics (*e.g.*, particle size and density).

5.2.2 Scaling

The next objective is to see whether or not Hazen number scaling works to accomplish the same sedimentation performance between the physical model and the prototype. The conceptual model was used for analysis since the prototype scale experimental results were not available. As shown in the physical model design section, length ratio, L_p / L_m, time ratio, t_p / t_m, and velocity ratio, $u_p(t_p) / u_m(t_m)$, were set to L_r, L_r, and 1 respectively. The orifice size ratio, $A_{e,p} / A_{e,m}$, was $L_r^{3/2}$ to keep the water level change between the model and the prototype consistent with the time and the length scales. The maximum water level of the prototype should be L_r times larger than that of the model, and the time required to drain water from the maximum water level to zero for the prototype should be L_r times longer than that of the model. Particle size distribution should be the same between model and prototype so that settling velocity ratio can be kept at 1. This is a big advantage for scaling because to prepare particles, which has exactly scaled up (or down) size distribution as particle size distribution in prototype, is very difficult. Inflow SSCs are not necessary to scale up since the outflow SSC is always normalized to the inflow SSC and the ratio is considered to be the same for any inflow SSC in the conceptual model. Table 5.7 summarizes the scaling ratio for parameters used for the physical model scaling.

Table 5.7. Scaling ratio of each variable

Variable	Description	Ratio X_p / X_m
L	Length of the detention basin	L_R
B	Width of the detention basin	L_R
h(t)	Height of the water level	L_R
Ts	Storm duration	L_R
v	Velocity	1
Q_{in} and $Q_{out}(t)$	Flow rate	$L_R^{\ 2}$
A_e	Effective Area of orifice	$L_R^{\ 3/2}$
C_{in} and $C_{out}(t^*)$	Concentration	1
λ and ζ	Parameters of particle size distribution	1
Rd	Removal ratio	1

To see the validity of these scaling assumptions, Run A, shown in the physical model section, was scaled up to the prototype with a length ratio, L_R, of 5. Inflow conditions for the model and prototype are shown in Table 5.8. The conceptual model was run for both the model and the prototype scale and time series outlet SSC and particle removal efficiency were calculated. Figure 5.18 shows water level change and outflow SSC change between the model and prototype.

Table 5.8. Dimensions and inflow conditions of prototype to have the same particle removal efficiency of run A in model scale

	Inflow rate, Qin (L/s)	Runoff duration, Ts (min)	Effective area of orifice, Ae (cm^2)	Basin length, L (m)	Basin width, B (m)	Inflow mean SSC (mg/L)
Model	0.53	40	0.43	6.96	0.62	202
Prototype	2.65	200	4.81	34.8	3.1	202

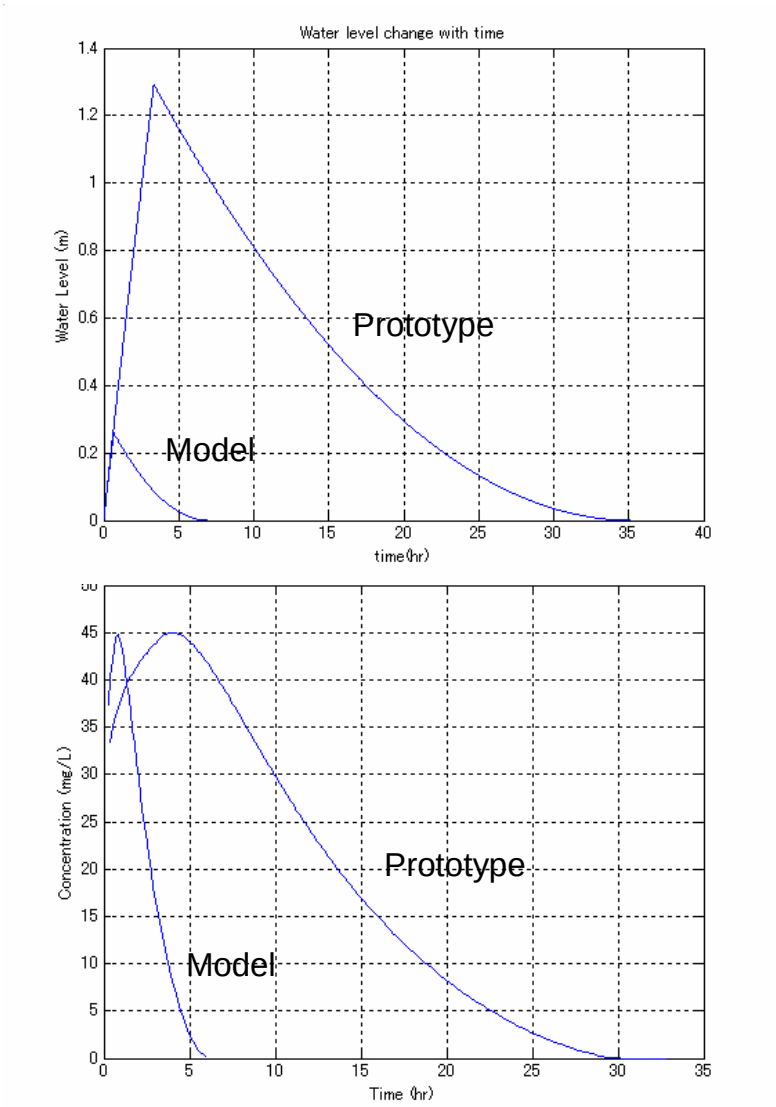

Figure 5.18. Time series water level change (above) and outflow SSC change (below) between model and prototype

The figure shows that both water level and SSC were properly scaled. The calculated removal efficiencies were 88% for both. This result implies that Hazen number scaling would work for the physical scaling of the sedimentation process in the rectangular detention basin since the conceptual model explained the sedimentation process, at least for the model scale. However, this comparison was done by using the conceptual model and not by using physical models. Therefore, Hazen number scaling should be verified using at least two similar physical models. This is not covered by this paper.

5.2.3 Analyses for Designing

Several typical design questions are presented and are attempted to be answered by either the conceptual model results or the experimental results. All the following analyses were done with the particles which have the same size distribution as the ones used for the physical models.

(A) Which storm has worse removal efficiency of suspended sediment: a strong but short storm, or a weak but long storm?

Experimental results can answer this question. Figure 5.4 shows the removal efficiency with respect to the theoretical overflow rate, which is a good index of how storm strength influences removal efficiency. The figure shows removal efficiency is worse if the storm strength is greater. However, this is not a good comparison because the storm volume is different for each run. Therefore, several simulations were done with the conceptual model keeping the runoff volume constant. Figure 5.17 shows the relationship between removal efficiency and theoretical overflow rates for three different storm volumes (0.82, 0.41, and 0.20 of the basin volume). As shown in the graph, storms with larger runoff volumes have lower suspended solid removal efficiency, although 80%

removal was calculated even for the worst case. This graph suggests that intense storms would result in a lower removal ratio than less intense storms. The removal efficiency doesn't drop significantly when the theoretical overflow rate is very strong. It is because no matter how large the storm is, the detention basin will have almost the same or even slightly longer drainage time for emptying period.

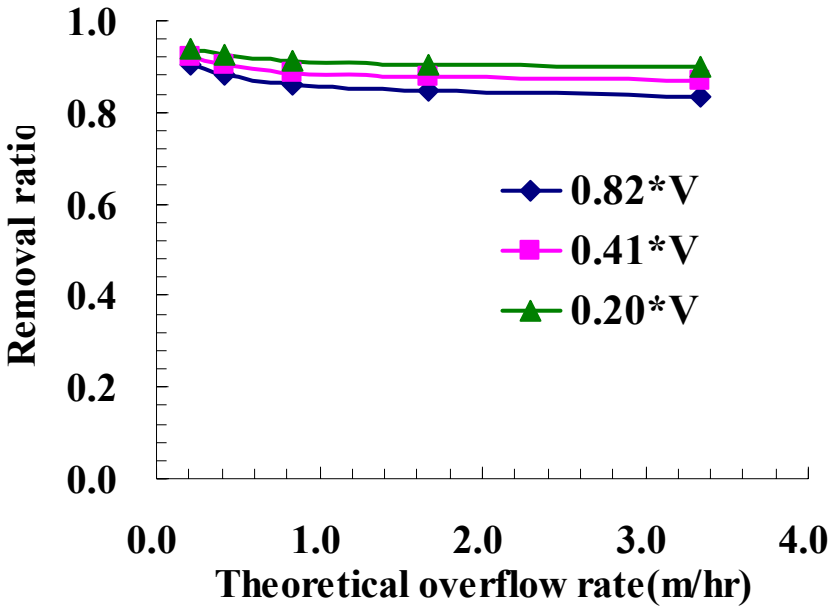

Figure 5.19. Removal ratio change with different theoretical overflow rates and different runoff volumes

(B) How does the length/width ratio affect removal efficiency?

In the conceptual model, which employs the plug flow concept, the calculated removal efficiency didn't change when only length/width ratio, L/B, changed. This is because a narrower basin results in a faster advection velocity. However, this may not be true in an extreme case such as for the length/width ratio less than 1. For this case, plug

flow cannot exist and the short cutting and large dead space may result in a lower removal efficiency.

(C) How does drainage time affects removal efficiency?

The process to determine the drainage time is equivalent to the process used to determine the outflow orifice size. The theoretical drainage time, t_d (hr), is defined as the time to drain all the water from full (h=H(m)) to empty.

$$\sqrt{h} = \frac{A_e}{B \cdot L}\sqrt{\frac{g}{2}} \cdot t_d$$

$$A_e = \frac{B \cdot L}{t_d}\sqrt{\frac{2h}{g}}$$

$$A_e\left(cm^2\right) = \frac{B(m) \cdot L(m) \cdot 10^4 (cm^2/m^2)}{3600(s/hr) \cdot t_d(hr)}\sqrt{\frac{2h(m)}{g(m/s^2)}} \qquad (5.34)$$

$$A_e\left(cm^2\right) = \frac{0.62 * 6.96 * 10^4}{3600} * \sqrt{\frac{2 * 0.34}{9.81}} \cdot \frac{1}{t_d(hr)} = \frac{3.16}{t_d(hr)}$$

Then, removal efficiency of suspended solid was calculated for four different orifice sizes (0.41, 0.82, 1.23, and 1.64 (cm^2)), which correspond to theoretical drainage times of 7.7, 3.9, 2.6, and 1.9 hours for three different flow rates (Q_{in}=0.5, 1.0, and 2.0 (L/s)). However, the runoff volume is the same for all cases. The calculation results are shown in Figure 5.18. Removal efficiency decreased significantly with increasing orifice size when compared to increasing flow rate. Table 5.9 shows the maximum water level and removal efficiency for the same cases shown in Figure 5.20.

Table 5.9. Particle removal ratio and corresponding maximum water level for different flow rate and different orifice sizes.

	Effective area of orifice (cm^2)	0.41	0.82	1.23	1.64
Q_{in}=0.5	Particle removal efficiency	0.88	0.82	0.78	0.76
(L/s)	Maximum water level (m)	0.25	0.21	0.19	0.16
Q_{in}=1.0	Particle removal efficiency	0.86	0.79	0.75	0.71
(L/s)	Maximum water level (m)	0.26	0.25	0.23	0.21
Q_{in}=2.0	Particle removal efficiency	0.85	0.77	0.72	0.68
(L/s)	Maximum water level (m)	0.27	0.26	0.25	0.25

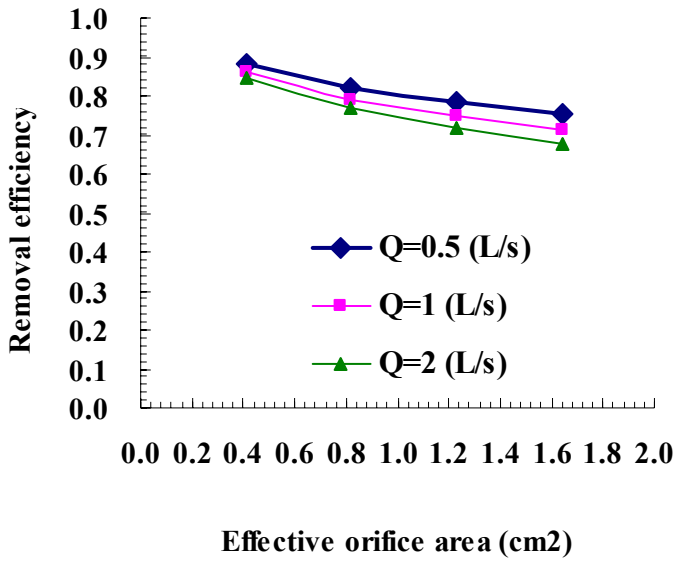

Figure 5.20. Removal ratio change with different effective orifice sizes

The table shows for a short but strong storm, a smaller orifice works much better than a larger orifice and the maximum water level is almost the same. However, for a weak but long storm, the difference in removal efficiency for different orifice sizes is not as big as the difference for a short but strong storm. For a flow rate of 0.5 L/s, the

maximum water level was 16 cm, or 47% of the overflow weir height, for an orifice area of 1.64 cm^2. However, for the same storm event (0.5 L/s), the maximum water level was 25 cm, or 74 % of the overflow weir height, for the orifice area of 0.41 cm^2. Therefore a smaller orifice opening is preferred if the design is for an intense short duration storm. However, a larger orifice opening can be effective when the design is for less intense storms since the volume which can be captured by the basin before overflow will occur will increase.

(D) How does the density of suspended solids affect removal efficiency?

To answer this question, particle removal efficiency was calculated for particles with different densities, and simulations with different flow rates were compared while keeping the runoff volume the same. Of primary interest are particles with densities less than 2.65 g/cm^3. Figure 5.21 shows the removal efficiency of suspended solids for particles with densities ranging from 1.2 to 2.65 (g/cm^3), using the assumption that density is uniform for all the particle sizes. Removal efficiency is lower if density is lower, and the decrease is more significant for lighter particles. The density of smaller particles in stormwater runoff can range from 1.1 (g/cm^3) (Cristina, *et al*., 2001) for typical highway organic soil to around 3.0 (g/cm^3) for larger particles (Zanders, 2005). When combined with the influence of density on removal efficiency, these results suggest that characteristics of particle density should be considered in analysis and design of stormwater treatment sysmtems.

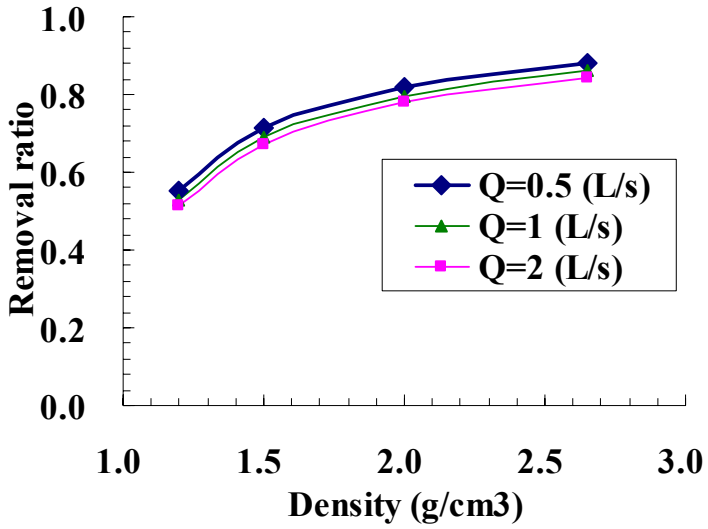

Figure 5.21. Removal ratio change with different particle densities

5.2.4 Nonideality

The ideal plug flow solution always underestimates the removal efficiency to some extent although the errors were not significant. To understand the reason and to see how the flow in the basin is different from the plug flow, conductivity tracer tests were done with salt as a tracer. Also, dye tests were conducted using the view window at the side of the tank to see the velocity profile.

(A) Conductivity test

Three conductivity tests were done using salt adding to the water as a tracer. A conductivity meter (Check mate 90, Corning) was used for detecting salt concentration at inlet and outlet.

Calibration test

To know the relationship between salt concentration and conductivity, a calibration test was done. Fig.5.20 shows the calibration line obtained from 6 different samples, salt concentrations of which were known.

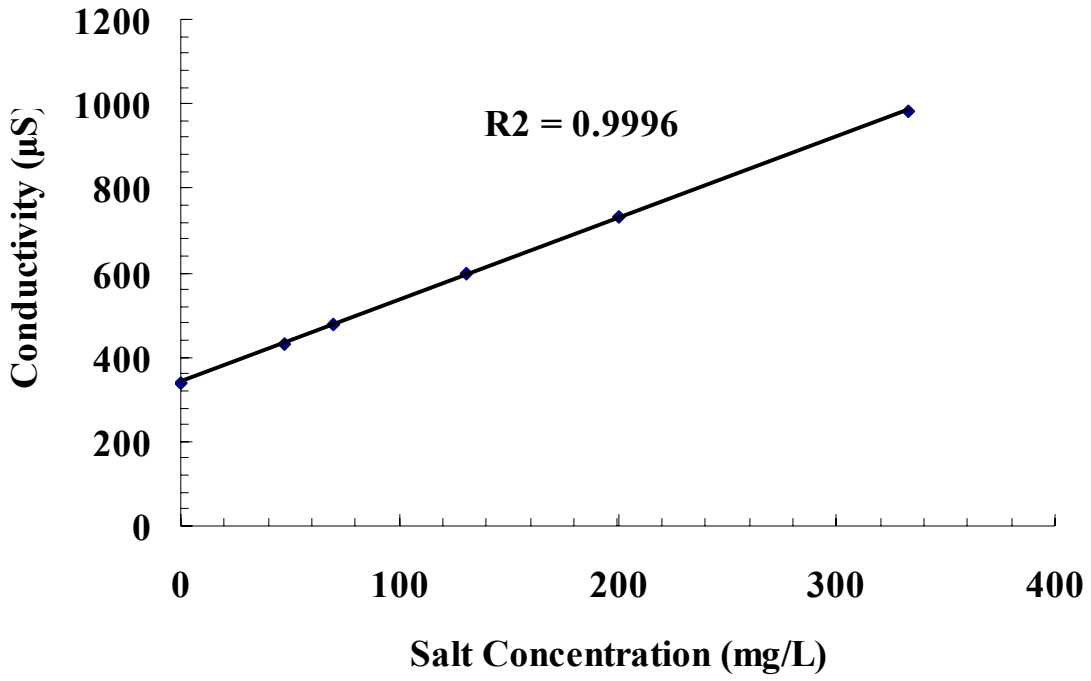

Figure 5.22. Calibration line between conductivity and salt concentration

Salt concentration can be obtained from the measured conductivity as follows:

$$C(\mathrm{mg/L}) = \frac{\mathrm{Cond}(\mu\mathrm{S}) - 341}{1.93} \tag{5.35}$$

341 (μS) is the tap water conductivity, which was used as the background concentration. Therefore, nondimensionalized conductivity was defined subtracting background concentration as follows:

$$C^* = \frac{Cond - 341}{\overline{Cond_{in}} - 341} \tag{5.36}$$

Where Cond is the measured outflow conductivity and $\overline{Cond_{in}}$ is the mean inflow conductivity.

Methodology

Three tracer tests were conducted with the same detention time of approximately 35 minutes and inflow rates of approximately 0.4 L/s. These experiments were done without injecting sediment. Therefore, salt was put into the inflow system using the mixing tank which was used to mix suspended sediemnt particles. Table 5.10 shows the experimental conditions of these three tracer tests. Salt was introduced as a step function for runs A and B while salt was injected as an inverse step function for run C. For example in the run A, the basin was continuously filled with water for 35 minutes but the tracer was injected only from 15 to 35 minutes during the filling period. These experiments were conducted with low salt concentration, which was always lower than 150 (mg/L), so that the density effect on the flow pattern was negligible.

Table 5.10. Experimental conditions of three different tracer tests

	Qin (L/s)	Ts (min)	Total Q (L)	Tracer from (min)	Tracer to (min)
A	0.42	35	882	15	35
B	0.38	38	866	28	38
C	0.4	35	840	0	10

Test results

Fig 5.23 shows the test results. Each graph has nondimensionalized inlet and outlet tracer concentration. In Run A, tracer was first detected at 26 minutes, which is 11

minutes after the tracer was added at 15 minutes. The traveling time of the tracer front was 12 minutes for Run B and the traveling time of clean water front was 11 minutes for Run C. Another interesting point is that tap water (runs A and B) or tracer (run C) was never depleted. If this detention basin is a plug flow reactor, the outlet tracer concentration should become 1 for Runs A and B, and 0 for Run C eventually. Therefore, these conductivity test results show that there is some sort of mixing or dispersion process in the basin and these processes prevent the detention basin from being a plug flow reactor.

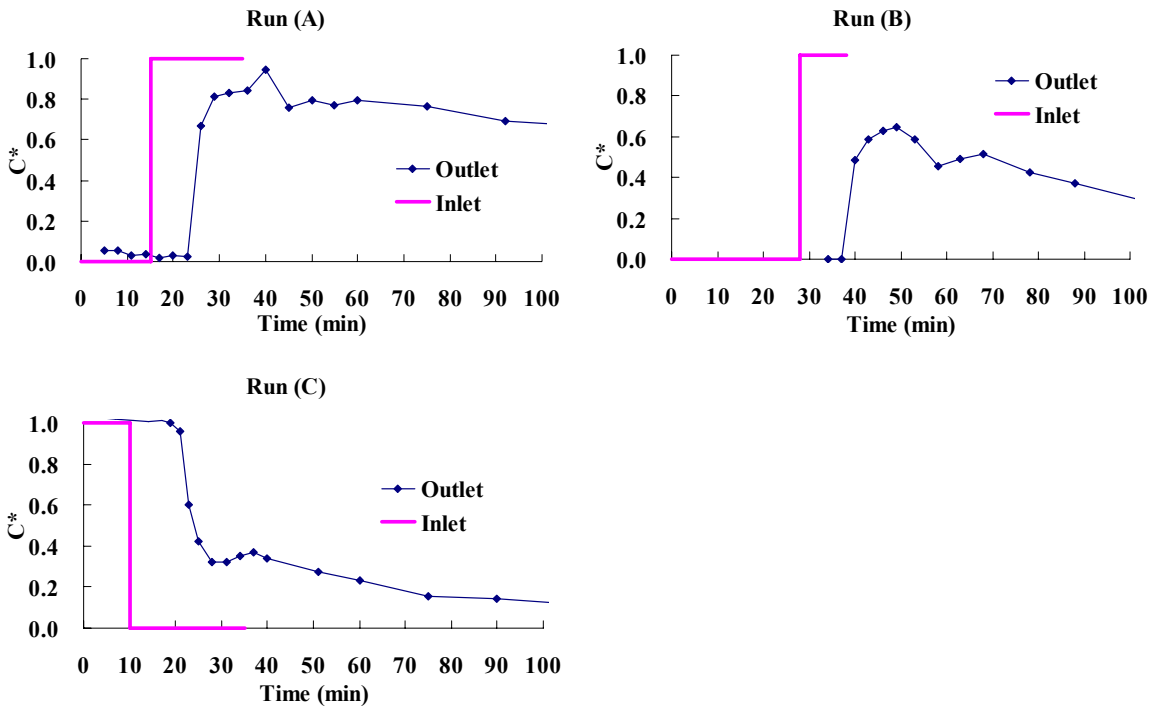

Figure 5.23. Nondimensionalized tracer concentration at inlet and outlet

(B) Model comparisons

Outflow tracer concentrations were calculated using plug flow and CSTR model. These model results were compared with the measured outlet tracer concentrations in order to see if the settling basin works more like plug flow or CSTR.

Plug flow model

Outflow tracer concentration was calculated using the conceptual model. In the case of step function input, such as Runs A or B, the outflow tracer concentration should jump from 0 to 1 when the tracer front reaches to the outlet. The time when the tracer front reaches to the outlet was calculated using the conceptual model since the conceptual model employed the plug flow model. Specifically, t_{out} in equation (3.10) was solved numerically as follows with the tracer input time and the shortened basin length of $\frac{2}{3}L$:

$$\frac{2}{3}L = \frac{1}{B \cdot h(t)} \int_{tin}^{tout} Q_{in}(t)dt \qquad (5.37)$$

CSTR model

Consider the case with the tracer injected from time 0 to T and the runoff duration is T_s ($T<T_s$) such as Run C. Outflow tracer concentration should be 1 for the time 0 to T since tracer is injected with a constant concentration. After the tracer injection stops, concentration change can be calculated by the mass balance equation (5.38). During the period, tracer concentration keeps declining because of the dilution by clean water.

$$\begin{aligned} &C^* \text{ for } T \le t \le T_s \\ &h(t)\frac{dC^*}{dt} = -\frac{A_e\sqrt{2gh(t)}}{BL} \cdot C^* \\ &\text{I.C.} \quad C^* = 1.0 \end{aligned} \qquad (5.38)$$

Equation (5.38) was numerically calculated by writing a code in C++. Time was discretized with forward differencing. Water level was explicitly calculated, followed by the concentration calculation so that tracer concentration can be solved explicitly. After

the runoff stops, the outflow tracer concentration becomes constant because there is no longer dilution.

In the case with tracer injected from time T to the end of the runoff, T_s, such as Runs A and B, outflow tracer concentration can be calculated with transforming equation (5.38) by changing datum concentration from 0 to inflow tracer concentration, C_{in}*, which is 1. Therefore, the solution of outflow tracer concentration for step input can also be obtained from the same equation form of (5.38).

$$\begin{aligned} h(t)\frac{dC^*}{dt} &= \frac{Q_{in}}{BL}\cdot C_{in}^* - \frac{A_e\sqrt{2gh(t)}}{BL}\cdot C^* \\ h(t)\frac{d\left(C^* - C_{in}^*\right)}{dt} &= -\frac{A_e\sqrt{2gh(t)}}{BL}\cdot\left(C^* - C_{in}^*\right) \\ h(t)\frac{d\left(1 - C^*\right)}{dt} &= -\frac{A_e\sqrt{2gh(t)}}{BL}\cdot\left(1 - C^*\right) \quad \because C_{in}^* = 1 \end{aligned} \tag{5.39}$$

Results

Fig 5.22 shows the measured and modeled outflow results.

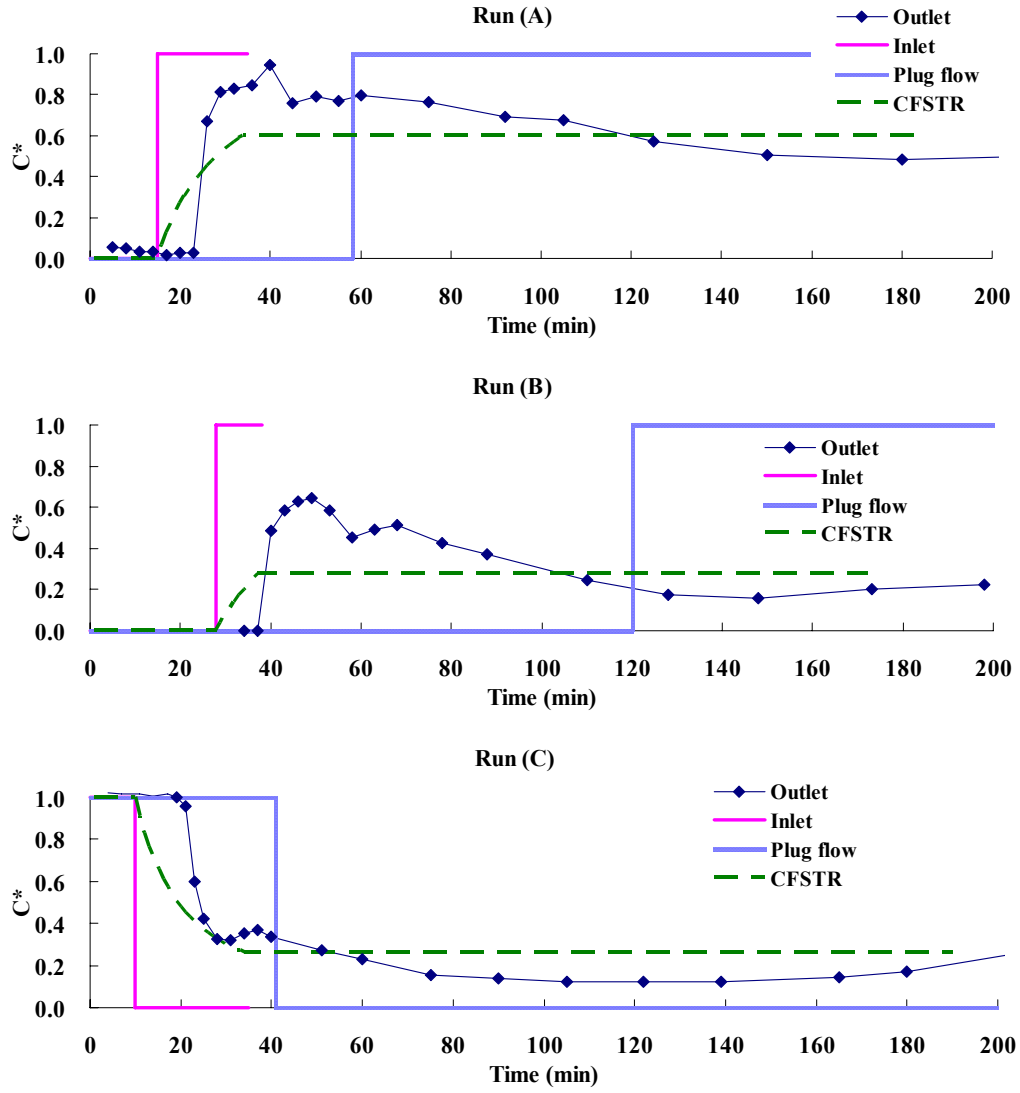

Figure 5.24. Measured outflow tracer concentration with calculated results from plug flow and CSTR model.

The graphs show that the interface between tracer and water traveled much faster than the interface calculated with plug flow model. The measured results are also different from CSTR model because the measured results show that the concentration rises for Runs A and B or drop for Run C at certain point, which cannot be explained by a

CSTR model. Among the three experimental results, deviation between measured and plug flow model is the largest in Run B with the tracer injected for the last 10 minutes among 38 minutes runoff duration.

1-D dispersion coefficient is sometimes employed for modeling the outflow tracer concentration change of column tests. However, this model would not well describe the situation. This is because 1-D dispersion term can only smooth out the sharp concentration rise of the plug flow solution.

(C) Observation from view window

The tracer tests imply that the flow is different from CSTR, plug flow, or plug flow with 1-D diffusion. The flow pattern was observed visually using the view window. Dye was used to visualize the velocity profile in the cross section for both the filling and emptying period. For the filling period, the velocity pattern looked like the plug flow except near the very bottom of the cross section due to the friction until water level reached approximately 12 cm. As water level increased during the filling period, an interface was created approximately at the height of 12 cm. the flow was still like the plug flow beneath the interface, while the flow above the interface was very slow and went backward. The height of the interface did not change much throughout the filling period. The velocity profile when the water level was approximately 20 cm during the filling period is shown in Fig 5.23. The pictures were captured from the videos for the filling and emptying period. Three layers can be seen in each picture. The top layer is the water surface, which is covered by scum, the middle layer is the other side of the basin wall painted gray, and the bottom layer is the bottom of the basin covered by white silica particles. The profile implies that a big counterclockwise direction eddy was developed during the latter half of the filling period.

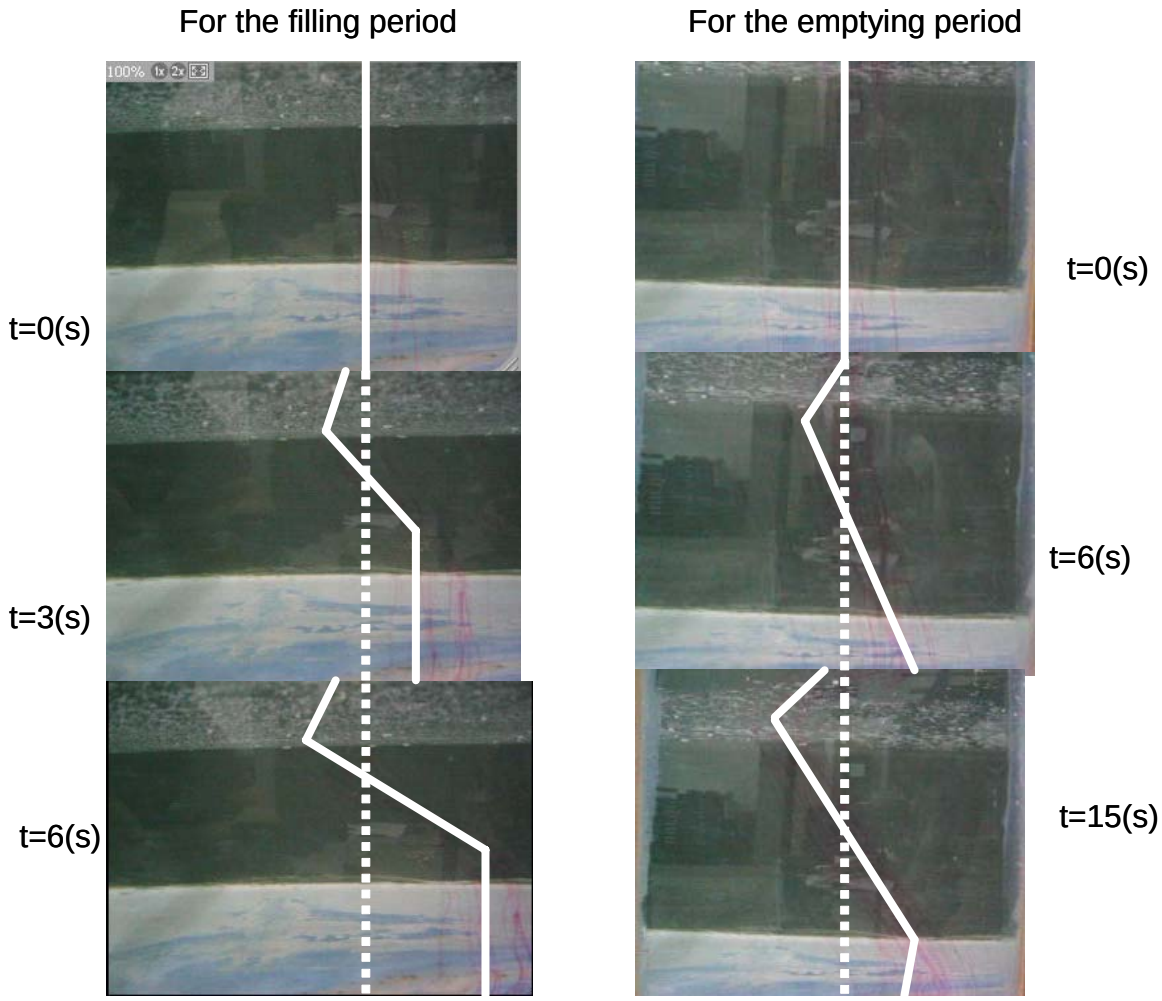

Figure 5.25. Typical velocity profiles with velocity interfaces for the filling period (left) and the emptying period (right)

For the emptying period, mean flow flux across a cross section was much smaller than the flux for the filling period because the mean flux is determined only by outflow. At the beginning of the emptying period, there remained the backwater caused by the big slow eddy developed during the filling period. The backwater circulation in the upper

layer disappeared approximately 10-15 minutes after the runoff stopped. Figure 5.25 shows the velocity profile observed 8 minutes after the runoff stopped. The figure shows that there was a weak backward flow for 1/2 depth of the basin from the top and there is also a weak forward flow for 1/2 depth of the basin from the bottom. After the backwater disappeared in the upper layer, the velocity profile becomes close to the plug flow except for the very top and bottom of the cross section.

The pictures also shows the reason for the short circuiting observed in the tracer test results such as Runs A and B. The tracer velocity in the bottom layer is much larger than the calculated average velocity of a cross section, which shorten the traveling time of the tracer front from the inlet to the outlet. However, some of the tracer might be dispersed in the basin due to the shear stress created by the large velocity gradient at the velocity interface and some of the tracer, which happened to be in the top layer, will be carried backward by the large vertical counterclockwise eddy. This can be a reasonable explanation of the tracer concentration graph, which never reached 1 throughout runs.

The reason why the plug flow model underestimated the results is speculated using the nonideality results on flow patterns. The particle sedimentation rate can be theoretically calculated as follows;

$$M(t) = \int_0^L \int_0^B v_s \cdot C_B(x, y, t)\,dy\,dx \tag{5.40}$$

Where M(t) is the total sedimentation rate and C_B is the particle concentration close to the bottom. The particle concentration in the bottom layer in the real situation is higher than that in the plug flow model since inflow was introduced to the lower part of the sedimentation basin when the water level is higher than a certain height. The particle concentration profile during the filling period was conceptually drawn in the Figure 5.26. Assume the settling velocity for the both situations are the same, the sedimentation rate,

M(t) in equation (5.41), for the real situation is higher than that of the plug flow model since the mean SSC is higher in the bottom layer.

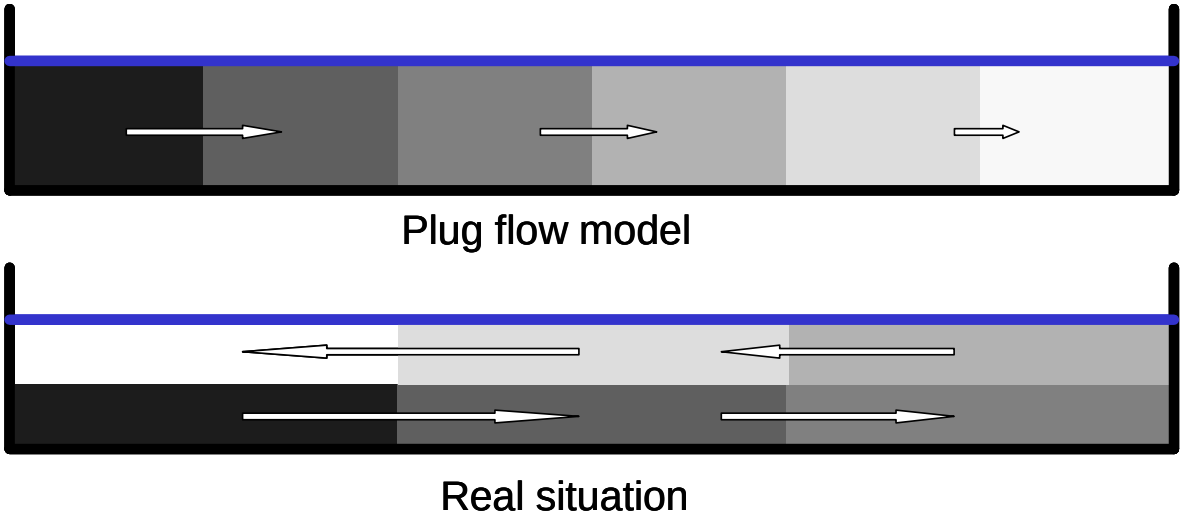

Figure 5.26. Particle concentration profile in the sedimentation basin in the plug flow model and the real situation during the filling period.

This could be a reasonable explanation of the situation that plug flow model underestimated the removal ratio. In this sense, the plug flow model estimates the removal efficiency conservatively. However, advection velocity in the lower layer is much higher than that in the plug flow model as shown in the Figure 5.26. Therefore, the higher advection velocity might enhance the resuspension of particles sitting on the bottom and entraining particles which are going to settle out. Therefore, it is necessary to use devices such as an energy dissipator or diffuser around the inlet and a sill around the outlet to prevent these resuspension and entrainment effects.

Chapter 6 Conclusions and future work

Conclusions drawn from the research and recommendations for future work are discussed in this chapter.

6.1 CONCLUSIONS

This research work is part of a research project funded by TxDOT. Four research objectives were set to fulfill the research project. How these research objectives were achieved and what kinds of findings that were drawn for each objective are discussed.

Objective 1: Build a rectangular sedimentation basin as a physical model, which can reproduce and vary input conditions such as inflow rate and SSC, and can be used to take samples at any time from inlet and outlet to measure SSC

Two physical model basins were built in the laboratory of CRWR (Center for Research in Water Resources). The first one, which unfortunately was not used, provided many insights about how the sedimentation basin should be built and protected from water leakage and how measurements should be taken. The second one had the same size of the first basin, but had a modified particle delivery system and better waterproofing. This second physical model could reproduce inflow conditions well except for controlling inflow SSC at a constant value. However, the particle mixing and delivery system was also modified and achieved 80% uniformity of inflow SSC during the filling period using a better peristaltic pump and mixing method. The system has an inflow nozzle right before the sedimentation basin and outflow nozzle right after the outlet orifice, and these nozzles were successfully used for taking samples. Therefore, the first research objective was successfully achieved.

Objective 2: Build a conceptual model which can estimate time series outflow SSC, event mean concentration (EMC), and particle removal efficiency; and verify the conceptual model using physical model results

A conceptual model used to calculate outflow SSC and particle removal efficiency was theoretically developed based on the assumptions and concepts that are used in the ideal horizontal flow reactor theory, and a program to apply the theory to simple cases was developed in MATLAB. The code can handle either constant flow rates or SCS triangular hydrographs as inflow rates. As a result, outflow SSCs were accurately calculated by the conceptual model except for a few cases, which had increasing trends of inflow SSC. Particle removal efficiencies were underestimated by a few percent for all cases. That's may be because highly concentrated inflow rather stay in the lower part of the tank and effectively be settled out than spread out and evenly be distributed vertically around at inlet, which is the assumption in the conceptual model.

Several simulations and analyses were conducted with the conceptual model. When the overflow rate is increased, removal ratio will decrease but not significantly. This may be because no matter how strong the storm is, the detention basin will have almost the same or a slightly longer drainage time for emptying period. However, the length/width ratio of the sedimentation basin will not affect removal efficiency when surface area of the basin is constant. This may not be true when the length of the sedimentation basin is nearly equal to or shorter than the width of the sedimentation basin because the flow will be far from plug flow. When the drainage time is decreased, by increasing the area of outlet orifice, the removal efficiency will decrease. This result is consistent with the analysis done from physical model results. Finally, particle removal efficiency was calculated when particle density is lower than 2.65 (g/cm^3). The decrease

of particle density will affect removal efficiency especially when the density is smaller than 2 (g/cm^3), which is possible for smaller particles with a high organic carbon fraction.

The tracer tests and the dye tests from the view window shows that there were some mixing in the basin and it may be because of a large scale vertical counterclockwise eddy formed in the basin, which resulted in the flow pattern different from plug flow. An example solution to make the flow close to the plug flow is to put a series of baffles in the basin to minimize the momentum created by the strong inflow. If it is necessary to understand the effect of the eddy on sedimentation, numerical simulations would be required to calculate at least 2-D (longitudinal and vertical axes) flow profile in the basin.

Objective 3: Test different lengths of the basin and outlet orifice sizes in the physical model to evaluate how the overflow rate and detention time affect particle removal ratio

Eight runs were conducted with different inflow conditions and setups with two different orifice sizes and two different basin lengths. To compare these results, which have different conditions, a time nondimensionalization method was developed for the system such that all runs have the same length of nondimensionalized filling and emptying period. As a result, time series outflow SSCs of all runs were compared efficiently.

For the filling period, outflow SSC was almost constant and was proportional to the theoretical overflow rate. The phenomenon was explained by a semi steady state CSTR model using effective settling velocity, which was calculated to 2.17 (m/hr). For the emptying period, outflow SSC decreased with time as if particles have a settling velocity which is the same as the speed of water level dropping except for few cases. These exceptional cases are runs with the two highest theoretical overflow rates and two

shortest durations, which implies almost all the bigger particles will settle out for a filling period if runoff duration is long enough and the overflow rate is not too large compared to particle settling velocity. Overall removal efficiency will decrease if the effective orifice area is increased; however, the mass of particles flowing out during the emptying period may be decreased if the effective orifice area is increased because the increased speed of water height drop will push particles down to settle out.

Table 6.1 shows the summary of the two different models developed in this research. One is the conceptual model with the plug flow assumption and the other is the empirical model developed using CSTR model concept and the physical model results. As shown in the table, the empirical model is easier to handle and as accurate as the conceptual model. The empirical model should determine the effective settling velocity, which would be different for different inflow particles, and sizes and shapes of the sedimentation basin. However, the behavior of the effective settling velocity was not studied yet.

Table 6.1. Summary of the model characteristics between the plug flow base conceptual model and the CSTR base empirical model.

	Conceptual	Empirical
Model base	Plug flow	CFSTR + experimental data
Required inflow data	Mean flow rate, duration, Mean SSC	Mean flow rate, duration, Mean SSC
Water level change	Time series water level change should be calculated	Only maximum water level should be calculated
Required software	MATLAB or any programming compiler	Excel spread sheet
Required inflow particle size distribution (PSD)	Lognormal mean and standard deviation	N/A
Calibration parameter	N/A	Effective particle settling velocity
Model accuracy	Good, but model results always underestimates for a few %	Good, but better for less intense and longer runoffs
Nonideality	Not considered	Incorporated with the effective settling velocity
Applicability with different sizes of particles	Fine if inflow particle size distribution is known	Effective settling velocity should be determined experimentally

Objective 4: Study how geometric and hydraulic parameters should be scaled to have identical particle removal efficiency in physical model and prototype using conceptual and physical model results

This scaling study was done using the conceptual model since prototype SSC data are not available yet. As a result, Hazen number scaling, which sets the velocity ratio between model and prototype equal to each other, was found to be the proper scaling method. With this scaling method, particles do not need to be scaled, which makes experiments much easier. However, the physical model has a weak but large vertical eddy in the basin, which made the system a little different from plug flow. This kind of nonideality may occur in the prototype, but it has not been studied yet.

6.2 FUTURE WORK

For the conceptual model, application methods can be modified a little bit more. For example, the current program cannot handle discrete inflow SSC but can only handle constant inflow SSCs. This is good enough when outflow SSC results are compared with physical model results or when only the removal ratio is to be estimated. However, inflow SSC sometimes significantly fluctuates or has a declining trend when so called first flush effect is significant. In these cases, using mean inflow SSC as an input will result in a large deviation from the actual removal ratio. Also, it is convenient if the conceptual model can calculate removal ratio of particles with known size especially when particle size distribution of inflow is unknown.

For the physical model, larger orifice sizes should be tested to see if the empirical model continues to works well and the calculated effective settling velocity has the same value. Also, several test results of the prototype should be acquired from the Texas A&M group and reproduce runs with properly scaled input to see if the Hazen value scaling works well.

Finally, optimization of removal efficiency should be done. For example, nonideality should be studied more. How the large vertical eddy makes the sedimentation different from the plug flow based sedimentation should be studied. Also, ways to minimize the resuspension effects around inlet and outlet area should be studied because the resuspension effects were significant especially with a strong runoff and the effect may be more significant for the prototype.

Appendix A   Conceptual Model Program in MATLAB

The following is the MATLAB program developed for calculating particle removal efficiency of the rectangular detention basin by the conceptual model. Water level, outflow rate, and outflow SSC are also calculated in the program. The same kinds of calculation can be done for prototype by setting the flagScale to be 1.

```
%%%%%%%%%%%%%%%%%%%%%%%%%%%%%%%%%%%%%%%%%%%%%%%%%%%%%%%%%%%
%%%%%%%%%%%%%%%%%%%%%%%%%%%%%%%%%%%%%%%%%%%%%%%%%%%
%This is a MATLAB code to calculate Water level change, Outflow rate, outflow SSC, and SS removal ratio
%Author: Masatsugu Takamatsu
%%%%%%%%%%%%%%%%%%%%%%%%%%%%%%%%%%%%%%%%%%%%%%%%%%%%%%%%%%%
%%%%%%%%%%%%%%%%%%%%%%%%%%%%%%%%%%%%%%%%%%%%%%%%%%%

clear all

%<<Define flags>>
    flagScale=0;        %Model or Prototype (0 for model scale and 1 for scaled model)
    flagInflow=0;       %Inflow hydrograph type (0 for constant inflow, 1 for SCS triangular inflow)
    flagInput=1;        %Among eight data, A=1, B=2, C=3, D=4, E=5, F=6, G=7, H=8
    flagGraph=0;        %Graph options
                          %0 for no graph
                          %1 for water level change
                          %2 for flow rate
                          %3 for PDF of inflow PSD
                          %4 for CDF of inflow PSD
                          %5 for PDF of particle settling velocity of inflow
                          %6 for CDF of particle settling velocity of inflow
                          %7: dp-vp relationship
    flagSSC=1;           %0 for not calculating sedimentation process
                          %1 for calculating sedimentation process

%<<Define Variables>>
%%%%%%%%%%%%%%%%%%%%%%%%%%coeff for model%%%%%%%%%%%
                g=9.81;          % Gravity acceleration, g (m/s^2)
                B=0.62;          % Width of the tank, B (m)

        if flagInflow==0 %parameter for constnat Qin
            if flagInput==1
                Ae=0.43*4;L=6.96;C0=202;Qconst=0.53;Ts=40*60;%runA
            elseif flagInput==2
                Ae=0.43;L=6.96;C0=267;Qconst=0.32;Ts=80*60;%runB
            elseif flagInput==3
                Ae=0.48;L=6.96;C0=246;Qconst=0.9;Ts=20*60;%runC
            elseif flagInput==4
                Ae=0.48;L=6.96;C0=258;Qconst=1.17;Ts=15*60;%runD
            elseif flagInput==5
                Ae=0.48;L=6.96;C0=212;Qconst=0.73;Ts=30*60;%runE
            elseif flagInput==6
                Ae=0.48;L=6.96*2/3;C0=192;Qconst=0.93;Ts=15*60;%runF
            elseif flagInput==7
                Ae=0.48;L=6.96*2/3;C0=255;Qconst=0.51;Ts=30*60;%runG
            elseif flagInput==8
                Ae=0.48;L=6.96*2/3;C0=277;Qconst=0.32;Ts=40*60;%runH
            end
```

```
         K2=(Ae/10000*(2*g)^0.5/2/B/L)^2; %K2 from (3.1.5)
    elseif flagInflow==1 %parameters for SCS triangular hydrograph
        Ae=0.43;            % Effective area of orifice
        L=6.96;             % Length of the tank, L=6.96 (m)
        C0=202;             %C0=constant inlet SSC (Suspended Solid Concentration)
        K2=(Ae/10000*(2*g)^0.5/2/B/L)^2; %K2 from (3.1.5)
        Qp=1.5/4;           %Peak flow rate (L/s)
                Tp=20*4*60;     %Peak time (s)
    end


    %%%%%     Variables on particles    %%%%%%%%%%%%
            densP=2.65;     %density of silica particle (g/cm^3)
            densL=1.00;     %density of water (g/cm^3)
            viscs=1e-3;  %viscs (viscosity of water) (Pa*s)=0.1*viscosity of water(=0.01)(g/cm/s)
    rmdPsize=2.286; %mean of ln(particle size) (particle size (micron)) 2.252 from Ana's data and 2.651 for best fit, 2.642 for manufacture data, (2.287, 0.906) is Jeff's data
    tyetaPsize=0.908;    %standard deviation of ln(particle size) 0.876 from Ana's data and 1.102 for best fit, and 0.588 for manufacture data
    k=g/18/viscs*(densP-densL)*3.6e-6; %(vs(m/hr)=k*dp(micron)^2)
            rmd=2*rmdPsize+log(k);%rmd is mean of ln(vp) and tyeta is std dev of ln(vp)
    tyeta=2*tyetaPsize;    %tyeta is std dev of ln(vp)


%%%%%%%%%%%%%%%%%%%%%Coeff for Scaled up model%%%%%%%%%%%%%%%%
     if flagScale==1
                Lr=5;               %Length ratio
            Ae=Ae*Lr^1.5;    % Orifice area, Ap (cm^2)
            L=L*Lr;          % Length of the tank, L (m)
            B=B*Lr;          % Width of the tank, B (m)
    %parameters for SCS triangular hydrograph
    if flagInflow==0
        Qconst=Qconst*Lr^2;
        Ts=Ts*Lr;
    elseif flagInflow==1
        Qp=Qp*Lr^2;%Constant inflow rate, Qin (L/s), 0.53(L/s) and Ts=40 (min) is default value
                Tp=Tp*Lr;% TS is the time when the runoff stops
    end
  end

%%%%%%%%%%%%%%%%%%%%%%%%      Program for hydraulics     %%%%%
  i=1;
  dt=1;               %dt: time interval (min)
  WL=1e-4;            %Water level(m)

  %%%%%%%%%%Constant Inflow%%%%%%%%%%%%%%%%%%%%%%

  if flagInflow==0        %Constant flow rate case
    QQ=0;
    tautau=0;
    while i<= 20*Ts/60/dt & WL>1e-5
        time(i)=i*dt;
        if i<(Ts/60+1)/dt
            WL=WL+60*dt/B/L*(Qconst/1000-Ae/10000*(2*g*WL)^0.5);      %WL (m)
            WLL(i)=WL;
            Qin(i)=Qconst;                                        %Qinn (m^3/s)
            Q(i)=1000*Ae/10000*(2*g*WL)^0.5;           %Q (L/s)
            tau(i)=Q(i)*i*dt;
        else
            WL=WL+60*dt/B/L*(-Ae/10000*(2*g*WL)^0.5);
```

```
                WLL(i)=WL;
                Qin(i)=0;
                Q(i)=1000*Ae/10000*(2*g*WL)^0.5;
                tau(i)=Q(i)*i*dt;
            end
            QQ=QQ+Q(i);
            tautau=tautau+tau(i);
            i=i+1;
        end
        tmax=Ts/60/dt;
        detention=tautau/QQ-Ts/2/60
        WL_max=WLL(tmax);
        ni=Ts/60/dt;     %ni:Number of i

%%%%%%%%%%SCS Triangular inflow%%%%%%%%%%%%%%%%%%%
elseif flagInflow==1         %SCS triangular hydrograph case
    while i<= 30*Tp/60/dt & WL>1e-5
        time(i)=i*dt;
        if i<(Tp/60+1)/dt
            WL=WL+60*dt/B/L*(i*dt/(Tp/60)*Qp/1000-Ae/10000*(2*g*WL)^0.5);
            WLL(i)=WL;
            Qin(i)=1000*i*dt/(Tp/60)*Qp/1000;
            Q(i)=1000*Ae/10000*(2*g*WL)^0.5;
        elseif i<(8/3*Tp/60+1)/dt
            WL=WL+60*dt/B/L*((1.6-0.6*i*dt/(Tp/60))*Qp/1000-Ae/10000*(2*g*WL)^0.5);
            WLL(i)=WL;
            Qin(i)=1000*(1.6-0.6*i*dt/(Tp/60))*Qp/1000;
            Q(i)=1000*Ae/10000*(2*g*WL)^0.5;
        else
            WL=WL+60*dt/B/L*(-Ae/10000*(2*g*WL)^0.5);
            WLL(i)=WL;
            Qin(i)=0;
            Q(i)=1000*Ae/10000*(2*g*WL)^0.5;
        end

        i=i+1;
    end
    ni=8/3*Tp/60/dt;     %ni:Number of iteration during runoff period
end


%Water level (m) change with time
if flagGraph==1
    plot(time/60, WLL);
    hold on
    title('Water level change with time')
    xlabel('time(hr)');
    ylabel('Water Level (m)')
elseif flagGraph==2
    plot(time/60, Q);
    hold on
    plot(time/60, Qin);
    title('In and outflow change')
    xlabel('time(hr)');
    ylabel('Flow Rate (L/s)')
end


%%%%%%%%%%%%%%%%%%%%%%%%Program for calculating TSS outlet
concentration     %%%%%%%%%%%%%%%%%
```

```
if flagSSC==1
    tic

    %%Calculating time to reach outlet zone
    for i=1:ni-1
        time=0;
        RHS=0;LHS=1;
        tDrain(i)=0;
        n=1;
        t0(i)=i*dt;
      while RHS<LHS %t0=TT*i and T=time(i)
          if i+n<ni
              iRange=[i:i+n];
          else
              iRange=[i:ni];
          end
          LHS=L;
          RHS=1/B/WLL(i+n)*trapz(iRange,Qin(iRange))*60/1000;
          RHSS(i)=RHS;
          tDrain(i)=i+n;
          tDetention(i)=n;
          n=n+1;
       end
    end
%          plot(t0, tDetention);
%          title('Figure2. Detention Time')
%          xlabel('Inflow time(min)');
%          ylabel('Detention time (min)')


      %%%%%%%%%%Time series TSS Concentration Calculation%%%%%%%%%%%%%%%
      for i=1:ni-1
          C00(i)=C0;
          vpMini=(densP-densL)*(100*g)*(1.5*1e-4).^2/18/(10*viscs)/100*3600; %vp(m/hr) for 1.5 micron
particle
          vp=0;%vpMini;
                        %Calculating critical velocity
          time=[t0(i):tDrain(i)];
          vp=60*1./trapz(time,1./WLL(time));
          vpp(i)=vp;
          %Calculating critical particle size
          cpp(i)=10000*(vp/3600*100*10*viscs*18/((densP-densL)*100*g))^0.5;
          vp_interval=0.00001;
          if vp> vpMini
              criticalVP=vpMini:vp_interval:vp;%0.0073(m/hr) is settling velocity for dp=1.5(micron)
               %P_Conc is the ratio of particles smaller than critical particle size, which means 1-P_Conc is the
portion all of which settles down
               P_Conc(i)=1/(tyeta*(2*pi)^0.5)*trapz(criticalVP, exp(-0.5*((log(criticalVP)-
rmd)./tyeta).^2)./criticalVP);
               %E2_out is the portion that settles down among whole PSD
               E2_out(i)=60*trapz(time,1./WLL(time))*1/(tyeta*(2*pi)^0.5)*trapz(criticalVP, 1/3600*exp(-
(log(criticalVP)-rmd).^2/(2*tyeta^2)));
               E_out(i)=P_Conc(i)-E2_out(i);
               C(i)=C0*E_out(i);
          else
              C(i)=0;
          end

      end
      plot(tDrain/60, C);
```

```
    hold on
    title('Figure2. Time series TSS concentration')
    xlabel('Time (hr)');
    ylabel('Concentration (mg/L)')

     %%%%%%%%%%%%5%Total removal ratio calculation%%%%%%%%%%%%
     timeIn=[1:ni-1];
     totalMassIn=C0/1000*60*trapz(timeIn,Qin(timeIn));
     totalMassOut=60/1000*trapz(timeIn,Qin(timeIn).*C(timeIn));
     RemovalRatio=1-totalMassOut/totalMassIn
end


%%%%%%%%%%%%%%%%%%%%% PSD graphs %%%%%%%%%%%%%%%%%%%%%%%%
lndp=[-5:0.1:4];
x_dp=exp(lndp);
lnvp=[-8:0.1:2];
x_vp=exp(lnvp);
if flagGraph==3 | flagGraph==4
    pPDF=1./((2*pi)^0.5*tyetaPsize.*exp(lndp)).*exp(-0.5*((lndp-rmdPsize)/tyetaPsize).^2);
    pCDF=cumtrapz(exp(lndp),pPDF);
    if flagGraph==3
        plot(x_dp,pPDF);
        title('PDF of Particle Size Distribution')
        xlabel('Particle Size (micron)');
        ylabel('PDF')
    else
        plot(x_dp,pCDF);
        title('CDF of Particle Size Distribution')
        xlabel('Particle Size (micron)');
        ylabel('CDF')
    end
end

if flagGraph==7
    vp=(densP-densL)*(100*g)*(exp(lndp)*1e-4).^2/18/(10*viscs)/100*3600; %vp(m/hr)
    plot(x_dp,vp)
    title('Relationship between particle size and settlign velocity')
    xlabel('Particle Size (micron)');
    ylabel('Particle Settling velocity (m/hr)')
end

if flagGraph==5 | flagGraph==6
    pPDF=1./((2*pi)^0.5*tyeta.*exp(lnvp)).*exp(-0.5*((lnvp-rmd)/tyeta).^2);
    pCDF=cumtrapz(exp(lnvp),pPDF);
    if flagGraph==5
        plot(x_vp,pPDF);
        title('PDF of Particle Settling Velocity')
        xlabel('Particle settling velocity (m/hr)');
        ylabel('PDF')
    else
        plot(x_vp,pCDF);
        title('CDF of Particle Settling Velocity')
        xlabel('Particle settling velocity (m/hr)');
        ylabel('CDF')
    end
end
```

Appendix B Nomenclature

Symbols	Descriptions
A_0	Actual orifice area
A_e	Effective area of an orifice
B	Width of the sedimentation basin
C	Concentration
C_D	Drag coefficient
Cd	Orifice coefficient
C_{in}	Inflow SSC
C_{out}	Outflow SSC
CU	Uniformity coefficient
d_p	Diameter of a particle
$d_{p,c}$	Critical particle diameter
EMC	Event Mean Concentration of particles
F	Force (in Chapter 2)
F	Potential settling function (except Chapter2)
F_b	Body force
F_d	Drag force
F_g	Gravitational force
F_r	Froude number
g	Gravitational acceleration
h	Water level
H_a	Hazen number
L	Length of the sedimentation basin
L_R	Length ratio of prototype to model
M	Mass
M_{in}	Total mass of inflow particles
M_{out}	Total mass of outflow particles
Q	Flow rate
Q_{in}	Inflow rate
Q_{out}	Outflow rate
Q_p	Peak flow of a triangular hydrograph
R	Removal efficiency
R_e	Reynolds number
R_{out} (t_{in})	Removal ratio of particles which flows into the basin at t_{in}
t	Time
tin	Time when a particle flows into the basin

t_{out}	Time when a particle flows out of the basin
T_p	Peak time of a triangular hydrograph
T_s	Duration of a runoff
u	Longitudinal fluid velocity
u_p	Longitudinal particle velocity
v	Velocity
v	Vertical fluid velocity
V_{in}	Total inflow volume
v_{or}	Overlflow velocity
V_{out}	Total outflow volume
v_p	Vertical particle velocity
v_s	Particle settling velocity
$v_{s,c}$	Critical particle settling velocity
x	Longitudinal position
x_p	Longitudinal position of a particle
x_w	Longitudinal position of water molecules
ζ	Lognormal standard deviation
ζ_p	Lognormal standard deviation of particle diameter
ζ_v	Lognormal standard deviation of particle settling velocity
λ	Lognormal mean
λ_p	Lognormal mean of particle diameter
λ_v	Lognormal mean of particle settling velocity
μ	Viscosity of a fluid
ν	Kinematic viscosity of a fluid
ρ	Density
ρ_f	Density of a fluid
t_d	Drainage time
ρ_p	Density of a particle
Superscript	
M	Model
P	Prototype
*	Nondimensionalized
k	Time step
Subscript	
E	Emptying period
F	Filling period

References

Adams, E.W., and Rodi. (1990). "W. Modeling Flow and Mixing in Sedimentation Tanks." Journal of Hydraulic Engineering. 116(7), 895-913.

Andral, M. C., Roger, S., Montrejaud-Vignoles, M., and Herremans, L. (1999). "Particle Size Distribution and Hydrodynamic Characteristics of Solid Matter Carried by Runoff from Motorways." *Water Environment Research*, 71 (4), 398-407.

ASCE. (1992). "Design and Construction of Urban Stormwater Management Systems." 101.

Bartosh, N. (2004). "Inventory and Analysis of Proprietary, Small-Footprint Storm Water Best Management Practices." Master Thesis, University of Texas at Austin, Texas.

Brown, P.P., Lawler, D.F. (2003). "Sphere Drag and Settling Velocity Revisited" Journal of Environmental Engineering, ASCE, 129, 3, 221-231.

Buchan, G.D. (1989). "Applicability of the simple lognormal model to particle-size distribution in soils." Soil Sci. 147:155–161.

Camp T. R. (1946). "Sedimentation and the design of settling tanks." Trans. ASCE, 111, 895-958.

Campbell, G.S. (1985). "Soil physics with BASIC: Transport models for soil-plant systems." Elsevier, Amsterdam.

Cristina, C., Tramonte, J., Sansalone J. J. (2002). "A granulometry-based selection methodology for separation of traffic-generated particles in urban highway snowmelt runoff." J. Water, Air, and Soil Pollution, 136: 33-53.

Currie, I.G. (1974). "Fundamental Mechanics of Fluids." McGraw-Hill, Inc, New York., 38-39.

DiToro, D.M., and Small. M.J. (1979). "Stormwater Interception and Storage." J.Environemtnal Engineering Division, ASCE, Vol.105, No.EE1, February.

Fenner, R. A., and Tyack, J. N. (1998). "Physical modeling of hydrodynamic separators operating with underflow." J. Envir. Engrg., ASCE, 124(9), 881-886.

Fair, G. M. and Geyer, J.C. (1954). “Water Supply and Wastewater Disposal.” John Wiley & Sons, New York.

Ford, D. T., and Hamilton, D. (1996). “Computer models for water-excess management.” 28.7 Larry W Mays ed., Water resources handbook, McGraw-Hill, NY.

Henderson, F. M (1966). “Open Channel Flow”, MacGrowhill, NY, 1966, pp.488-493.

Hwang, Ned H.C. and Houghtalen, J. R. (1996). “Fundamentals of hydraulic engineering system.” Pentice-Hall Inc., 308.

Jensen, M. (2005). “Sediment retention in rectangular storage tanks: Computations with a mass transport model and comparison with laboratory experiments.” 10th International Conference on Urban Drainage, Copenhagen/Denmark, 21-26 August 2005.

Jin, Y., Guo, Q., and Viraraghavan, T. (2000). “Modeling of Class 1 Settling Tanks.” J. Hydr. Engrg., ASCE 126 (8), 754-760.

Karamalegos, M. A. (2006). “Particle Size Distribution of Highway Runoff and Modification Through Stormwater Treatment.” Master Thesis, UT Austin. CRWR online report 05-10.

Lawler, D. F., and Benjamin, M.M. (2007). "Gravity Separations," Chapter 13 (draft) in "Water Quality Engineering: Physical-chemical Treatment Processes." to be published by McGraw-Hill, New York.

Lee, B., Shimizu, Y., Matsuda, T., and Matsui, S. (2005). “Characterization of Polycyclic Aromatic Hydrocarbons (PAHs) in Different Size Fractions in Deposited Road Particles (DRPs) from Lake Biwa Area, Japan.” Environ. Sci. Technol. 39, 7402-7409.

Luyckx, G., Vase, G., and Berlamont, J. (1998). “Experimental investigation on the efficiency of a high side weir overflow.” 3rd International Conference on Innovative Technologies in Urban Storm Drainage, Novatech, Lyon, France, 347-354.

Luyckx, G., Vase, G., and Berlamont, J. (2002). “Surface load as predominant factor for CSO efficiency.” *Global Solutions for Urban Drainage.*, ASCE, 1-14.

Luyckx, G., Vase, G., and Berlamont, J. (2005). “Solids separation efficiency of combined sewer overflows.” Water Science and Technology Vol51 No2, IWA Publishing 2005, 71-78.

Minton, G. (2002). “Stormwater treatment.” Amica International Inc.

National Pollutant Discharge Elimination System (NPDES):

"Phases of NPDES stormwater program." U.S. Environmental Protection Agency. http://cfpub.epa.gov/npdes/stormwater/swphases.cfm (as of April 27, 2006)

NURP. (1983). "Results of the Nationwide urban runoff program." US EPA Water Planning Division WH-554 Washington, DC 20460.

Reeve, Dominic., Chadwick, Andrew., and Fleming Christopher. (2004). "Coastal engineering." Spon Press., 300.

Shimadzu. (2006). "Mechanism of particle size distribution measurements using lazer diffraction particle analyzer." http://www.shimadzu.co.jp/powder/lecture/middle/m01-2.html, (in Japanese).

Small. M.J., DiToro. D.M. (1979). "Stormwater Treatment System." Journal of Environemntal Engineering Devision, ASCE, Vol.105, No.EE#, June.

Stovin, V. R., Saul, A.J., Drinkwater, A., and Clifforde, I. (1999). "Field testing CFD-based predictions of storage chamber gross solids separation efficiency." *Water Science and Technology*, v 39, n 9, 161-168.

Stokes, G. G. (1851). "On the Effect of the Internal Friction of Fluids on the Motion of Pendulums." Transactions of the Cambridge Philosophical Society, Vol.9, pt.2, 8-106.

Su, Y. and Mitchell, G.F. (2006). "Characteristics of First Flush Effects in Storm Water Runoff via a Retention-Detention System." TRB 2006 Annual Meeting CD-ROM

Swamee, P. K., and Tyagi, A. (1996). "Design of Class-1 sedimentation tanks." J. Envir. Engrg., ASCE, 122(1), 71-73.

Takamatsu, T, Naito, M, Shiba, S, Ueda, Y. (1974). "Effects of Deposit Resuspension On Settling Basin", J of the Environemtnal Enginnering., EE4, 883-903.

Thompson, D. M. (1969). "Scaling laws for continuous flow sedimentation in rectangular tanks." Proceedings The Institution of Civil Engineers, Vol.43, May, 453-461.

TTI. (2000). "Design Methods, Selection, and Cost-Effectiveness of Stormwater Quality Structures." Research Report 1837-1, 6.

Urbonas, B. and Stahre, P. (1993). "Stormwater-Best management practices and detention for water quality, drainage, and CSO management." PTR, Prentice Hall, Englewood Cliffs, New Jersey.

Walesh, S.G. (1987). "Course Notes on Stormwater Detention Facility Design." ASCE Continuing Education Program ASCE, New York, NY.

Young, G.K., Stein, S., Cole, P., Kammer, T., Graziano, F., and Bank, F. (1996). "*Evaluation and Management of Highway Runoff Water Quality."* Publication No. FHWA-PD-96-032, U.S. Department of Transportation, Federal Highway Administration, Office of Environment and Planning.

Zanders, J.M., (2005). "Road sediment: characterization and implications for the performance or vegetated strips for treating road run-off." J. Science of Total Environment., ELSEVIER, 339 (2005), 41-47.

Zhou, S., and McCorquodale, J. A. (1992). "Modeling of rectangular settling tanks." J. Hydr. Engrg., ASCE, 118(10), 1391-1405.

Zhou, S., McCorquodale, J. A., and Godo, A.M. (1994) "Short Circuiting and Density Interface in Primary Clarifiers." J. Hydr. Engrg., Volume 120, Issue 9, 1060-1080.